Lehigh University
Lehigh Preserve

Fritz Laboratory Reports | Civil and Environmental Engineering

1976

Experimental local buckling of fabricated high-strength steel tubular columns, M.S. thesis, October 1976

Stephen Xavier Gunzelman

Follow this and additional works at: http://preserve.lehigh.edu/engr-civil-environmental-fritz-lab-reports

Recommended Citation
Gunzelman, Stephen Xavier, "Experimental local buckling of fabricated high-strength steel tubular columns, M.S. thesis, October 1976" (1976). *Fritz Laboratory Reports.* Paper 2174.
http://preserve.lehigh.edu/engr-civil-environmental-fritz-lab-reports/2174

This Technical Report is brought to you for free and open access by the Civil and Environmental Engineering at Lehigh Preserve. It has been accepted for inclusion in Fritz Laboratory Reports by an authorized administrator of Lehigh Preserve. For more information, please contact preserve@lehigh.edu.

EXPERIMENTAL LOCAL BUCKLING OF FABRICATED HIGH-STRENGTH STEEL TUBULAR COLUMNS

by

Stephen Xavier Gunzelman

FRITZ ENGINEERING
LABORATORY LIBRARY

A THESIS

Presented to the Graduate Committee

of Lehigh University

in Candidacy for the Degree of

Master of Science

in

Civil Engineering

Lehigh University

October, 1976

406.81

This thesis is accepted and approved in partial fulfillment of the requirements for the degree of Master of Science.

September 17, 1976
(date)

Professor Alexis Ostapenko
Professor in Charge

Professor David A. VanHorn
Chairman, Department of
Civil Engineering

ACKNOWLEDGEMENTS

This investigation is part of a research project on the local buckling of round tubular steel columns above the proportional limit, sponsored by the American Iron and Steel Institute and conducted at Fritz Engineering Laboratory, Lehigh University. Dr. Lynn S. Beedle is the director of the laboratory and Dr. David A. VanHorn is the chairman of the Civil Engineering Department.

The author wishes to gratefully acknowledge the help of Dr. Alexis Ostapenko, his thesis advisor, who has devoted a considerable amount of time and effort to making pertinent comments and suggestions concerning the author's work.

Sincere gratitude is expressed to Kenneth C. Loush, Marc A. Marzullo, and Gerry Weimann, graduate students at Lehigh, for their help in reducing the experimental data and in preparing many of the figures. Special thanks are due to Kenneth R. Harpel, Robert R. Dales, Kermit Eberts, and the rest of the laboratory's technical staff who helped plan, set-up, and run the tubular column tests. Hugh T. Sutherland and Russel Longenbach were most helpful with the test instrumentation. John M. Gera, Douglas Wiltraut, Sharon Balogh, and Rick Troxell did a fine job of drafting. Last but not least, the typists of the laboratory's Word Processing Center, Ms. Debra Zappasodi and Ms. Antoinette Larkin, are acknowledged for their patience and effort.

TABLE OF CONTENTS

LIST OF TABLES

LIST OF FIGURES

ABSTRACT

The designers of round tubular columns are handicapped by the discrepancies between the design rules currently used for local buckling.

Local buckling tests were conducted on eight short tubular specimens. The specimens were fabricated from 6.35 mm (1/4 in.) and 7.94 mm (5/16 in.) high-strength steel plate with a yield stress (F_y) of 345 MPa (50 ksi). The plate was cold-rolled and then welded. The diameters ranged from 0.72 m (28 in.) to 1.79 m (70 in.), and the diameter-to-thickness (D/t) ratios ranged from 85 to 248.

The maximum stress was limited by the formation of ring bulge or lobular buckles or by the simultaneous formation of both. The buckling stress values ranged from 0.814 F_y to 1.009 F_y.

The buckling stress and strain, the type of initial buckling, and the post-buckling behavior were found to be a function of D/t. Longitudinal welding residual stresses did not appear to affect the location of the buckles, and the initial geometric imperfections had very little effect on the intensity of the buckling stress. By forming successive sets of lobular buckles, the tubes were found capable of dissipating large amounts of energy at approximately 15-25% of the buckling stress.

When the buckling stress values were plotted against the geometric and material properties of the test specimens, they formed a smooth curve with very little scatter. All the current design rules are conservative in comparison to these tests.

1. INTRODUCTION

1.1 Background

Columns of circular shape are equally resistant to buckling in any direction, and this is one reason why they are often used in structures subjected to three-dimensional loading such as offshore oil drilling platforms, elevated storage tanks, transmission towers, and light poles. Indeed, as long as the end conditions are uniform, the circular tube provides the most efficient shape for a centrally loaded column which is not supported laterally between its ends.

Tubes are produced by two methods, manufacture in a mill and fabrication from the flat plate. The manufacturing process can be accomplished in a variety of ways including extrusion, fusion welding, and electric resistance welding (6). The fabrication process is carried out by rolling a flat plate into a cylindrical shape and welding the joint. The distinction between the processes is important because fabricated tubes usually have greater geometric imperfections and different levels of residual stress than do manufactured tubes.

Depending on the dimensions of the tubular column, failure can occur by either local or overall buckling or by a combination of both. For tubes with a large ratio of length to radius-of-gyration, L/r, and a small ratio of diameter to wall thickness, D/t, failure will occur by overall buckling. On the other hand, a large D/t and

a small L/r will cause the tube to buckle locally. Furthermore, buckling can be classified as elastic or inelastic depending on whether it occurs below or above the proportional limit.

At the present time, there are significant discrepancies between the design rules used to predict local buckling. The substantial disagreement between the test data and the classical theory and the wide scatter amongst the test points have been largely responsible for these discrepancies. The vast majority of tests have been performed on manufactured tubes made from thin gauge aluminum or Mylar. Very little research has been conducted on fabricated tubes made from steel, even though such members are widely used. It is not feasible to extrapolate the test results on the manufactured tubes to fabricated steel tubes because of the differences between the two with respect to imperfections, residual stresses, and the materials from which they are made. Therefore, more research on the fabricated steel tubes is necessary.

Of greatest importance for engineering structures are fabricated members whose D/t is such that local buckling can be expected at stresses between the proportional limit and the yield stress. Some of the numerous parameters which are expected to influence local buckling within this range are: residual stresses, out-of-roundness, out-of-straightness, and the locations of weld seams. Since, at the present time, these factors are difficult or impossible to consider analytically, the need for more empirical studies is again established.

1.2 Present Design Curves

Figure 1 shows some of the design curves currently used for local buckling. The ordinate is the ratio of the buckling stress to the yield stress, and the abscissa is the nondimensional parameter α which is inversely proportional to the D/t ratio and is defined by

$$\alpha = \frac{Et}{F_y D} \tag{1}$$

where E is the modulus of elasticity, t is the wall thickness, F_y is the yield stress of the steel, and D is the diameter of the tube. Parameter α has proved to be convenient for plotting test results with different values of yield stress and, therefore, for formulating general design formulas. The following design curves are shown in Fig. 1: Donnell & Wan (5), AISI (American Iron and Steel Institute) (1), Plantema (10), Marshall (6), and DNV (Det Norske Veritas, 1973, Amended) (4).

There are more curves in practical use, such as AWWA (American Water Works Association), but they generally fall within the extremes of the curves shown in Fig. 1 (6). Since the AWWA curve and some others, not shown in Fig. 1, were originally developed as allowable stress curves for a particular grade of steel, a direct comparison between these curves and others in a nondimensional form may not be valid.

Of particular interest are the AISI and Marshall curves since they are recommended by AISI and API (American Petroleum Institute) for practical use in the design of fabricated tubular members in this country. The disagreement between these curves is rather substantial, especially in the range of F_c/F_y = 0.5 to 0.8. The optimistic DNV curve makes the range of uncertainty even more pronounced; for example, the difference in F_c/F_y between the DNV and Marshall curves is 40% for α = 3.0 (D/t = 200 when F_y = 345 MPa (50 ksi)).

1.3 Previous Work

Prior to the research described here, the only local buckling tests conducted on fabricated tubes which failed in the inelastic range were made by Wilson and Newmark (14,15) during the 1930's. Most of their results are plotted in Fig. 1. The test points shown in the figure represent D/t ratios ranging from 69 to 320 and wall thicknesses ranging from 0.8 mm (0.031 in.) to 12.55 mm (0.494 in.). There is substantial scatter between the test results for the same α values.

One trend found by Wilson and Newmark was that for the same D/t the thicker tubes developed a greater buckling stress than the thinner ones. Wilson and Newmark attributed this result to geometric imperfections which they said were greater, relatively, for the thin than for the thick walls. However, they did not take

measurements of the imperfections to confirm their contention.

In 1950, Donnell and Wan introduced an initially deflected shape into the analysis of tubular buckling in order to account for geometric imperfections (5). This initial shape was characterized by an "imperfection factor," and, by varying this factor, Miller has recently shown that predicted curves can be made to fit the test data quite accurately (9). However, to accomplish this fit, Miller found it necessary to establish different categories for the type of material, the type of process by which the tube is made, the wall thickness, and the D/t ratio. Furthermore, since the imperfection factor was selected only for agreement with the test data and without knowledge or consideration of the actual specimen imperfections, this procedure becomes a direct curve fitting process for each special case.

Koiter raised serious objections of a theoretical nature against the Donnell and Wan analysis by pointing out that when Donnell and Wan applied variational methods to the free parameters in their assumed buckling mode, they simultaneously varied their assumed initial imperfection pattern (7). Taking a different approach, Koiter showed that if the post-buckling behavior of a perfect structure is unstable (that is, there is a loss of stress upon increasing deformation), as is the case for a tube under axial compression, small imperfections will result in a significant reduction in the maximum load (8).

Most of the recent theoretical work has assumed an axisymmetric configuration of initial imperfections. However, Arbocz has noted that measurements conducted on laboratory specimens during the 1960's and early 1970's indicate that most imperfections are asymmetric (13). Though asymmetry increases the complexity of the analysis, work is proceeding in this area, and several excellent state-of-the-art discussions on this work are included in Ref. 13. So far, such analyses have been limited to elastic buckling. Despite the advances in the methods of analysis, specific design recommendations cannot yet be made based on theory alone.

1.4 Topics of this Investigation

Eight high-strength steel tubular columns were subjected to axial compression, and they failed by local buckling above the proportional limit. In the analysis of these tests, the following topics are covered:

1.) Description of the eight test specimens.

2.) The test procedures employed.

3.) The results of out-of-roundness, out-of-straightness, and residual stress measurement.

4.) The test behavior of the specimens.

1.5 Brief Summary of the Test Results

The test results showed that the API and AISI design curves are adequately conservative. A consistent relationship between the buckling stress and α and the post-buckling behavior and α was found. The tubular specimens possessed a capacity for dissipating large amounts of energy by the formation of successive sets of buckles. The patterns of residual stress in the longitudinal direction due to welding were seen to have little correlation with the patterns of buckling, and the initial imperfections were found to have little effect on the buckling stress of the specimens tested.

2. DESCRIPTION OF TEST SPECIMENS

2.1 Geometric and Material Parameters

A typical tubular specimen and the pertinent notation are shown schematically in Figure 2. The dimensions and other parameters for each of the specimens are listed in Table 1. The outside diameters (OD) ranged from 0.72 m (28 in.) to 1.79 m (70 in.) as seen in Column 4 of Table 1, and the wall thickness ranged from 7.2 mm (0.28 in.) to 8.4 mm (0.33 in.) as shown in Column 5. The D/t ratios correspondingly fell between 85 and 248. The specimens were short with lengths ranging from 2.03 to 3.05 m (80 to 120 in.), and this resulted in slenderness ratios of less than ten in all cases.

The specimens were made from ASTM A572 or A633 steel having a nominal yield stress of 345 MPa (50 ksi). They were fabricated by cold-rolling flat plate in a pyramid three-roll plate bending machine and then welding along one longitudinal seam. The submerged arc process was used to place three different kinds of welds:

1.) A multi-pass vee weld for Specimens P1 and P3.

2.) A single-pass butt weld for Specimens P2 and P4.

3.) A two-pass, single-vee groove weld for Specimens P5, P6, and P7.

These three weld types are shown in Figures 3a, 3b, and 3c, respectively.

After testing, Specimen P3 was modified into a new specimen, P3A, for retesting. The buckled portion of P3 was removed by flame cutting, and a 17 mm steel plate was welded to the shortened end. In the process, the length was reduced from 3.05 m (120 in.) to 2.03 m (80 in.) while all other dimensions (D, t) remained the same as for P3. This modification also produced mixed end conditions since one end of Specimen P3A was fixed by welding to a steel plate. Specimens P3 and P3A are shown in Figures 4a and 4b, respectively.

2.2 Preparation of the Specimen Ends

The ends of the specimens had to be prepared so that the load could be applied uniformly and concentrically. The ends of P1, P2, P3, P4, and P7 were machined flat and square. However, in the case of Specimens P5 and P6, the large diameters made machining difficult, and thus the method of end preparation was modified. In these cases, a 127 mm wide x 25.4 mm thick steel ring was welded to each end with the specimens centered on the rings. The end ring at the top of P6 can be seen in Figure 5.

2.3 Material Properties

Static yield stress values obtained from flat plate coupons at a zero strain rate were used in evaluating the test results. The

plate coupons were made in accordance with the ASTM Standards (3), utilizing a 203.2 mm (8 in.) gage length. The yield stress values were taken as the average of 3 to 4 coupon tests, and they are listed for each specimen in Column 3 of Table 1. The difference between the actual yield stress and the nominal value of 345 MPa ranged from -25.58 MPa to +32.41 MPa (-3.71 ksi to +4.70 ksi).

The static yield stress was chosen because it is a more consistent value than the dynamic yield stress whether in a test on the same coupon or from one coupon to the next. A dynamic strain rate or 52 micro-strains/sec. was used in the coupon tests conducted in this investigation. Shortly after the test coupon had achieved its yield plateau, the motion of the machine head was stopped, and, after a 5-minute wait, the static yield stress value was recorded. The machine was restarted and then stopped twice more during yielding in the same manner. Thus, three static yield stress values per coupon were obtained. Beyond strain hardening, the dynamic strain rate was increased to 417 micro-strains/sec., and the test was continued until fracture of the coupon occurred.

Experience of conducting coupon tests in this program showed that it was difficult to accurately maintain the maximum ASTM A370 strain rate of 1042 micro-strains/sec., even on a displacement controlled machine. This fast rate of strain also made it difficult to take readings accurately. However, much coupon testing in both industry and research is performed at the maximum ASTM A370

strain rate, and thus a method of correlating yield stress values obtained at different strain rates is required.

Empirical formulas for relating dynamic and static yield stress values for ASTM A36, A441, and A514 steels have previously been developed by Rao, Lohrman, and Tall (11). However, a few control tests run in the present study on ASTM A633 steel coupons suggested that a slight modification in the formula for A441 steel which is applicable to steel with F_y = 345 MPa, should be made. The formulas of interest are:

a.) From Rao, Lohrman, and Tall (11):

$$\frac{F_{yd}}{F_{ys}} = 1 + 0.020\,\dot{\varepsilon}^{0.18} \qquad \text{(from tests on A441 steel)} \tag{2}$$

b.) From Four Control Tests in this Investigation:

$$\frac{F_{yd}}{F_{ys}} = 1 + 0.021\,\dot{\varepsilon}^{0.20} \qquad \text{(from tests on A633 steel)} \tag{3}$$

where F_{yd} and F_{ys} are the dynamic and static yield stresses, respectively, and $\dot{\varepsilon}$ is the dynamic strain rate in micro-strains per second.

3. IMPERFECTIONS OF THE SPECIMENS

In this investigation, the measure of geometric imperfections was determined from the out-of-roundness and out-of-straightness of the test specimens. The out-of-roundness at any given cross section of the specimen was defined by:

$$\text{OUT-OF-ROUNDNESS} = \frac{OD_{max} - OD_{min}}{OD} \qquad (3)$$

where OD_{max} and OD_{min} are the maximum and minimum outside diameters of the cross section and OD is the mean outside diameter of the specimen. Out-of-roundness at the top, the bottom, and the mid-height levels of each specimen was evaluated. The maximum out-of-roundness values and their locations are given in Columns 3 and 4 of Table 2. These values varied from 0.00530 (P6) and 0.00569 (P5) to 0.03618 (P3) and 0.03799 (P4).

The out-of-straightness is defined as the maximum offset between a longitudinal straight line and the specimen wall in any 1.52 m (5 ft.) length. In all cases, the maximum value of out-of-straightness was on a line adjacent to the weld. These values are given in Column 5 of Table 2, and they varied from 1 mm (0.04 in.) for P5 and P6 to 2.5 mm (0.10 in.) for P2 and P4.

There was considerable variation in the amount of initial imperfections from specimen to specimen. For example, P4 was 2.3

times more out-of-round than P2 and 7.2 times more out-of-round than P6.

Specimens P1, P2, P3, P3A, and P4 were made by the same fabricator, and they are considered to have greater initial imperfections than would normally be encountered in practice. Specimens P5, P6, and P7 were made by another fabricator, and their imperfections appear to be much more representative of those found in practice.

There was no specific relation between the magnitude of initial imperfections and the dimensions of the tube. On the other hand, there was a pattern to the location of the maximum out-of-straightness since it consistently occurred along a line adjacent to the weld.

The American Petroleum Institute has set standards for the allowable out-of-roundness and out-of-straightness of a tube (2). According to these standards, the difference between the maximum and minimum outside diameters should not exceed 1% of the nominal diameter or 6.4 mm (1/4 in.) whichever is less. The maximum allowable out-of-straightness in any 3.05 m (10 ft.) length is 3.175 mm (1/8 in.). All the specimens, except P5 and P6, exceeded both of the out-of-roundness limits while P5 and P6 exceeded just the 6.4 mm limit. The out-of-straightness limit was exceeded by Specimens P1, P2, and P4.

4. RESIDUAL STRESSES

The primary types of residual stress in a fabricated tube are: the stresses due to cooling of the hot-rolled plate, the circumferential stresses caused by the bending of the plate into a cylindrical shape and the corresponding longitudinal stresses due to the Poisson's ratio effect, and the longitudinal and corresponding circumferential stresses due to welding the tube. Only the longitudinal residual stresses caused by welding were measured in this study. Although the circumferential and hot-rolling stresses may have an effect on the intensity of the buckling stress, they do not change around the circumference and thus should not affect the location of the local buckles in the circumferential direction. The longitudinal stresses due to welding, on the other hand, do vary with distance from the weld and therefore may affect the circumferential location of the buckles. Measurements of the latter residual stresses were made in five specimens: P1, P2, P3, P4, and P5.

4.1 Method of Measuring Residual Stresses

A non-destructive method was utilized for measuring residual stresses. Target holes were drilled 0.254 m (10 in.) apart in the longitudinal direction on the inside and outside surfaces of the test specimen as shown in Fig. 6. The 0.254 m gage section had to be located far enough from the end of the specimen to preclude the relaxation of residual stresses that might occur adjacent to the free

end and yet close enough so that readings could be conveniently taken. To meet these requirements, the gage section was chosen to be 0.61 m from the end as indicated in Fig. 6. The distance between target holes along each gage line was measured before welding (but after rolling) and after welding.

A typical target hole is shown in Fig. 7. The hole had a shoulder which seated the tip of the gage, and, by being countersunk, the shoulder was protected from mechanical damage during handling and rolling. Since even a tiny amount of rust would significantly affect the distance measured between the target holes, protection against rusting was provided by painting the holes with a silicon solution and by covering them with duct tape.

The target holes were drilled on the flat plate prior to rolling for P1, P2, P3, and P4 and on the rolled tube for P5. There was slight ovalization of the holes due to rolling in Specimens P1 through P4 which did reduce the repeatability of the readings. However, since the readings taken before and after welding were equally affected by this ovalization, the effect on the determination of the residual stresses was not critical.

Measurements were made with a Whittemore Gage as indicated in Figure 8. The following procedure for taking readings was employed. First, the specimen was placed on rollers and rotated until the gage

line under consideration faced upwards. This occurred at the bottom for holes on the inside surface and at the top for holes on the outside surface. The target holes were cleaned with an air hose, and the Whittemore Gage was inserted into the holes and maintained perpendicular to the surface of the tube with the help of a bubble level. The gage reading was recorded, and then the gage was repositioned in the opposite direction to account for differences in the geometry of the target holes. This process was repeated until two readings were taken in each direction per gage line. If these readings were divergent, the target holes were cleaned again and additional readings were taken until reasonable repeatability was obtained. To account for the variation in ambient temperature, intermittent control readings were made on a temperature insensitive reference bar made of Invar. After the readings for each gage line were averaged and adjusted for temperature, the residual stress was computed from

$$F_r = \frac{L_A - L_B}{L_B} E \qquad (4)$$

where F_r is the residual stress, L_B and L_A are the average distances between target holes before and after welding (adjusted to a standard temperature), and E is the modulus of elasticity of steel.

4.2 Longitudinal Residual Stresses Due to Welding

4.2.1 Method of Presentation

For purposes of presentation, the pattern of longitudinal residual stresses around the circumference of a tube is unfolded and laid out flat as shown, for example, in Fig. 9 for Specimen P1. A vertical line through the mid-point of the pattern corresponds to the weld seam, and the right and left edges correspond to the line which originally was diametrically opposite the weld. The distance from the weld is given by the abscissa, and the stress is given by the ordinate. The measured stress values for both the inside and outside surfaces are plotted. Values from both surfaces were necessary because welding caused some distortion of the tube wall which, in turn, resulted in changes in curvature along the gage lines. The effect of these curvature changes was eliminated by averaging the inside and outside readings corresponding to the same location. The smooth curve in Fig. 9 represents this average.

A similar process was used to obtain the curves shown in Figures 10 through 13 for Specimens P2 to P5, respectively. Wherever the inside and outside readings were too disparate for averaging, the curves were dotted as seen in Figures 10, 11, and 12. In portions where there were readings for just one surface, the curve was established by maintaining continuity with the previously determined parts of the curve.

4.2.2 Results of Residual Stress Measurements

The residual stress patterns of all five specimens exhibited considerable similarity. As an illustration, the pattern for Specimen P1, shown in Fig. 9, is considered.

Although no readings were taken immediately at the weld, other research has established that high tensile residual stresses approximately equal to F_y exist there[12]. Just 0.05 m (2 in.) from the weld, the residual stresses went into compression and formed a band of compressive stress which extended from approximately 0.05 to 0.4 m (2 to 15 in.) from the weld. Beyond this, the magnitude of stress diminished sharply and alternated between tension and compression in a wave-like pattern. The compressive stresses peaked at about 0.13 to 0.18 m (5 to 7 inches) from the weld with a value of 76 MPa (11 ksi).

For Specimens P2, P3, and P4 the peak compressive stresses varied only slightly, ranging from 69 MPa (10 ksi) for P2, to 62 MPa (9 ksi) for P3, to 76 MPa (11 ksi) for P4. For Specimen P5 the band of compressive stress nearest the weld covered a larger area than for the other specimens, extending from approximately 0.03 to 0.6 m (1 to 25 in.) from the weld. The compressive stresses in P5 peaked at about 0.05 to 0.08 m (2 to 3 in.) from the weld with a value of 103 MPa (15 ksi).

The differences in residual stress that exist between the five specimens can be attributed to variations in the yield stress and in parameters which affect the heat input and heat dissipation such as the type of weld and the wall thickness. A comparison of the five patterns indicates that the width of the compressive stress band nearest the weld increases somewhat with an increase in the diameter. On the other hand, the value of the maximum compressive stress does not appear to be affected by the diameter, at least over the range of diameters tested.

5. TEST SETUP AND INSTRUMENTATION

5.1 Test Arrangement for Specimens P1, P2, P3, and P4

Figure 14 shows one of the specimens, P1, at the beginning of the test. The tube is seen standing between the loading head above and the machine pedestal below. The specimen is white because it was painted with a solution of lime in order to give a visual indication of surface yielding. As mill scale flaked off the specimen during the test, the whitewash would come with it, leaving a clear pattern behind.

A schematic representation of the test setup is shown in Fig. 15. Again the test specimen is seen standing on the machine pedestal. Between the end of the specimen and the pedestal was a steel base plate for the distribution of bearing stresses. A thin copper sheet was laid between the specimen and the base plate. The copper sheet was intended to accommodate local imperfections in the surface of the base plate and/or in the machined end of the test specimen, and thus the copper helped to provide uniform end stress. The same arrangement was used at the top of the specimen. This setup was utilized for Specimens P1, P2, P3 and P4.

The instrumentation consisted of mechanical and electrical-resistance gages, large scale micrometers, and reference rings.

Four mechanical gages at the corners of the machine head were used to measure the longitudinal shortening of the test specimens as indicated in Fig. 15.

The lateral deflection of the specimen wall relative to the ends of the specimen was measured by means of the special movable dial gage rig shown to the right of the test specimen in Fig. 14. The rig consisted of eight mechanical dial gages permanently attached to a trussed frame. The bottom end of the rig sat on the base plate and touched the specimen wall, while the top end was held against the specimen by means of an electromagnet. Readings were taken at eleven to thirteen locations around the circumference by successively repositioning the dial gage rig.

The out-of-straightness was measured by comparing the dial gage readings taken at the beginning of the test with readings taken when the rig was placed against a machined flat surface. The readings for out-of-roundness were obtained by using micrometers which had the capacity to measure diameters as large as 1.24 m (49 in.).

The original and subsequent geometry of the specimen ends was determined by measuring the gap between the specimen wall and the edge of a circular cutout in a Masonite plate attached to the steel base plate at each end of the specimen (this plate is labeled "reference ring" in Fig. 15). The diameter of the cutout was made approximately 100 mm larger than the nominal diameter of the test specimen,

thus providing a 50 mm gap which was convenient for measurement by means of calipers. This gap was also adequate for the placement of the bottom end of the dial gage rig on the base plate.

Electric-resistance gages were placed at the top and mid-height levels of each specimen, as indicated in Fig. 15. Longitudinal gages were located on the inside and outside surfaces at four diametrically opposite locations, while transverse gages were located on the outside surface only at the midheight level. The electric gages served in the aligrment of the specimens and as an alternate means for determining longitudinal strains during the test.

5.2 Test Arrangement for Specimen P3A

Figure 4b shows Specimen P3A standing between the loading head above and the machine pedestal below. The test setup for this specimen is shown schematically in Fig. 16. As with Specimens P1 to P4, a steel base plate with a copper sheet on top was laid between the bottom end of the specimen and the pedestal. However, at the top end, 1.52 m X 1.52 m X 17 mm thick steel plate welded to the tube served to distribute the load.

The use of mechanical dial gages was the same as for Specimens P1 to P4, but the electric gages were located differently being mounted at the bottom and at 0.5 m from the top.

5.3 Test Arrangement For Specimens P5 and P6

Figure 17 shows Specimen P5 standing between the loading head above and the test floor below. Figure 18 shows the schematic setup for testing Specimens P5 and P6.

Steel rings, 127 mm wide X 25.4 mm thick, were welded to both ends of these specimens to serve in the distribution of the load. The use of mechanical dial gages was the same as for Specimens P1 to P4, but the use of electric gages was limited to longitudinal ones mounted on the outside surface at three equally spaced circumferential locations at the midheight level.

The original geometry of the specimen ends was determined (prior to placement of the specimen in the loading machine) by measuring the gap between the end rings and a circle scribed approximately 100 mm larger than the outside diameter of the end rings. By also knowing the distance between the outside edge of the end rings and the tube wall, the out-of-roundness at the ends was determined. The out-of-roundness at mid-height was obtained from readings taken with the dial gage rig.

5.4 Test Arrangement For Specimen P7

The schematic setup for testing P7 is shown in Fig. 19. The setup was the same as for Specimens P1 to P4 except that there

were no Masonite reference rings. In addition, since there were no steel rings welded to ends of P7, the out-of-roundness at its ends was determined by directly measuring the distance between the specimen wall and a circle scribed approximately 100 mm larger than the tube diameter.

The use of mechanical and electrical gages was the same as for Specimens P5 and P6.

6. TEST PROCEDURE

6.1 Alignment

The tests were conducted on a 5-million pound hydraulic Baldwin testing machine. The first phase of each test consisted of alignment of the specimen in the testing machine. The loading head of the machine has a mechanism for controlled tilting, and, by careful adjustment, a practically concentric load could be applied.

Three methods of alignment were used to account for the different specimen end conditions. For Specimens P1, P2, P3, P4, and P7, alignment was accomplished by applying a series of load increments (with the maximum total load reaching 35% of the estimated failure load) and measuring the longitudinal strain increments at the different circumferential locations. Unequal strain increments indicated load eccentricity and a need for an adjustment in the tilt of the loading head. When the strain increments came into acceptably close agreement, the load was considered to be concentric.

Tilting of the loading head was not sufficient for achieving a uniform load for P3A because the steel plate welded to the top end of this specimen was not truly flat. Instead, a layer of gypsum grout ("Hydrostone") was poured onto the plate, directly above the tube wall. The machine head was then lowered to spread the grout on the plate. After hardening overnight, the grout could transmit load

uniformly to the specimen without any further alignment.

For Specimens P5 and P6, a similar grouting procedure was used at both the top and bottom ends in order to transmit the load uniformly through the end steel rings, as depicted in Fig. 20.

6.2 Test Sequence

Following alignment, the test began with the application of 90 KN (20 kips) of load and the attachment of the four longitudinal dial gages as shown in Fig. 15. The readings taken at this load were used as the initial reference condition for all subsequent readings.

Generally, load increments of 445 KN (100 kips) for P1 and P2 and 890 KN (200 kips) for all the other specimens were used. At each load increment, readings were taken of the longitudinal dial gages and of the electric-resistance gages. The lateral displacement readings of the dial gage rig were taken at the initial load of 90 KN and at several times prior to buckling. In addition, the dial gage readings were taken after the formation of the initial buckles in Specimens P3, P4, P5, and P7. The "gap" measurements between the specimen ends and the reference Masonite rings were taken at the beginning of the test and several times prior to buckling for P1, P2, P3, and P4.

7. TEST RESULTS

The description of test behavior has been separated into three categories: pre-buckling, buckling, and post-buckling. The phenomena common to all the specimens are discussed first, and then individual items of interest are pursued.

7.1 General Test Behavior

7.1.1 Behavior Prior To Buckling

The behavior up to and including buckling of Specimens P1, P2, P3, P3A, and P4 is shown in Figure 21 and that of Specimens P5, P6, and P7 is shown in Figure 23. The load is given as the average axial stress nondimensionalized with respect to the static yield stress of the material (ordinate), and the deformation is given as the average longitudinal strain (abscissa).

Figures 21 and 23 show that after some initial nonlinearity due to self-adjustments in the grouted ends of Specimens P3A, P5 and P6 or squashing of the copper in the case of P1, P2, P3, P4, and P7, the test curves followed a linear elastic path. The proportional limits for the individual specimens were approximately as follows: 0.65 F_y for P1 and P2, 0.80 F_y for P3, P5, P6 and P7, and 0.85 F_y for P3A and P4. The smaller proportional limits for P1 and P2 may have been caused by the greater residual stresses produced through

the wall thickness by rolling these smaller diameter tubes.

7.1.2 Behavior at Buckling

The specimens with values of $\alpha > 4$ (P1, P2, P3, and P3A) achieved a maximum stress of essentially F_y. The maximum stress for the remaining specimens ($\alpha < 4$) ranged from 0.951 F_y for P4 to 0.814 F_y for P5. In the latter specimens, the maximum stress decreased with a reduction in α, that is, with an increase in D/t. The maximum stress values are given in Column 9 of Table 1.

In all cases, the maximum stress was limited by local buckling. The buckling was accompanied by an explosive sound in Specimens P5 and P6 with the level of sound being greater for the tube with the larger D/t, P5.

With one exception, the achievement of maximum stress occurred simultaneously with buckling in a range of strain between 1.8 and 2.7 X 10^{-3}. The one exception was P1 where the maximum average stress of F_y was reached at a strain of about 3 X 10^{-3}, but local buckling did not occur until a strain of approximately 4 to 5 X 10^{-3}. Thus, the consequence of local buckling in this specimen was to limit the strain to which the yield stress could be maintained.

Table 1 shows that the α value for Specimen P1 ($\alpha = 7.51$) is distinctly greater than for P2 ($\alpha = 6.42$) even though the D/t

ratios for both specimens are about the same. Since P2 buckled just after reaching the yield stress and P1 buckled only after significant plastification, there should be an α value in the range, $6.42 < \alpha < 7.51$, above which the tube could strain significantly beyond the initial attainment of the yield stress before local buckling occurred.

7.1.3 Post-Buckling Behavior

The post-buckling behavior of Specimens P1, P2, P3, P3A, and P4 is shown in Fig. 22 and that of Specimens P5, P6, and P7 in Fig. 24. The nondimensionalized stress (ordinate) is plotted against the average longitudinal deformation (abscissa). In Article 7.1.1, Figures 21 and 23 were referred to, and in those figures strain was plotted along the abscissa. However, in the post-buckling range, strain is not a valid parameter for plotting because the post-buckling deformation is not uniform over the length of the specimen.

After initial buckling, there was an immediate reduction in stress as seen in Figures 22 and 24. However, the rate of reduction was not the same for individual specimens. The reduction was most gradual for P1, somewhat steeper for P2, and steeper yet for P3, P4, P7, P6, and P5 in that order. Since this order also corresponds to a decrease in the α values for the individual specimens, it can be concluded that the rate of load reduction is greater

for smaller α (larger D/t).

Following the drop in stress, the load stabilized, and the stress-deformation curve levelled off. The post-buckling strength depended on α; the larger α was, the greater the post-buckling strength became. The amount of deformation sustained between buckling and stabilization of the load after buckling varied. For the specimens with $\alpha < 4$ (P4, P5, P6, and P7), the amount of this deformation increased with a decrease in α. The deformation values were about 2.5 mm (0.1 in.) for P4 and P7, 5.5 mm (0.22 in.) for P6, and 8 mm (0.31 in.) for P5. For the specimens with $\alpha > 4$ (P1, P2, P3, P3A), these deformations were only about 0.5 mm (0.02 in.).

7.2 Initial Buckling of Specimens P1 to P4 including Specimen P3A

For the specimens with values of $\alpha > 3.6$ (P1, P2, P3, P3A, and P4), initial buckling occurred by the formation of a ring bulge. The bulge appeared adjacent to the top or bottom end of the specimen and was generally uniform around the circumference. Specimen P3A deviated from this pattern in that an initial ring bulge formed simultaneously at the top and at the bottom end before the buckling at the top took over. A typical ring bulge is shown in Fig. 25; here, Specimen P3A is shown immediately after initial buckling. The width of the ring bulge was about 0.2 m (8 in.) for all five specimens.

7.3 Initial Buckling of Specimens P5, P6, and P7

7.3.1 General Comments

For Specimens P6 and P7 ($2.4 < \alpha < 3.6$), initial buckling occurred by the simultaneous development of ring bulge and lobular buckles. For Specimen P5 ($\alpha < 2.4$), only lobular buckles developed.

The buckles occurred adjacent to the ends of Specimens P5 and P6, but they formed over 0.50 m from one end of Specimen P7. Thus, P7 was the only specimen in this investigation in which the buckles developed away from the end.

7.3.2 Initial Buckling of Specimen P5

In Specimen P5, the lobular buckles formed near the bottom end as seen in Fig. 26. The lobes are alternating inward and outward displacements of the tube wall. The symmetrical pattern formed by the eight lobes around the circumference of this specimen is shown by the plan view in Fig. 52.

A side view of an inward lobe is shown in Fig. 27. This photograph clearly points our the absence of ring bulge buckles.

In the longitudinal direction, the lobular buckles typically took the form shown in Fig. 28. The axial length of the lobes was about 0.45 to 0.50 m (18 to 20 in.).

7.3.3 Initial Buckling of Specimens P6 and P7

In Specimens P6 and P7, the initial buckling occurred by the simultaneous formation of the ring bulge and lobular buckles. For both specimens, the width of the ring bulge buckles was the same as for Specimens P1 to P4, and the axial length of the lobes was the same as for Specimen P5. The buckling of the two specimens did, however, differ with respect to location.

In Specimen P6, buckling took place near the top end as shown in Fig. 29. The ring bulge was located about 0.10 m (4 in.) from the top, and it was generally uniform around the circumference. Six lobular buckles emanated from the bottom side of the ring bulge, and the pattern formed by these lobes around the circumference is shown in Fig. 53.

In Specimen P7, the buckles developed at two levels as shown in Fig. 30. One level was centered 0.58 m (23 in.) from the top of the tube, and the second (lower) level was centered 1.17 m (46 in.) from the top. The upper level of buckling extended about two-thirds of the way around the circumference, while the lower level covered the remaining one-third with a slight overlap. At each level, lobular buckles emanated from both sides of a ring bulge in such a manner that an outward lobe above the ring bulge lay opposite an inward lobe below it.

Plan views of the lobes located on the bottom side of each ring bulge in Specimen P7 are shown in Figures 54a and 54b. The lobes possessed a half-wavelength in the circumferential direction of approximately 58°. This configuration could be interpreted as resulting in either five or seven lobes around the full circumference.

7.4 Post-Buckling Behavior of Specimens P1 to P4 including Specimen P3A

7.4.1 Amplitude of the Buckles

The amplitude of the initial ring bulge buckles was measured after the load had stabilized at a reduced level following buckling. In Fig. 22, the stabilized loads are given by the first set of plotted points after the sharp drop in stress. The amplitude of the initial ring bulge increased with a decrease in α. This amplitude varied from about 1.25 mm (0.05 in.) for the smaller diameter tubes (P1 and P2) to about 6 mm (0.25 in.) for the larger diameter specimens (P3, P3A, and P4).

7.4.2 Development of Lobular Buckles

As the post-ultimate deformation proceeded, the initial ring bulge buckles in Specimens P1 to P4 were followed by the development of lobular buckles. The lobes emanated from the ring bulge and alternated in an inward and outward pattern around the

circumference as shown, for example, in Fig. 31 for Specimen P3. Once the lobes had formed, the size of the ring bulge remained unchanged. In other words, all further shortening occurred by way of increasing magnitudes in the lobular buckles. An inward lobe always developed at the weld, and its amplitude was slightly greater than the amplitude of the other inward lobes.

The lobular buckles consistently formed a symmetrical pattern around the circumference, and their number varied from three to five. Actual end views of Specimens P1 to P4 are shown in Figures 32 to 36, respectively. Plan views of the lobular buckle patterns for these specimens are shown in Figures 47 to 51. The type and location of the initial buckles and the number of lobular buckles which formed are tabulated for each specimen in Columns 6 and 7 of Table 2.

The deformation at which the lobular buckles developed varied from specimen to specimen. In Specimens P3 and P4, lobular buckles were first observed at a deformation of between 7.5 mm (0.30 in.) and 9 mm (0.35 in.), that is, immediately after the formation of ring bulges. On the other hand, for Specimens P1 and P2, lobular buckles could not be detected until a deformation of approximately 20.5 mm (0.8 in.) which is considerably after the ring bulge formation. Thus, it can be concluded that, while the ring bulge mode is only briefly stable for the specimens with larger D/t

(P3 and P4), it is stable over a greater range of strain for the specimens with smaller D/t (P1 and P2).

The formation of lobular buckles in Specimen P3A is a special case. In this specimen, lobular buckles were first observed at a deformation of approximately 11 mm (0.45 in.) which is nearly 1.5 times the deformation at which they were first detected in Specimen P3. Therefore, it appears that the edge fixity provided by the welded end of P3A had the effect of delaying the development of the lobular buckles.

The behavior of the specimens in the post-buckling range was affected by the end conditions. The development of lobular buckles forced the buckled ends of specimens P1, P2, P3, and P4 to rotate and to slide on the base plate. The non-circular configuration of the end of Specimen P4, shown in Fig. 36, illustrates these deformations. Had the buckled end of Specimen P1 been prevented from rotating, it is possible that a series of ring bulges instead of lobular buckles would have followed the first ring bulge. It was the excessive deformations of the specimen ends which dictated the termination of the tests on Specimens P1, P2, P3, and P4 between deformations of 25 mm (1 in.) and 35 mm (1.4 in.), as shown in Fig. 22.

On the other hand, the end at which lobular buckling took place in Specimen P3A was fixed by welding. This arrangement allowed the test on P3A to be continued until it had been shortened by nearly 300 mm (12 in.).

The maximum loads achieved by Specimens P3 and P3A were nearly identical, indicating that, had the ends of Specimens P1, P2, P3, and P4 also been welded to base plates, their maximum stress values would have been the same as found in this study.

In the post-ultimate range, at a deformation of 20 mm (0.8 in.) P3A carried 1.2 times as much load as did P3, and thus it can be surmised that the post-buckling strengths of P1, P2, and P4 would have been somewhat larger had their ends also been welded to base plates.

As long as the end conditions were the same, the post-buckling strength was found to be a function of α, and the difference between individual specimens was significant. For example, at a deformation of 18 mm (0.7 in.), the stress had dropped to 30% of its maximum value in Specimen P4 but to just 47% in Specimen P2. In general, as α decreased, the post-buckling strength decreased.

7.4.3 Post-Buckling Behavior of Specimen P3A

The stress deformation plots in Fig. 22 are shown terminated before completion of the tests. The remainder of the plots

for Specimens P1, P2, P3, and P4 would have only shown a continued gradual reduction in strength. However, since Specimen P3A regained strength further out in the post-buckling range, it warrants special discussion, and its complete stress-deformation plot is shown in Fig. 37a.

After Specimen P3A initially buckled, it continued to loose stress until it reached a low point of 0.16 F_y at a deformation 20 times the deformation at initial buckling. Beyond this point the specimen regained some strength and climbed to its second stress peak, equal to 0.34 F_y, at a deformation 50 times greater than the initial buckling deformation. As the second peak was approached, a new set of lobular buckles formed. These new buckles developed directly below the first set in such a manner that the inward lobes of the second set were located under the outward lobes of the first set. Figure 37b shows the first set of lobular buckles in Specimen P3A, and Fig. 37c shows the same location after the formation of the second set.

The test on Specimen P3A was terminated shortly after the attainment of the second stress peak. However, the deformation process between the formation of the first and second sets of lobular buckles indicates that, had the test been continued, additional sets of lobular buckles would have formed with the stress fluctuating between the low value after the first set and the high value of the

second set.

7.5 Post-Buckling Behavior of Specimens P5, P6, and P7

7.5.1 Amplitude of the Buckles

The amplitude of the initial lobular buckles was measured after the load had stabilized at a reduced level following buckling. In Figure 24, the stabilized loads are given by the first set of plotted points after the sharp drop in stress. The magnitudes of the initial inward lobular displacements averaged about 40 mm (1.60 in.) for Specimens P5 and P6 and about 25 mm (0.95 in.) for Specimen P7.

7.5.2 General Comments

The conclusion reached in Article 7.4.2 that the post-buckling strength decreased with a decrease in α was confirmed by the behavior of Specimens P5, P6, and P7. At a deformation of 18 mm (0.7 in.), the stresses for these specimens ($\alpha < 3.6$) ranged from 0.25 F_y for P6 to 0.29 F_y for P7 as compared, for example, to the stresses of 0.35 F_y and 0.47 F_y for Specimens P3 and P2 ($\alpha = 4.50$ and 6.42, respectively).

After initial buckling, the size of the ring bulge in Specimens P6 and P7 did not change. In other words, all the post-buckling deformation in these specimens occurred in the lobular

buckles. For Specimens P5 and P6, an inward lobe formed across the weld seam in a manner similar to Specimens P1 to P4.

In Article 7.3.3, it was noted that two levels of buckling developed in Specimen P7. The longitudinal weld seam was one dividing line between these two levels as shown in Fig. 30. The other dividing line, located about one-third of the circumference from the weld, is shown in Fig. 44. The photograph in Fig. 44 was taken when Specimen P7 had been shortened by about 9.1 mm (0.36 in.). By the time the specimen had been compressed by 12.7 mm (0.50 in.), the two buckled levels were joined by the "Z-shaped" buckle shown in Fig. 45. No "Z-shaped" connection developed along the dividing line at the weld.

The tests for Specimens P6 and P7 were terminated at deformations of 19 mm (0.75 in.) and 23 mm (0.9 in.), respectively. However, the test for Specimen P5 was terminated only after the specimen had been shortened by 0.40 m (15.6 in.).

7.5.3 Post-Buckling Behavior of Specimen P5

The complete stress-deformation curve for Specimen P5 is shown in Fig. 38a. After initial buckling, P5 continued to loose stress until it reached a low point of 0.10 F_y at a deformation 20 times the initial buckling deformation (0.11 m = 4.3 in.). Beyond this point, the specimen regained some strength and achieved its second peak in stress, equal to 0.22 F_y, at a deformation 44 times the initial buckling deformation (0.24 m = 9.5 in.).

Shortly before the second stress peak was reached, a second set of lobular buckles formed adjacent to and above the first set. The new set of lobes was generally staggered with respect to the first set in that an inward lobe of the second set formed opposite an outward lobe of the first set. However, just seven lobes formed in the second set as compared with eight in the first set. Thus, one buckle was "swallowed" between the two sets. This observation is depicted in Fig. 39 where both sets of lobes are shown relative to each other in plan view. The first set of buckles is shown in an advanced stage in Fig. 38b, and the second set is shown at the same circumferential location in Fig. 38c.

The second set of lobes was first observed at a deformation of about 0.20 m (7.9 in.). However, there buckles were not due to a bifurcation phenomenon. Instead, they appeared to result from a gradual acceleration in the curvature of the specimen wall which, in turn, was a result of the tube wall having to maintain compatibility with the adjacent regions of the tube. This continuous process is depicted in Fig. 40 where an inward lobe from the second set of buckles is shown at various stages of development.

Following the attainment of the second stress peak and the subsequent reduction in load, the test was terminated. Had the test been continued, it is expected that the stress-deformation curve would have continued to rise and fall as additional sets of lobular

buckles formed.

During the deformation process, two types of outward lobes were observed. In one case, the outward lobe remained vertical and rigid and tended to shear or punch through the folded section of the buckle beneath it, as shown in Fig. 41. The shearing action caused the steel to fracture and created loud, popping sounds. In the second case, the outward lobe folded over on itself as shown in Fig. 42. It appeared that, when enough outward lobes of the second type folded to the point where unbuckled sections of the tube made contact, the specimen regained strength. By extending this reasoning, the formation of a new set of lobular buckles would cause the load to drop off and the folding process to begin again.

8. DISCUSSION OF TEST RESULTS

8.1 Comparison With Design Curves

The buckling stresses of the eight specimens are plotted against α in Fig. 55. The eight test points form a smooth curve with very little scatter. The small magnitude of scatter enhances the reliability of these tests, especially in view of the considerable scatter exhibited by the other test points in the figure.

All the design curves, including the AISI and API curves, lie below the eight test points obtained in this study; they are therefore conservative. However, the DNV curve comes close to matching these test points.

8.2 Comparison of Specimens P3A and P5

Specimens P3A and P5 were the only tubes tested to the point where a second set of lobular buckles developed. The stress-deformation curves for these two specimens are plotted in Fig. 43, and their patterns of behavior are seen to be quite similar. Both reached a low point in stress at about 20 times their deformations at initial buckling. The second stress peaks for P3A and P5 were achieved at 50 and 44 times their initial buckling deformations, respectively. However, the value of the second stress peaks were significantly different as P3A carried 1.55 times more stress than did P5 at this point (0.34 F_y for P3A vs. 0.22 F_y for P5). It can

be concluded that, after the formation of additional sets of lobular buckles, the maximum stress achieved is a function of α. The larger α is, the greater this maximum stress becomes.

8.3 Effect of Residual Stresses

The pattern of longitudinal residual stresses due to welding and the pattern of lobular buckles for Specimen P5 are superimposed in Fig. 46. The inward and outward lobes that correspond to the pattern of lobular buckles are shown alternating across the bottom part of this figure. No direct correlation between the two patterns can be observed. Therefore, it can be concluded that, in P5, welding residual stresses had no detectable effect on the location of the buckles. This observation can be extended to Specimens P6 and P7 since residual stresses in these specimens are expected to be of the same general pattern and magnitude as measured in P5. Furthermore, since the initial buckling in Specimens P1 to P4 took the form of a uniform ring bulge, it appears that the welding residual stresses in these specimens had no effect on the location of the initial buckles either.

8.4 Effect of Initial Imperfections

For each specimen, the original shape and the shape after lobular buckling are superimposed in plan view in Figures 47 to 54b. For example, for Specimen P5 these shapes are shown in Fig. 52. The

perfect tube with a circumference equal to the actually measured circumference of the specimen is depicted by the light solid line and is labelled "reference circle."

The original shape of the specimen is shown by the dotted line and the shape after buckling by the heavy solid line. The original shape was generated from the set of dial gage rig readings taken at the beginning of the test (prior to loading). The readings of the dial gages located nearest the level of buckling were used for this purpose. The dial gage rig readings could not be used to generate the shape after buckling because the magnitude of the buckling deformations generally made it impossible to use the rig. Consequently, the buckled shape was obtained from measurements of the distance between a vertical reference line and the deformed tube wall at points of peak inward and outward radial displacement around the circumference.

The buckled shapes for Specimens P5, P6, and P7 shown in Figs. 52 to 54b represent the patterns of lobular buckles immediately after initial buckling. However, for Specimens P1 to P4, the ring bulge buckles appeared first; therefore, the buckled shapes for these specimens, shown in Figs. 47 to 51, represent the patterns of lobular buckles at the conclusion of their tests.

No definite correlation between the original and buckled

shapes for any of the specimens can be observed except at the weld. The initial inward displacement that was consistently seen to exist at the weld corresponds to the inward lobe that developed there for all the specimens except P7. In the case of P7, the two levels of buckling straddled the weld so that no specific buckle can be associated with it. In Figures 47 to 54b, the dial gage rig readings show the initial inward displacement at the weld to be pronounced only in Specimens P4, P5, and P6.

Specimens P1 to P4 essentially achieved yield stress dispite the fact that the out-of-roundness of each of these specimens and the out-of-straightness of three of them exceeded the allowable values specified by API (see Article 3 and Ref. 2). In fact, the out-of-roundness and out-of-straightness of Specimen P4 were, respectively, 4 times and 1.5 times greater than the maximum allowable values. Still, P4 achieved a peak stress of 0.95 F_y. Thus, the initial imperfections did not have a detectable effect on the buckling stress of these specimens.

The apparent lack of correlation between the initial imperfections and the buckled shape (except possibly at the weld) must be viewed cautiously. Other researchers have conducted some tests where they were able to link initial imperfections with buckling (13). However, these experiments were performed on tubes with very large D/t ratios in comparison to the specimens described here.

Therefore, the buckling was elastic. In this study, the buckling was inelastic, and it may be that inelastic local buckling is relatively insensitive to initial imperfections in comparison to elastic buckling.

8.5 Effect of α

Parameter α and the buckling stress for the eight specimens are listed in Columns 8 and 9 of Table 1, and the buckling stress is plotted against α in Fig. 55. In the figure, the eight test points form a smooth curve, thereby indicating a consistent relationship between the buckling stress and α.

The local buckling strain depended on α; the larger α was, the greater the local buckling strain became. There appeared to be a value of α in the range, $6.4 < \alpha < 7.5$, above which the tube could strain significantly beyond the initial attainment of the yield stress before local buckling occurred.

The type of initial buckling depended on α. Ring bulge buckles formed initially in Specimens P1 to P4 ($\alpha > 3.6$), a combination of ring bulge and lobular buckles developed in Specimens P6 and P7 ($2.4 < \alpha < 3.6$), and lobular buckles alone formed in Specimen P5 ($\alpha < 2.4$).

The axial deformation between the initial buckling and load stabilization immediately after buckling was a function of α. It

appeared that for $\alpha < 4$, this deformation increased with decreasing α. For $\alpha > 4$, no definite trend could be observed except that the magnitudes of this deformation were smaller than for those specimens with $\alpha < 4$.

For equivalent end conditions, the post-buckling strength decreased with a decrease in α. For example, at a deformation of 18 mm (0.7 in.), Specimen P2 ($\alpha = 6.42$) sustained a stress of 0.47 F_y while P7 ($\alpha = 3.32$) supported a stress of only 0.29 F_y.

The peak stress achieved in the post-buckling range after the formation of additional sets of buckles was dependent on α. The larger α was, the greater this peak post-buckling stress became. For example, after the formation of a second set of lobular buckles, the peak stress was 0.34 F_y for Specimen P3A ($\alpha = 4.50$) but just 0.22 F_y for Specimen P5 ($\alpha = 2.17$).

9. SUMMARY AND CONCLUSIONS

Local buckling tests were conducted on eight tubular specimens. The specimens were fabricated from high-strength steel plate with F_y = 345 MPa (50 ksi) by cold-rolling and then welding along one longitudinal seam. The specimen diameters were 0.72 m (28 in.), 1.19 m (47 in.), 1.53 m (60 in.), and 1.79 m (70 in.), and the wall thicknesses ranged from 7.2 mm (0.28 in.) to 8.4 mm (0.33 in.). The D/t ratios correspondingly fell between 85 and 248. To preclude the effect of overall column buckling, the specimens were made short with a slenderness ratio less than 10.

The maximum stresses achieved in the tests were limited by local buckling. The buckling stress of each specimen was greater than its proportional limit, and thus the buckling was inelastic. The behavior of the specimens beyond initial buckling was also studied.

The following conclusions can be drawn from the results of these tests:

1) The design rules for local buckling currently recommended by AISI and API are adequately conservative for tubular members fabricated from 345 MPa (50 ksi) steel and falling within the range of parameters tested: $85 \leq D/t \leq 248$ and $2.17 \leq \alpha \leq 7.51$.

2) The type of initial local buckling is a function of α. Approximate guidelines are: ring bulge for $\alpha \geq 3.6$, transition

between ring bulge and lobular for $2.4 \leq \alpha \leq 3.6$, and lobular for $\alpha \leq 2.4$.

3) The strain at which local buckling occurs is a function of α. The larger α is, the greater the local buckling strain becomes. There is a value of α in the range, $6.4 \leq \alpha < 7.5$, above which the tube can strain significantly beyond the initial attainment of the yield stress before local buckling occurs.

4) The post-buckling strength is a function of α. In general, for equivalent end conditions, the post-buckling strength decreases with a decrease in α.

5) By forming successive sets of lobular buckles, tubular columns can dissipate large amounts of energy at approximately 15-25% of the buckling stress. The peak stress achieved in the post-buckling range is a function of α. The larger α is, the greater this peak post-buckling stress becomes.

6) There is no apparent correlation between the pattern of longitudinal residual stresses due to welding and the pattern of local buckling. Thus, these residual stresses do not appear to be significant in influencing the location of the buckles for the range of parameters tested (D/t, F_y, etc.).

7) The initial geometric imperfections had little effect on the local buckling stress of the specimens tested. The reason for this may be that inelastic local buckling is relatively insensitive to initial imperfections in comparison to elastic buckling.

Before the results of these tests can be translated into sound design recommendations, it is necessary that more experimental and theoretical work be conducted. Specifically, the following items must be investigated:

1) Yield stresses different from the value of 345 MPa tested here.

2) The interaction between local and overall column buckling.

3) The effect of circumferential weld seams.

4) Larger D/t in order to extend the results of this study to smaller values of α.

5) The effect of initial imperfections for larger D/t where there is a transition from inelastic to elastic buckling.

10. TABLES

TABLE 1: ACTUAL SPECIMEN DATA

No.	Steel	Coupon Static F_y (MPa)	Measured			D/t	α	F_c/F_y
			OD (m)	t (mm)	L (m)			
1	2	3	4	5	6	7	8	9
P1	A572 Gr50	319.17	0.717	8.349	2.05	84.85	7.51	0.998
P2	A633 GrD	346.68	0.741	8.037	2.05	92.26	6.42	1.008
P3	A572 Gr50	319.17	1.190	8.349	3.05	141.53	4.50	0.989
P3A	A572 Gr50	319.17	1.190	8.349	2.03	141.53	4.50	1.009
P4	A633 GrD	346.68	1.217	8.037	3.05	151.39	3.88	0.951
P5	A572 Gr50	377.16	1.787	7.165	3.03	248.38	2.17	0.814
P6	A572 Gr50	372.05	1.533	7.262	3.03	210.05	2.60	0.889
P7	A572 Gr50	372.05	1.203	7.262	3.03	164.62	3.32	0.941

Notes: 0.0254 m = 25.4 mm = 1 in.

6.895 MPa = 1 ksi

OD = Outside Diameter, t = Thickness, D = OD - t

L = Length, $\alpha = Et/F_yD$

E = 203.403×10^3 MPa = 29.5×10^3 ksi

F_c = Critical Local Buckling Stress

TABLE 2: SPECIMEN IMPERFECTIONS AND BUCKLING DETAILS

Spec. No.	α	Maximum Imperfections			Type and Location of Initial Buckles	No. of Lobes Around Circumf.
		Out-of-Roundness		Out-of-Straightness (mm in 1.52 m)		
		Value	Locn.			
1	2	3	4	5	6	7
P1	7.51	0.02757	Top	2.03	Ring Bulge At Top	3
P2	6.42	0.01647	Top	2.54	Ring Bulge At Bottom	3
P3	4.50	0.03618	1.02 m from Bottom	0.51	Ring Bulge At Bottom	4
P3A	4.50	Not Measured		Not Measured	Ring Bulges At Top and Bottom	5
P4	3.88	0.03799	Bottom	2.54	Ring Bulge At Bottom	5
P5	2.17	0.00569	Top	0.89	Lobular At Bottom	8
P6	2.60	0.00530	Top	0.99	Ring Bulge and Lobular At Top	6
P7	3.32	0.03136	Bottom	1.50	Ring Bulge and Lobular At 0.58 m and 1.17 m from Top	5 or 7

NOTE: 0.0254 m = 25.4 mm = 1 in.

11. FIGURES

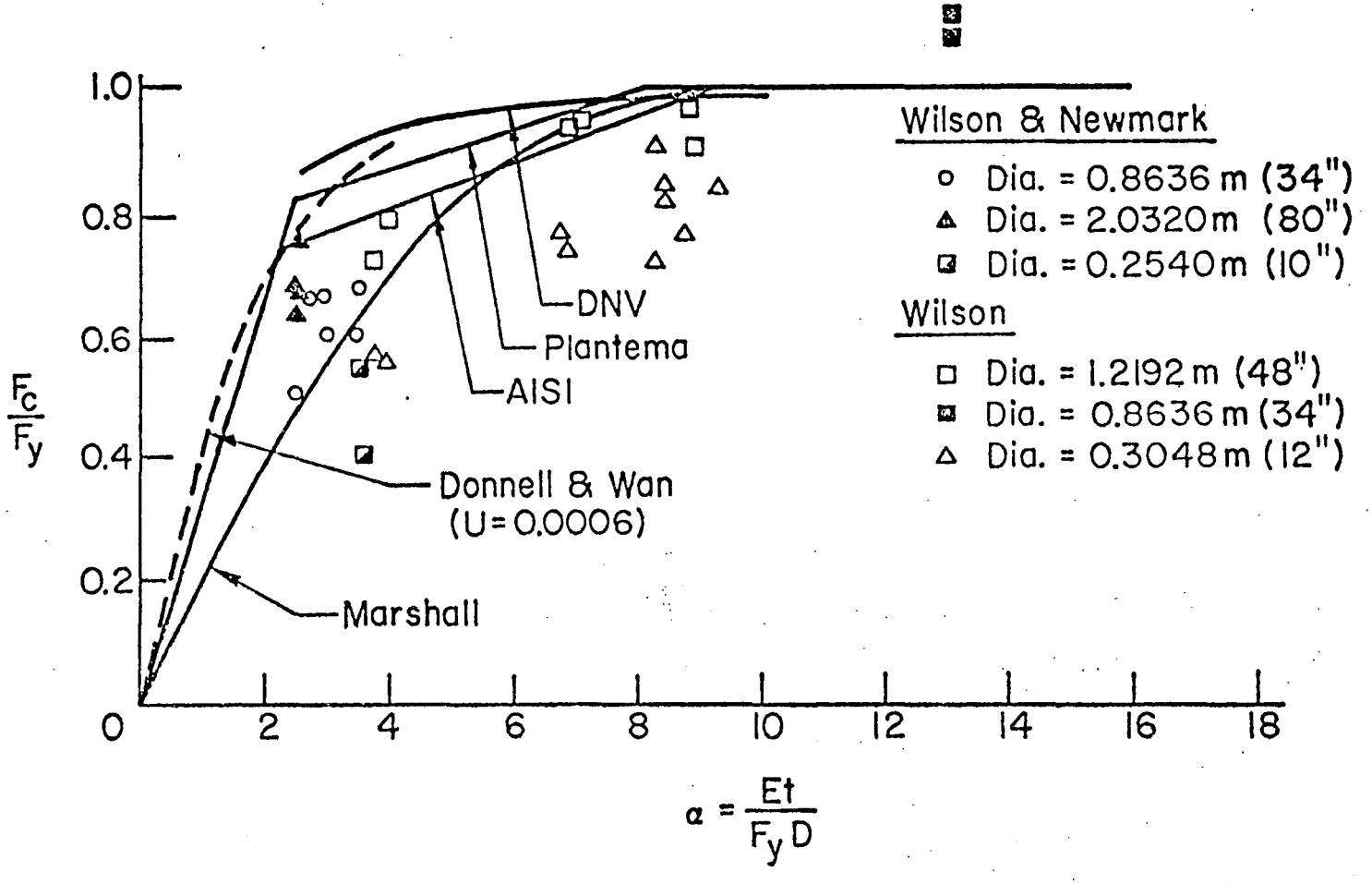

Fig. 1 Design Curves and Previous Test Results for Local Buckling of Tubular Columns

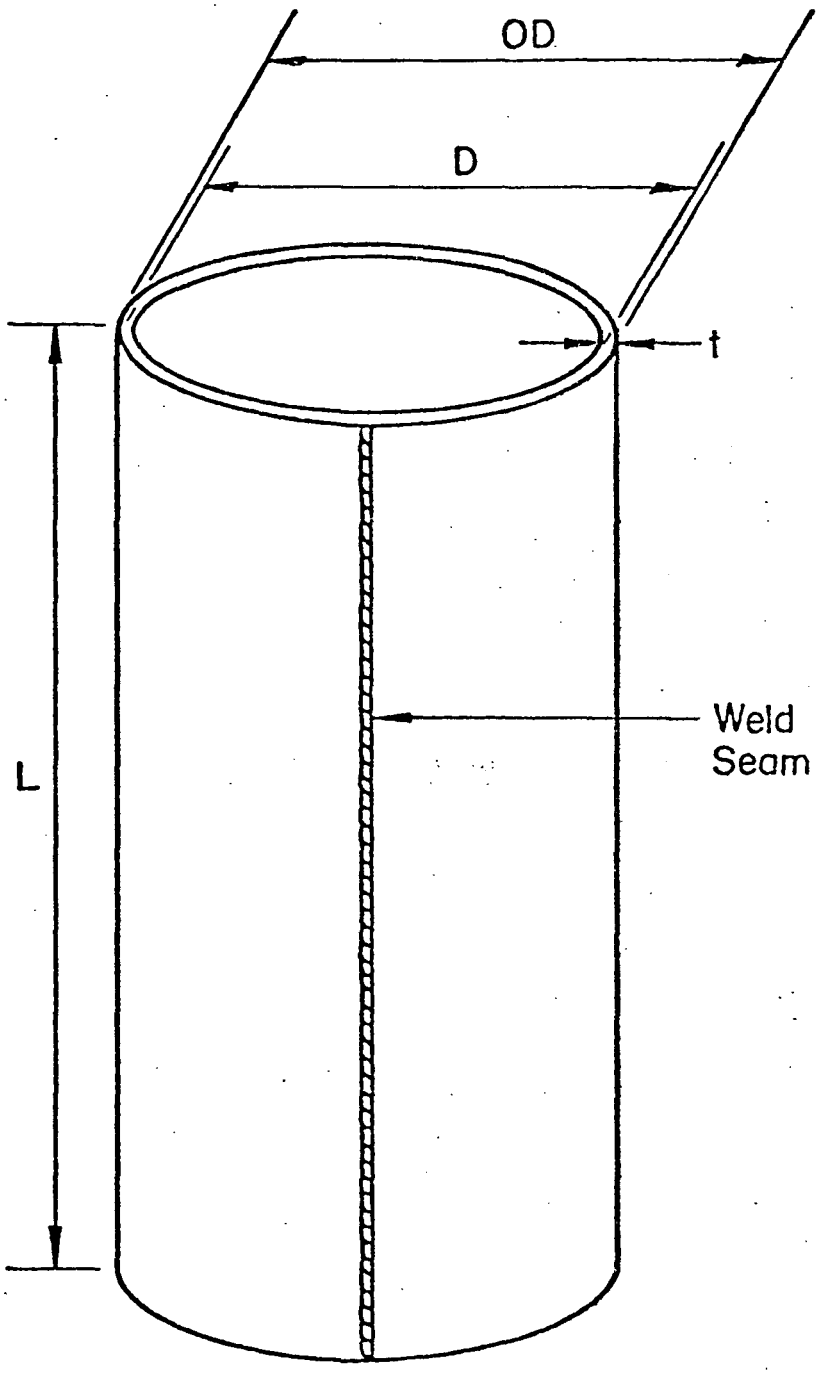

Fig. 2 Typical Test Specimen and Pertinent Notation

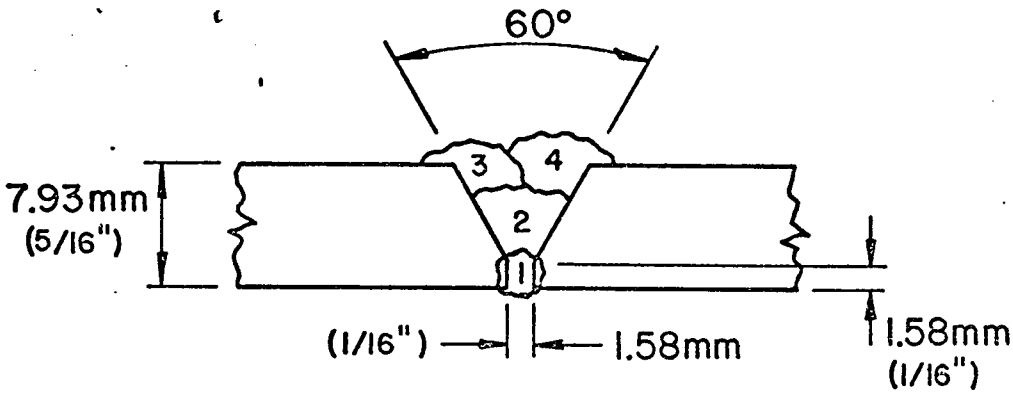

Multi-Pass, Single-Vee, Submerged Arc Weld
(Except First Pass Is Gas Metal Arc)

PASS	ELECTRODE		AMPS	VOLTS	TRAVEL SPEED
	TYPE	DIA.			
1	Linde 65	0.89 mm (.035")	150±	22±	229 $\frac{mm}{min}$ (9 $\frac{in.}{min}$)
2, 3, 4	EM12K	3.18 mm (1/8")	300 ±	23±	432/483 $\frac{mm}{min}$ (17/19 $\frac{in.}{min}$)

Fig. 3a Welding Details for Specimens P1 and P3

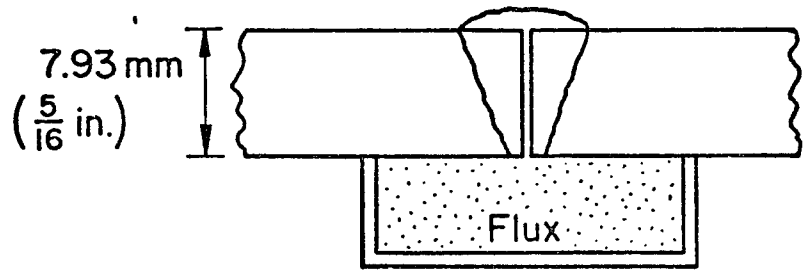

Single Pass, Square Butt, Submerged Arc Weld

PASS	ELECTRODE		AMPS	VOLTS	TRAVEL SPEED
	TYPE	DIA.			
1	EM12K	3.18 mm (1/8")	400±	30±	406/450 mm/min (16/18 in./min)

Fig. 3b Welding Details for Specimens P2 and P4

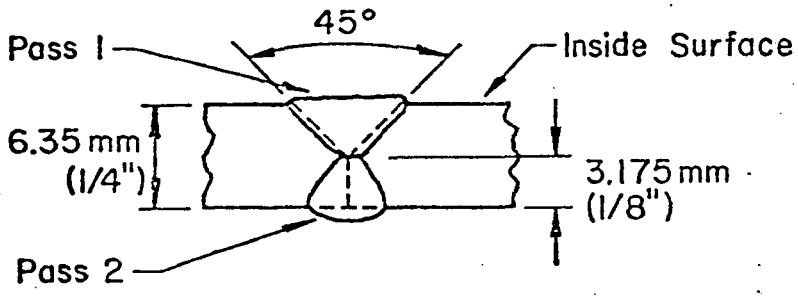

Single-Vee Groove, Submerged Arc Weld

PASS	ELECTRODE		AMPS	VOLTS	TRAVEL SPEED
	TYPE	DIA.			
1	EM12K	2.38 mm (3/32")	460/500	26/30	305/406 $\frac{mm}{min}$ (12/16 $\frac{in.}{min}$)
2	EM12K	2.38 mm (3/32")	460/500	26/30	305/406 $\frac{mm}{min}$ (12/16 $\frac{in.}{min}$)

Fig. 3c Welding Details for Specimens P5, P6, and P7

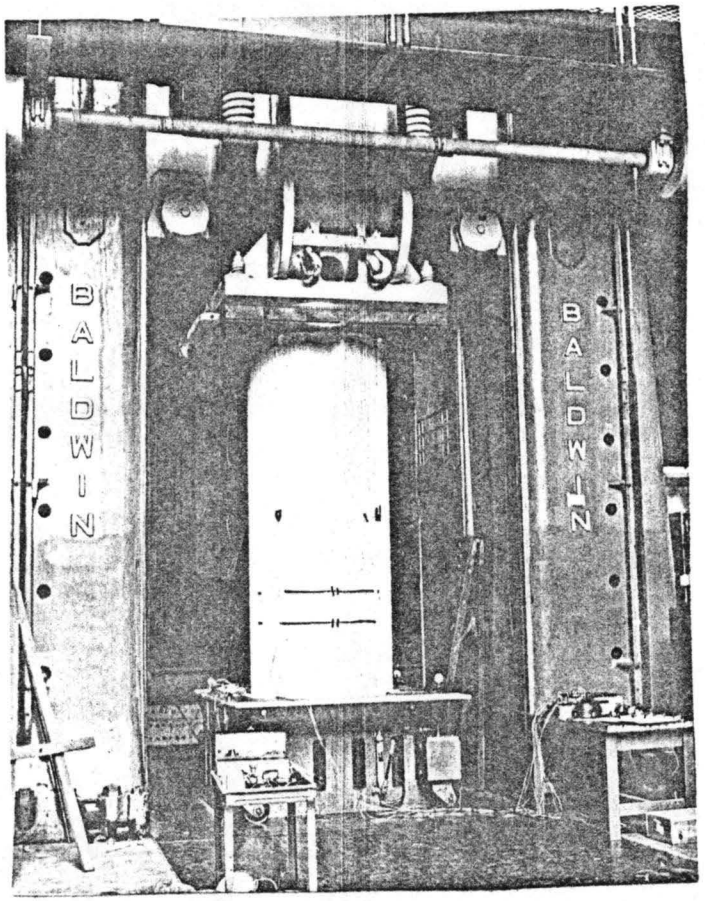

Fig. 4a Specimen P3 Prior To Testing

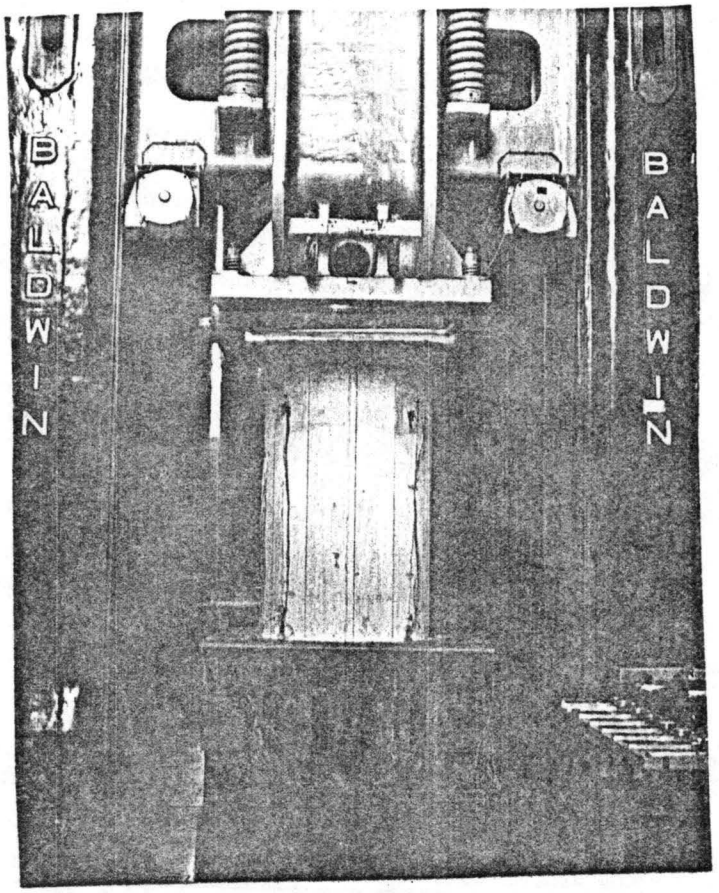

Fig. 4b Specimen P3A Prior To Testing

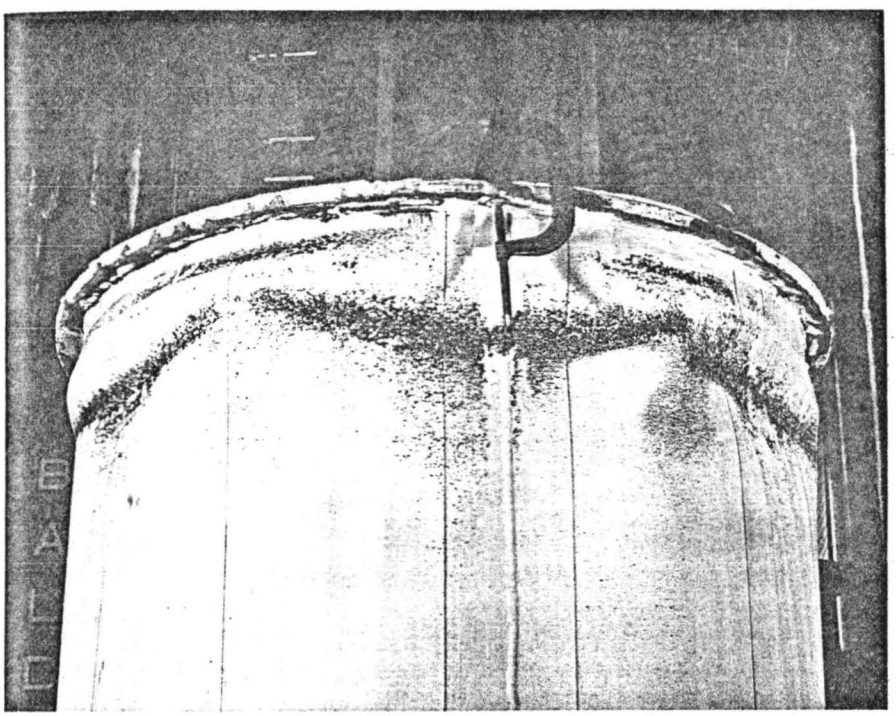

Fig. 5 Steel Ring welded to the top end of Specimen P6

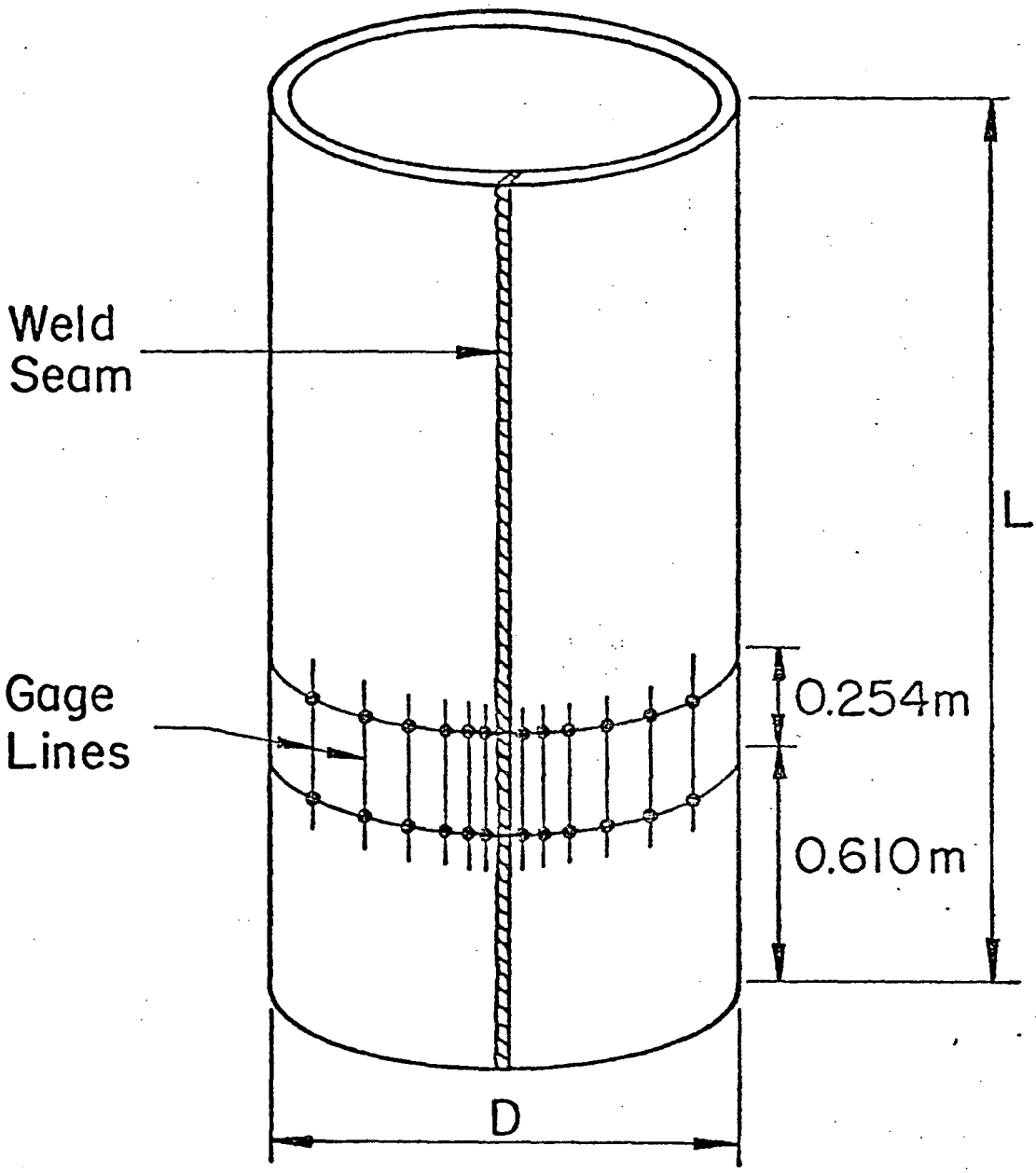

Fig. 6 Target Holes on Test Specimen for Measuring Residual Stresses

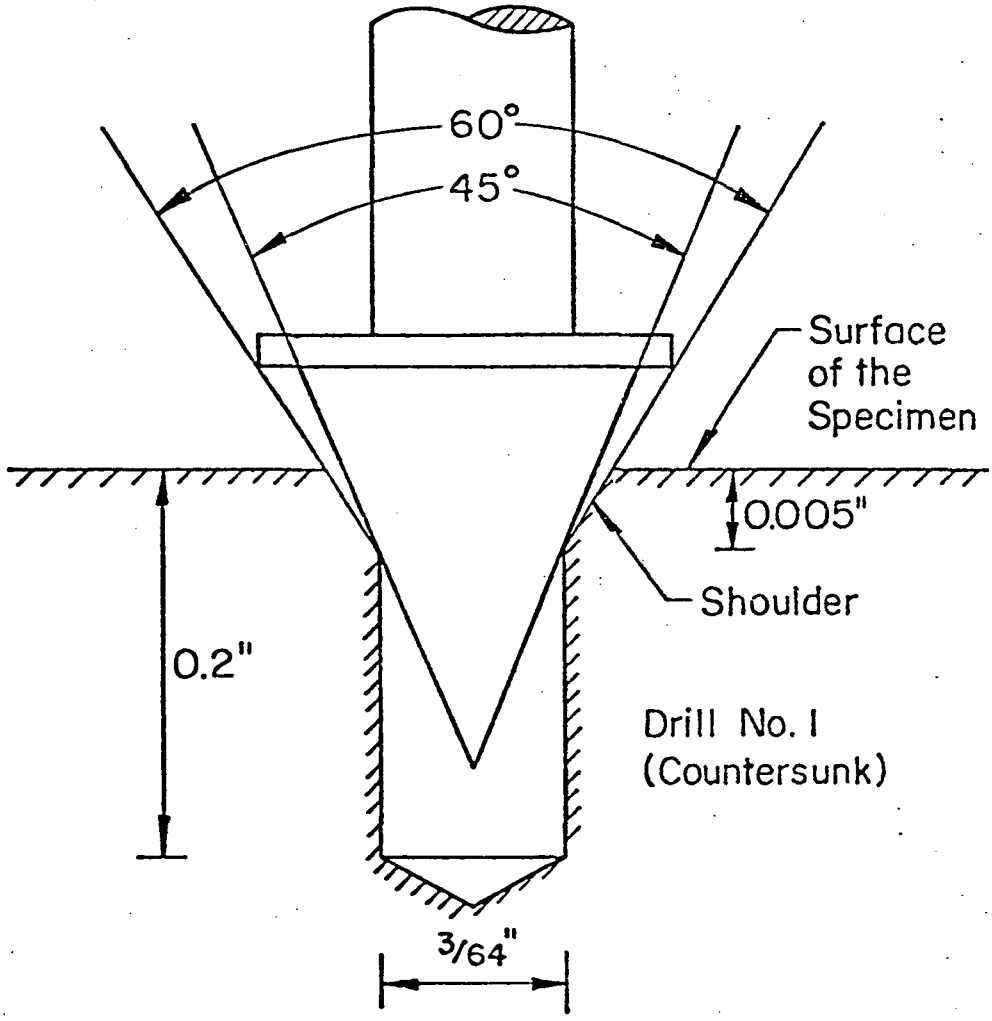

Fig. 7 Typical Target Hole Used in Residual Stress Measurements

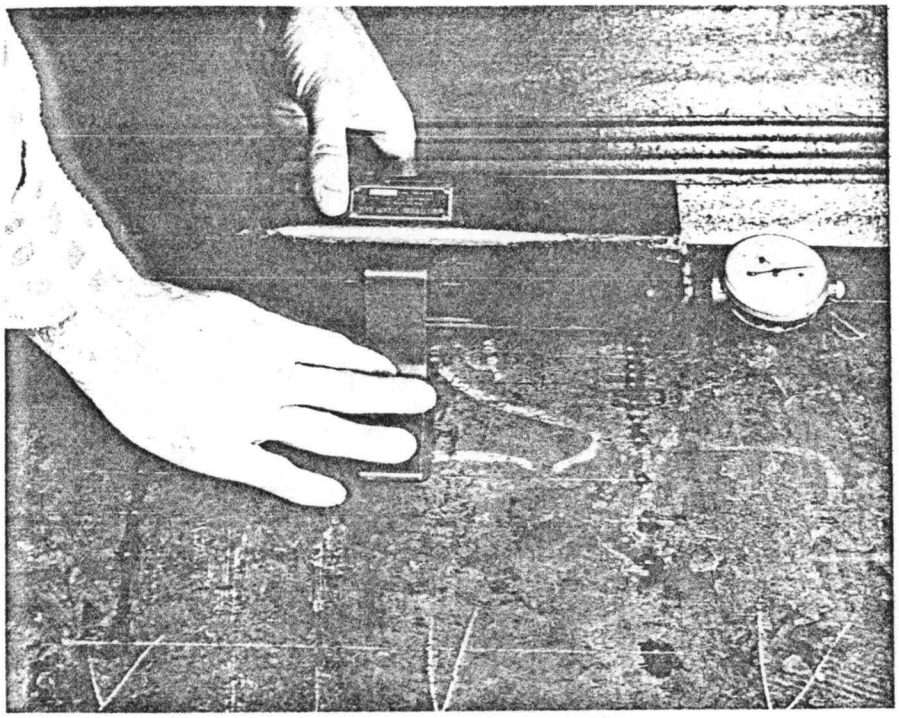

Fig. 8 Whittemore Strain Gage Used in Residual Stress Measurements

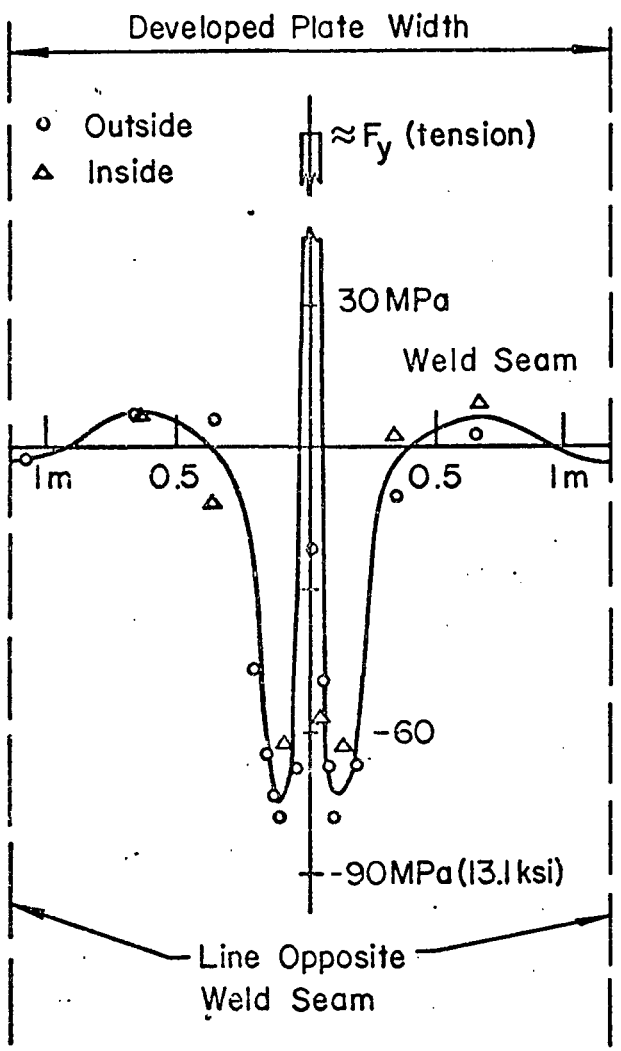

FIG. 9 WELDING RESIDUAL STRESSES IN SPECIMEN P1

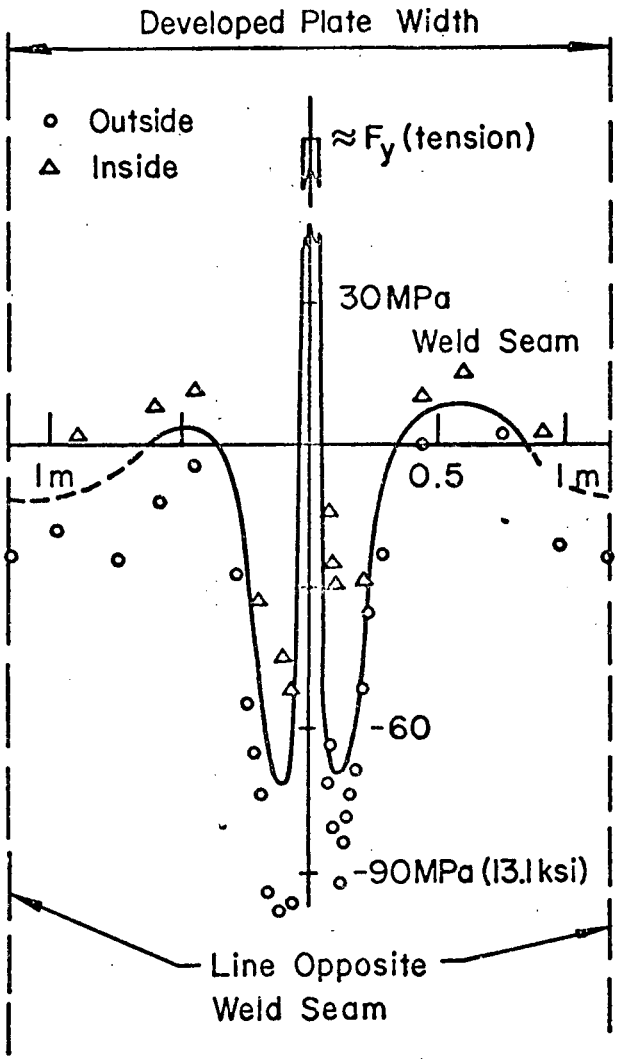

FIG. 10 WELDING RESIDUAL STRESSES IN SPECIMEN P2

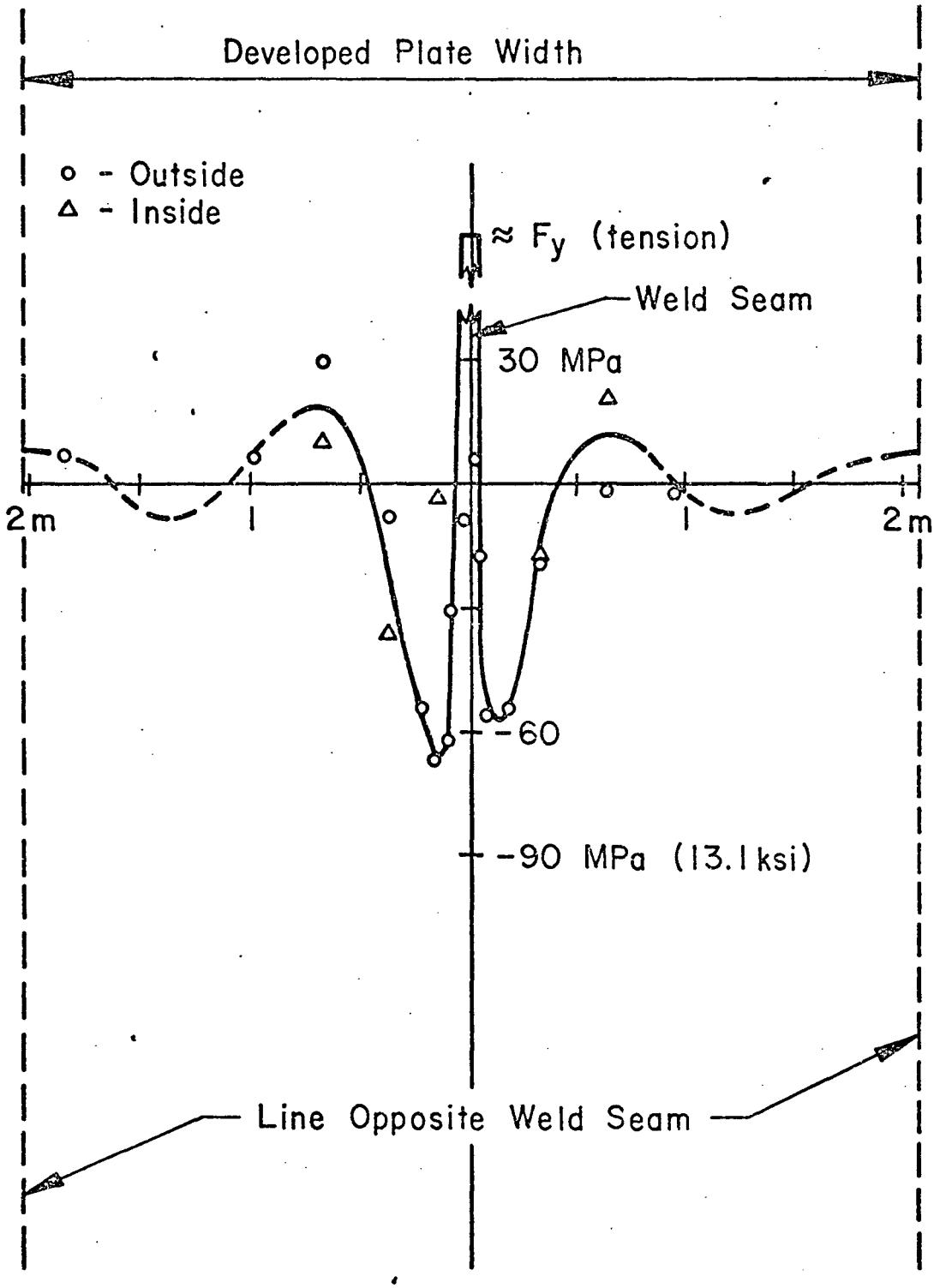

FIG. 11 WELDING RESIDUAL STRESSES IN SPECIMEN P3

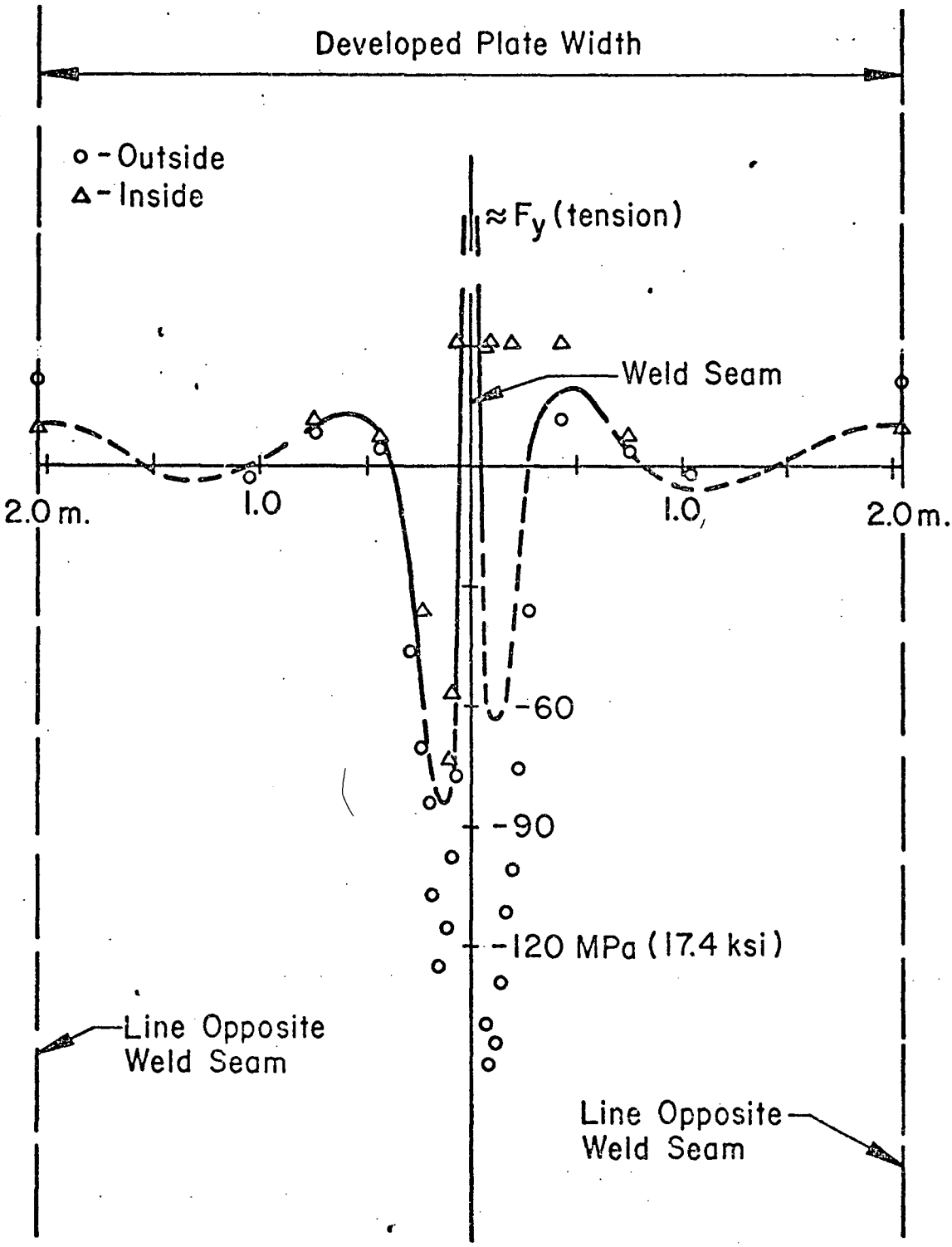

FIG. 12 WELDING RESIDUAL STRESSES IN SPECIMEN P4

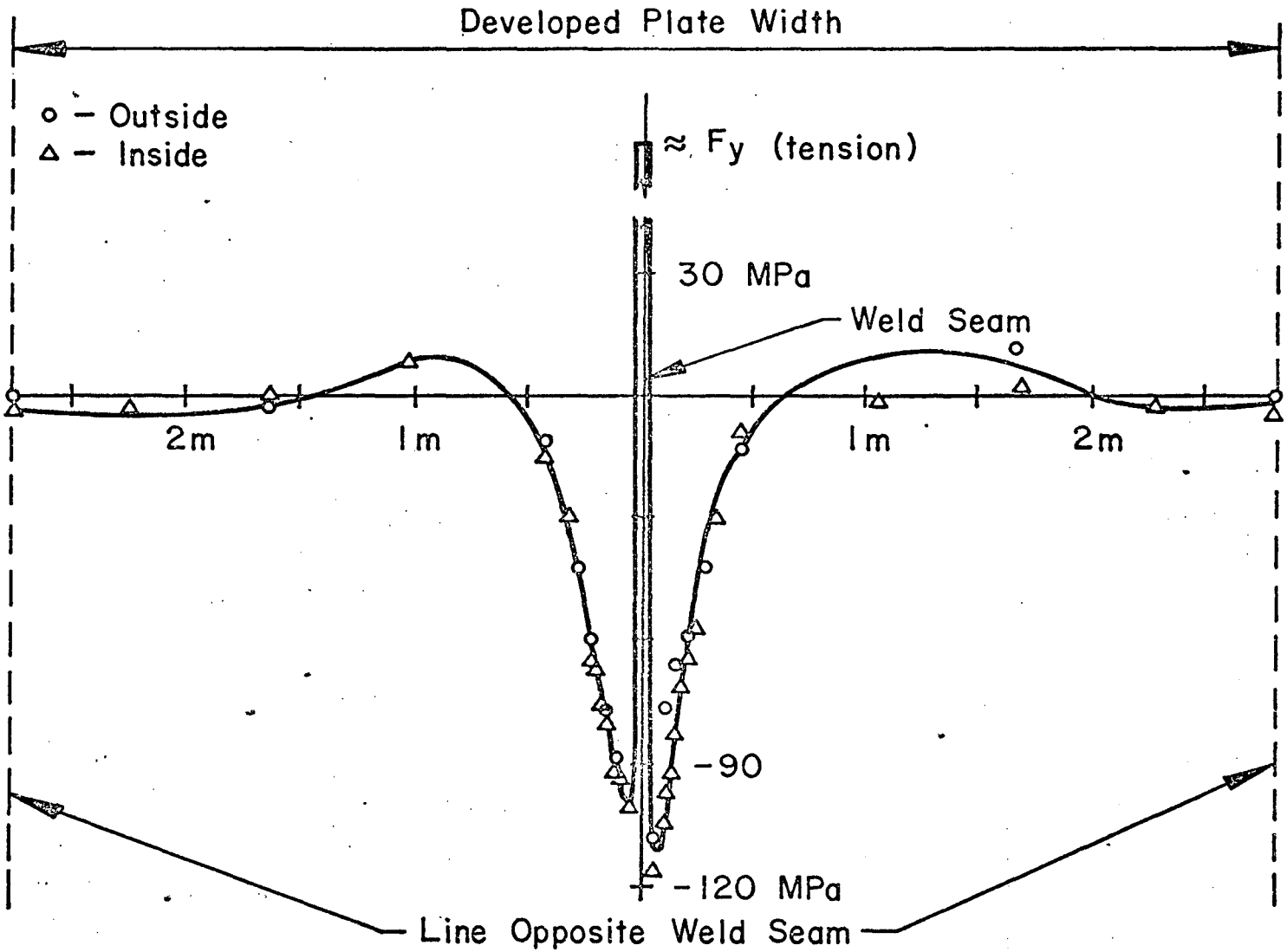

FIG. 13 WELDING RESIDUAL STRESSES IN SPECIMEN P5

Fig. 14 Specimen P1 with the Dial Gage Rig Prior to Testing

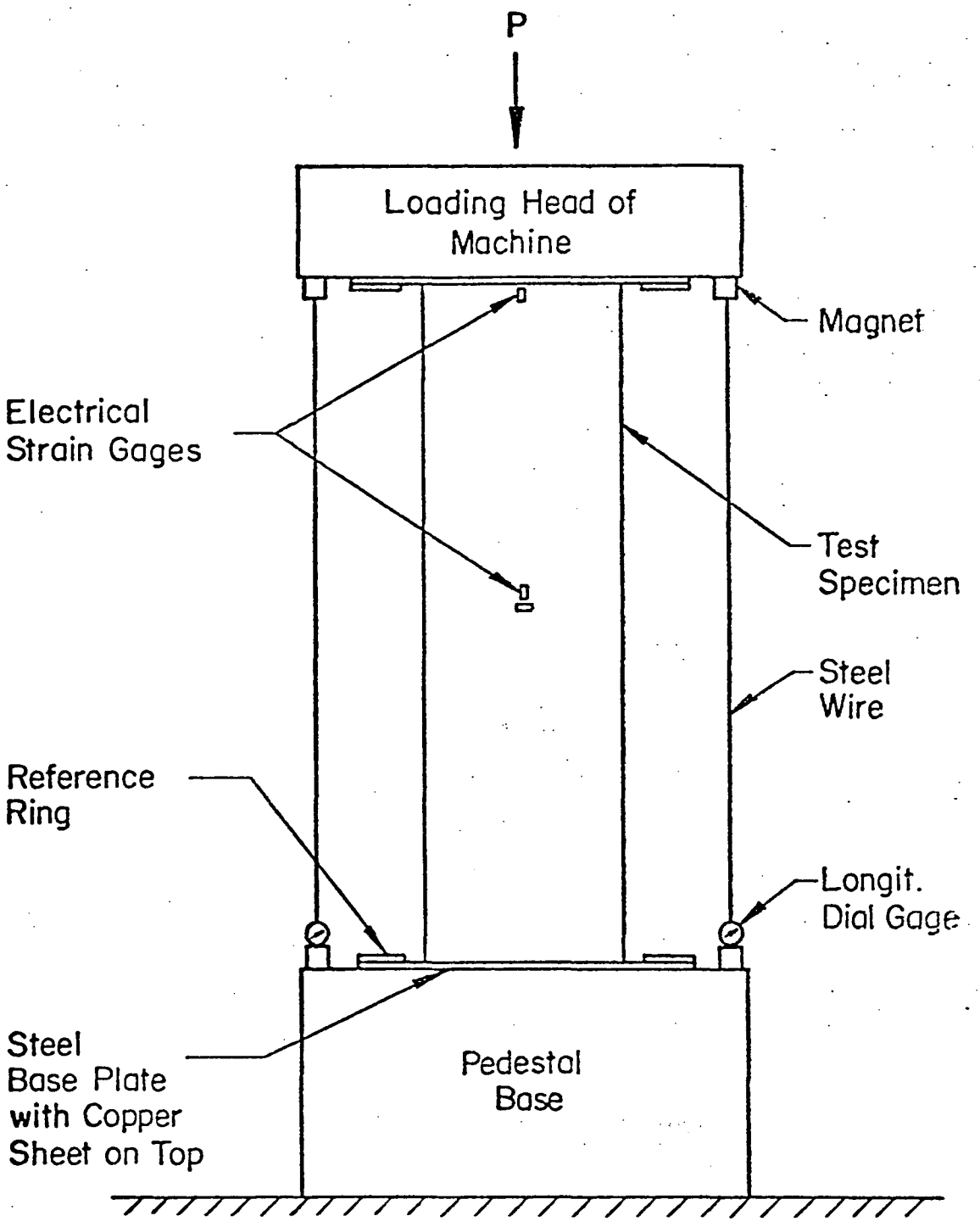

Fig. 15 Test Setup and Instrumentation for Specimens P1, P2, P3, and P4

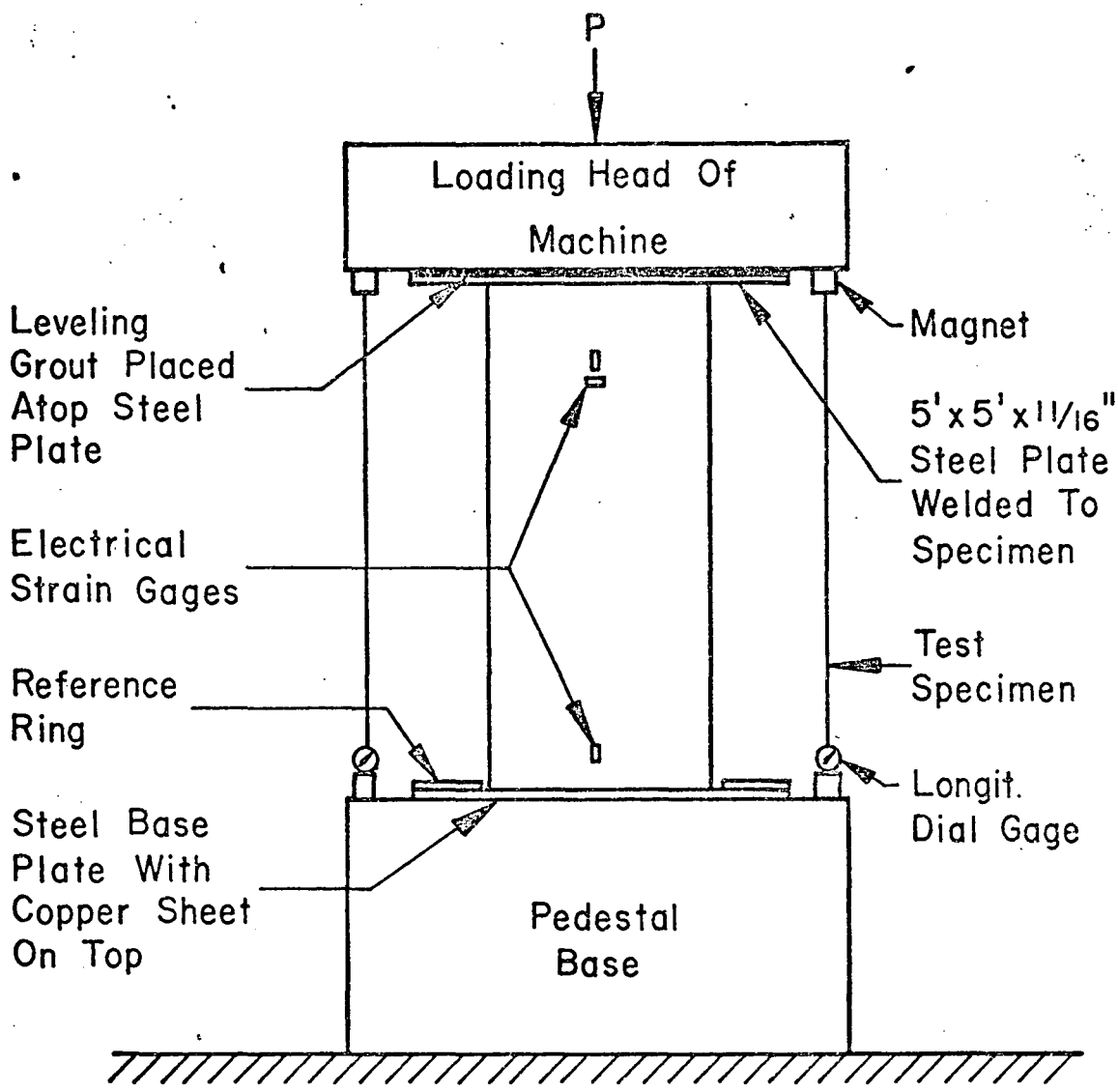

FIG. 16 TEST SETUP AND INSTRUMENTATION FOR SPECIMEN P3A

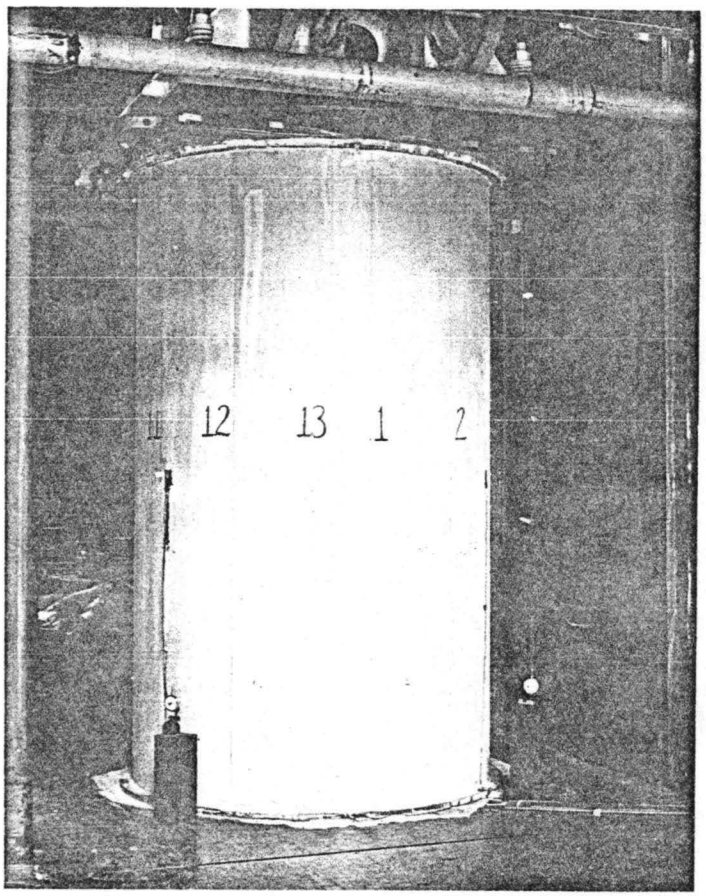

Fig. 17 Specimen P5 Prior to Testing

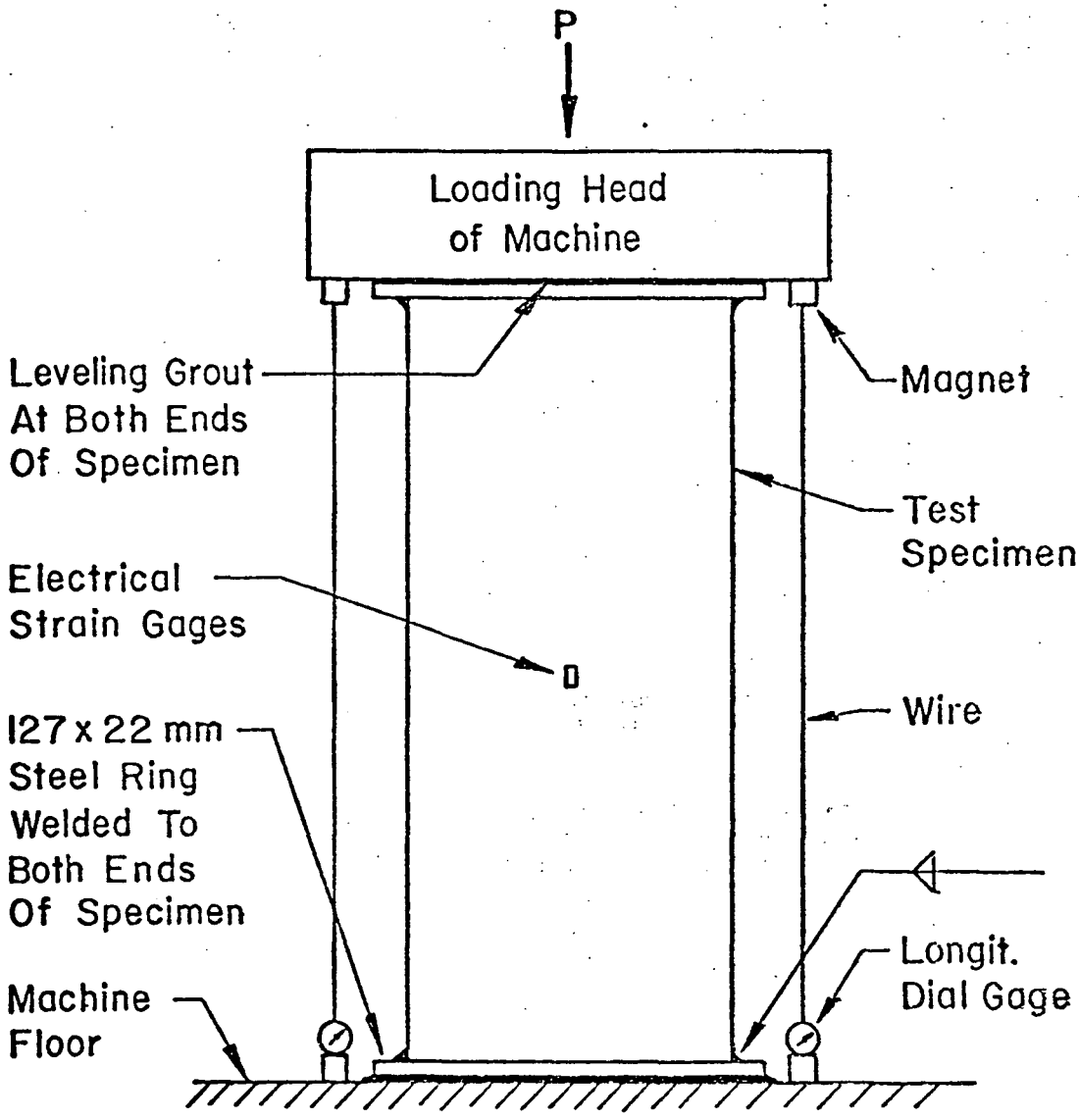

Fig. 18 Test Setup and Instrumentation for Specimens P5 and P6

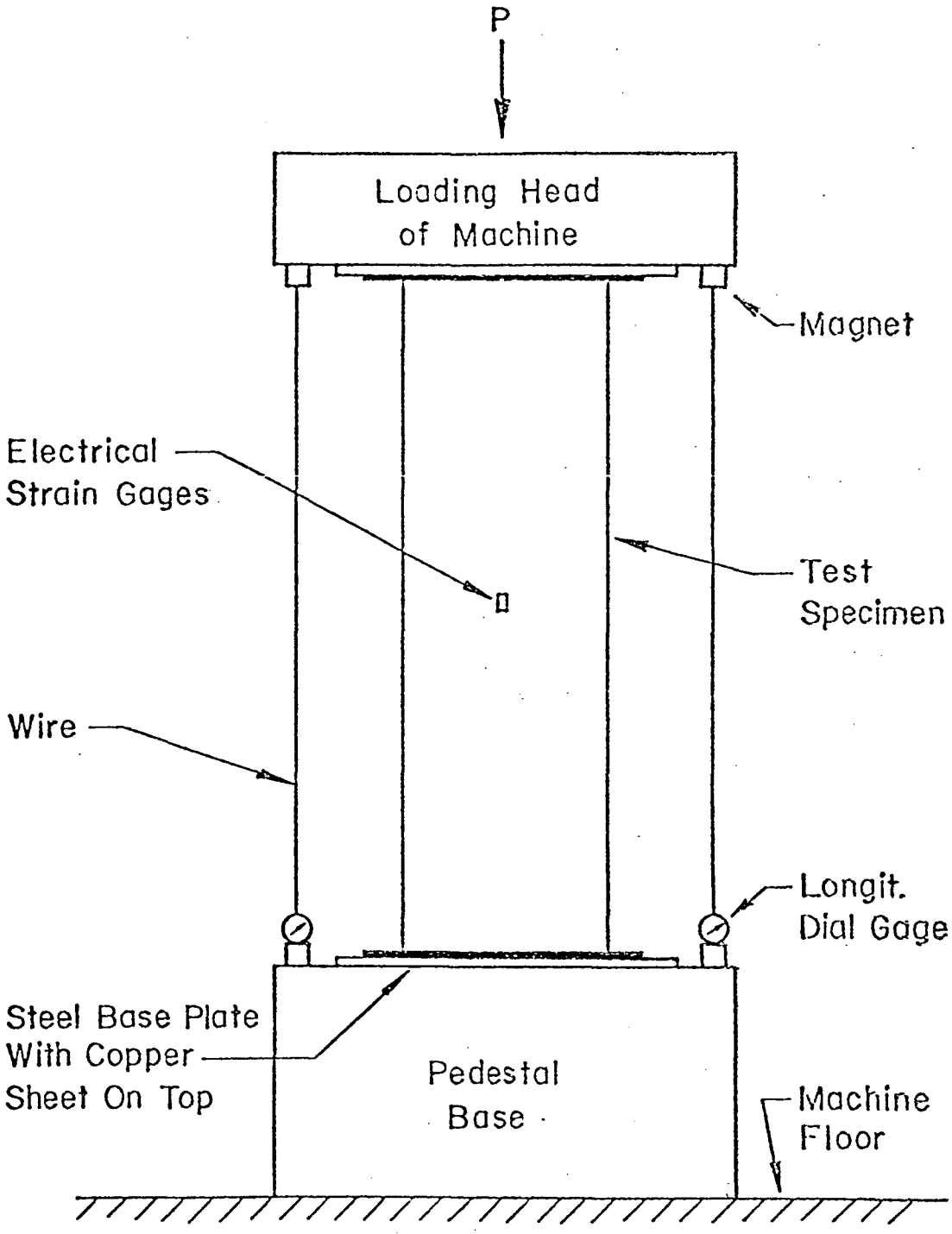

Fig. 19 Test Setup and Instrumentation for Specimen P7

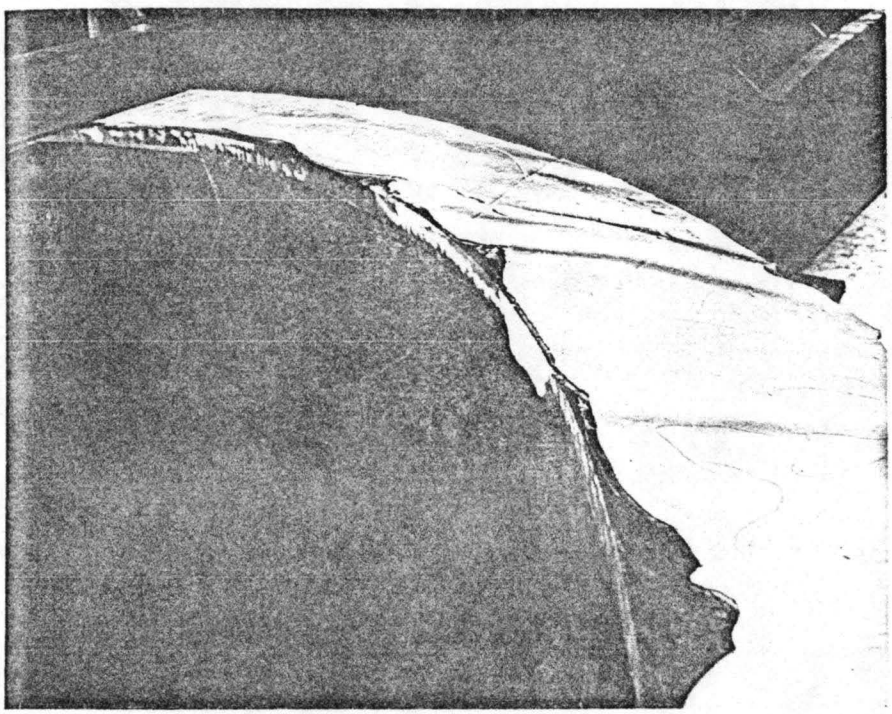

Fig. 20 Leveling Grout on Steel Ring at Top of Specimen P6

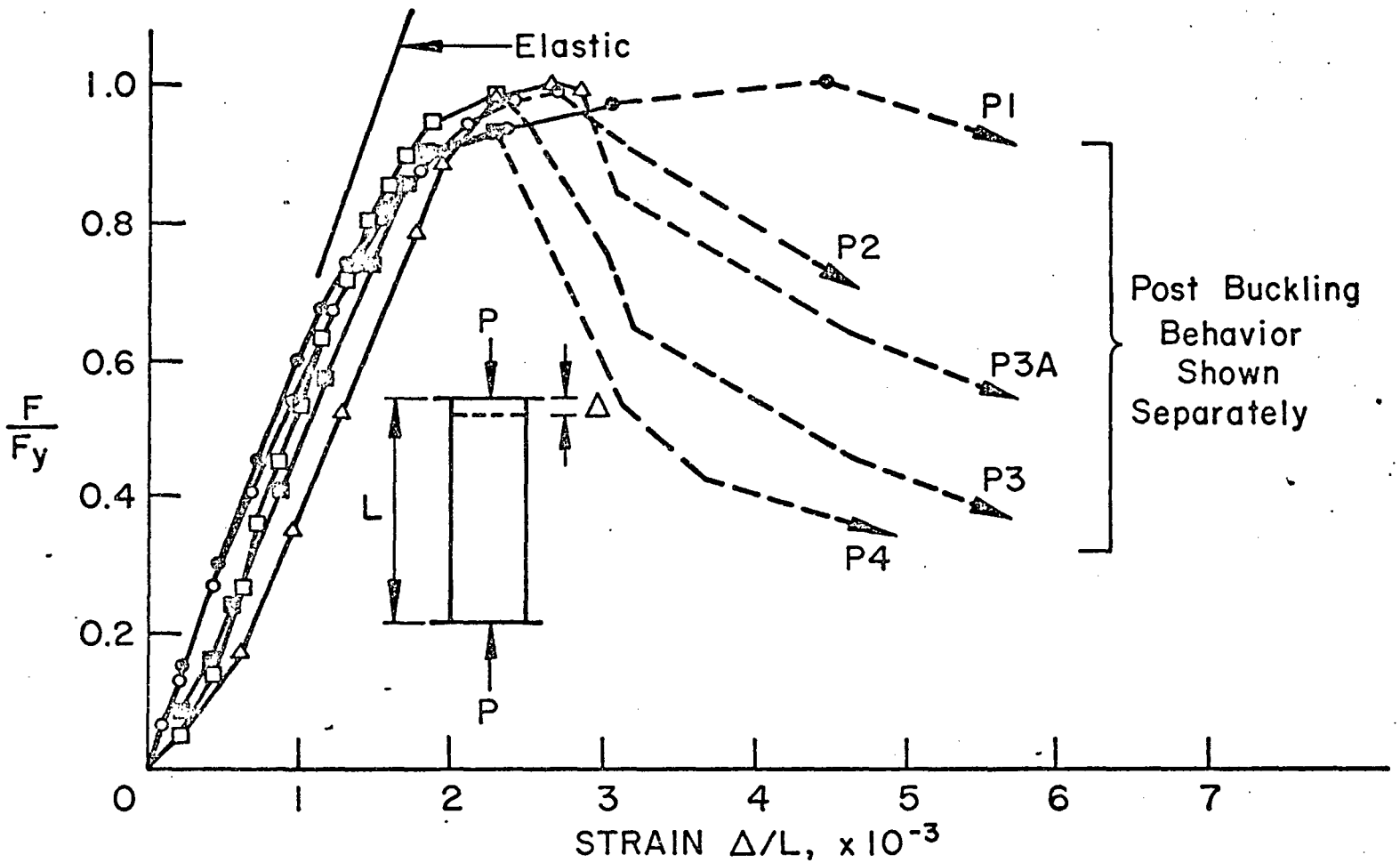

FIG 21• AVERAGE STRESS-STRAIN BEHAVIOR OF SPECIMENS P1, P2, P3, P3A, AND P4

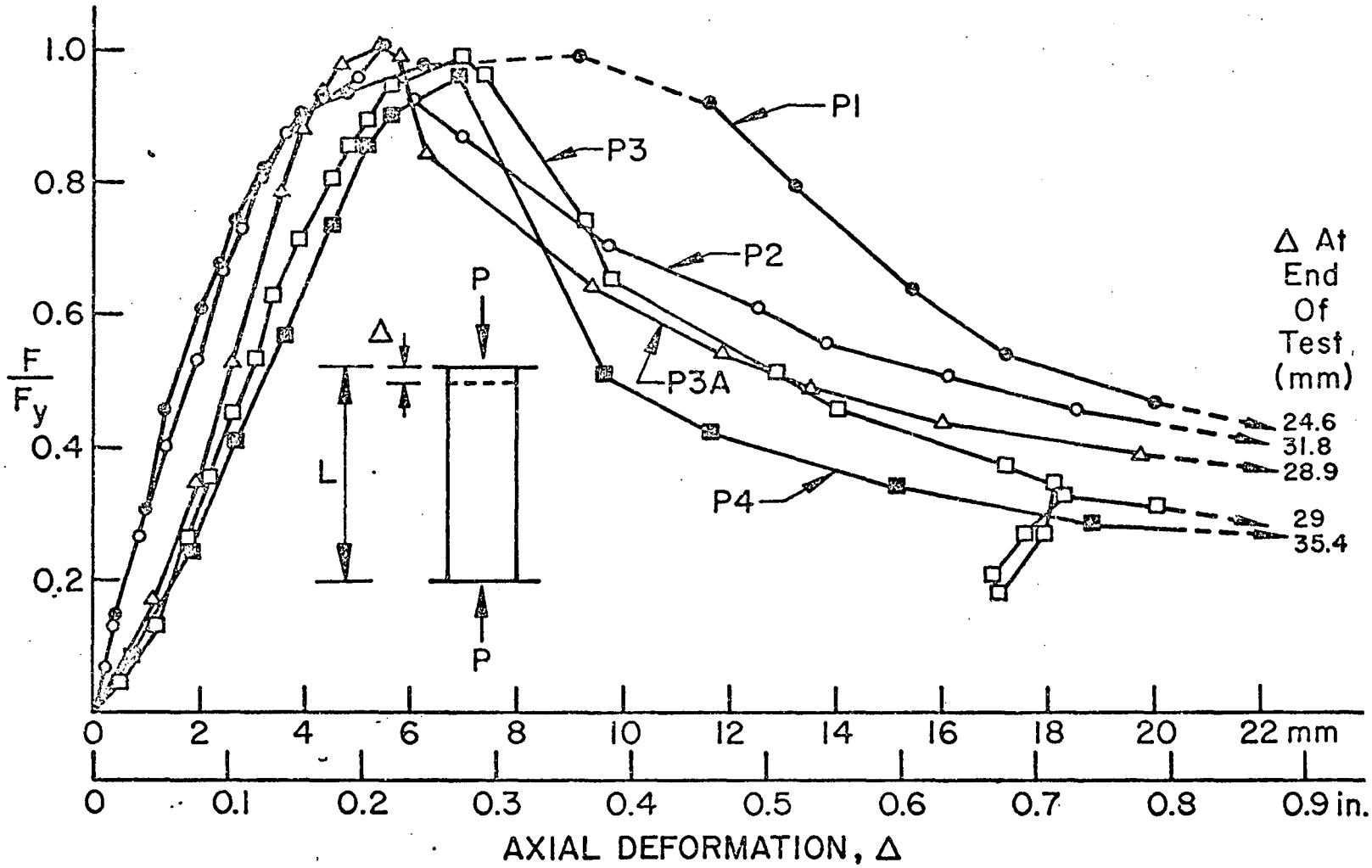

FIG. 22 AVERAGE STRESS-DEFORMATION BEHAVIOR OF SPECIMENS P1, P2, P3, P3A, AND P4

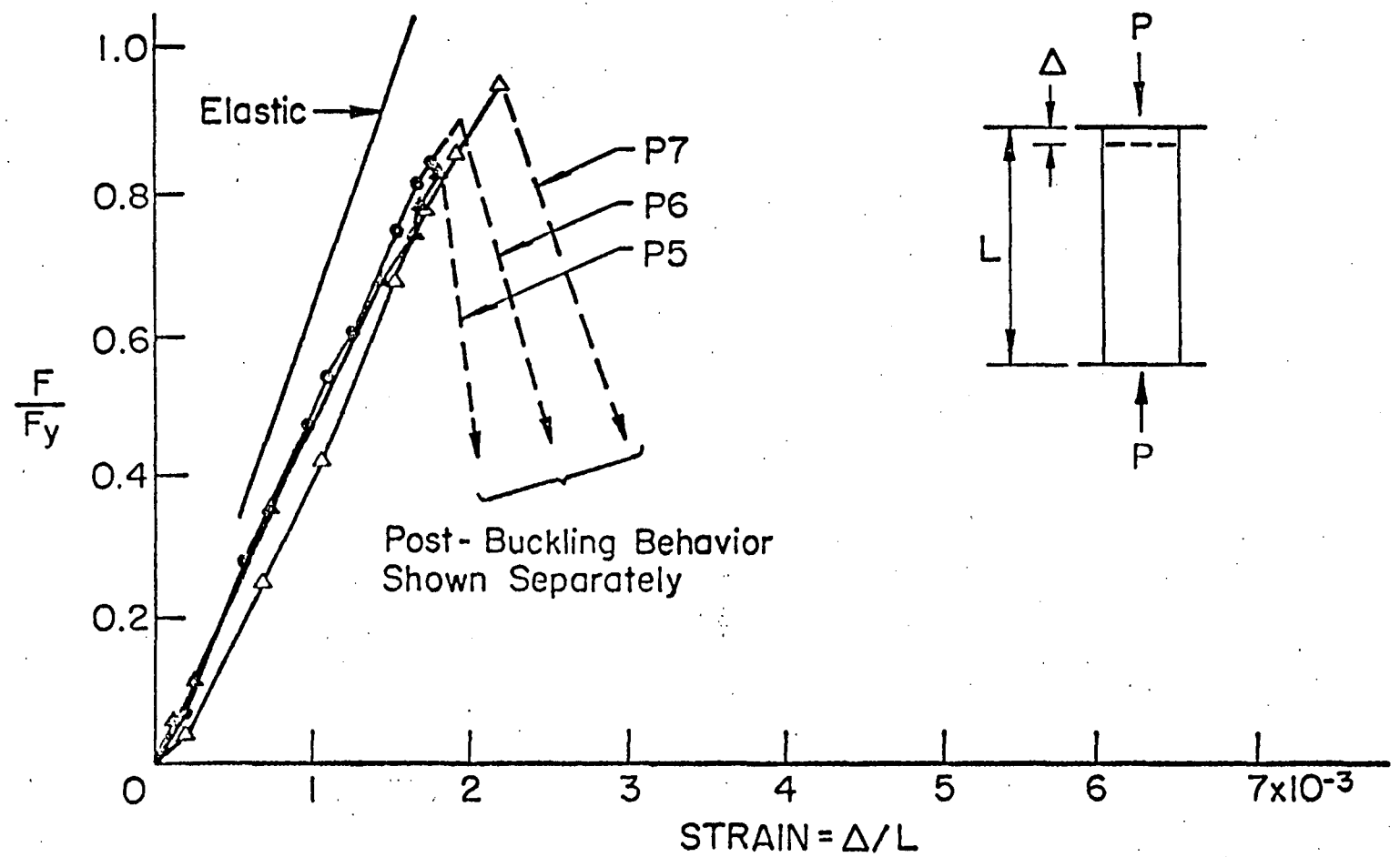

Fig. 23 Average Stress-Strain Behavior of Specimens P5, P6, and P7

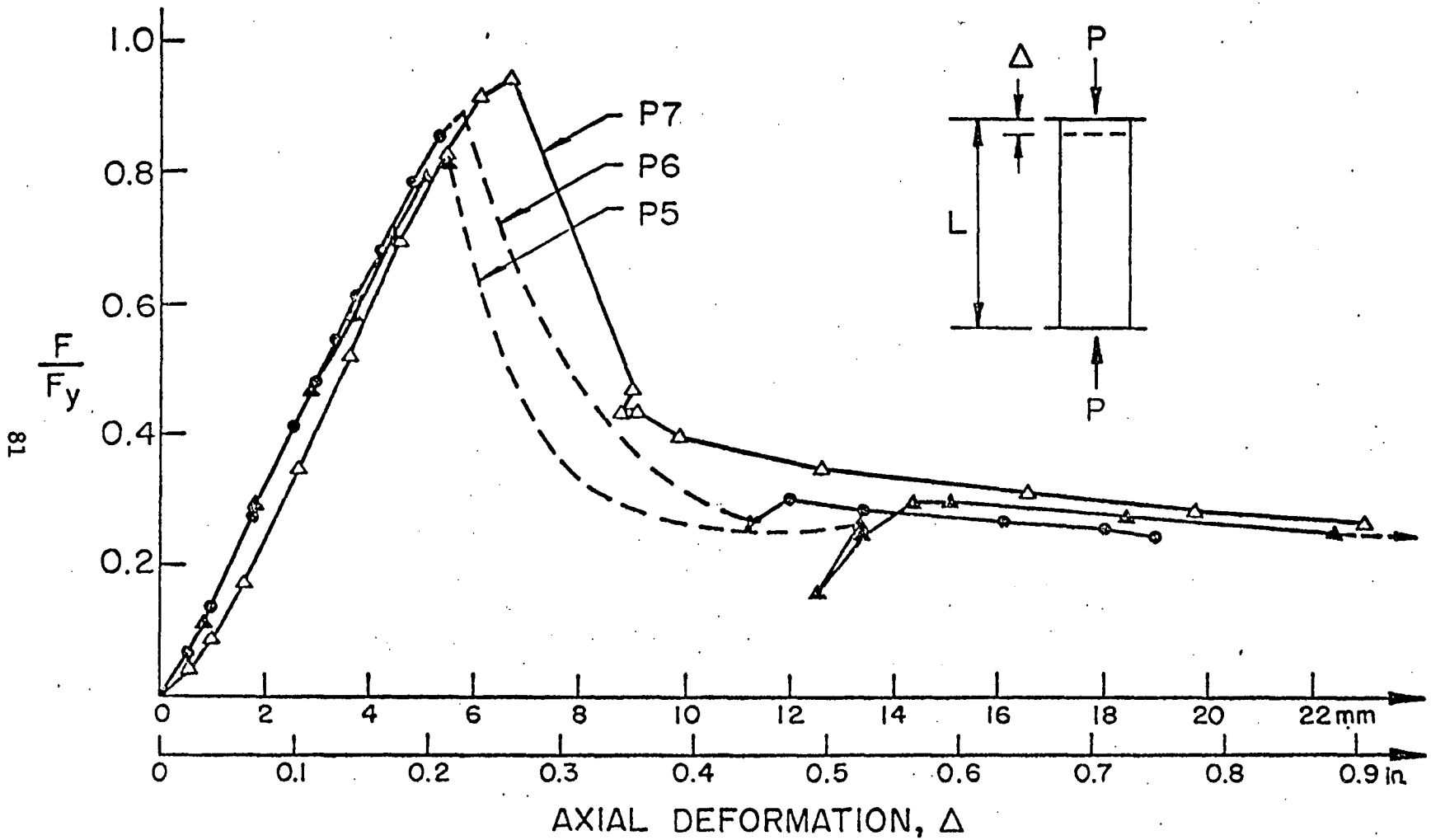

Fig. 24 Average Stress-Deformation Behavior of Specimens P5, P6, and P7

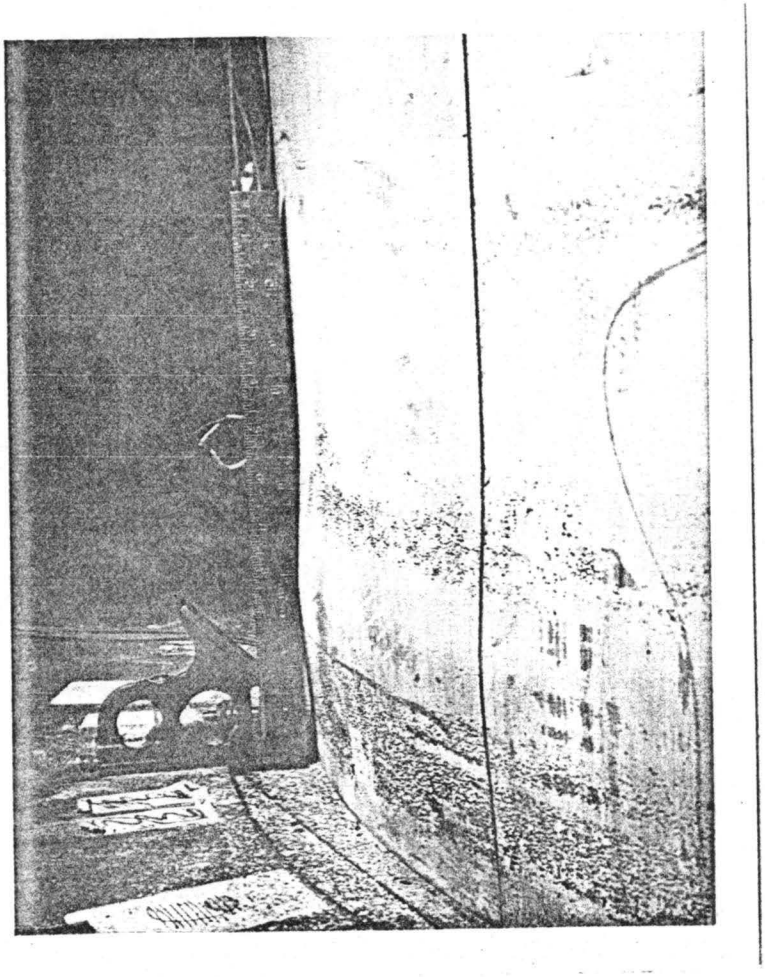

Fig. 25 Typical Ring Bulge After Initial Buckling.
Bottom End of Specimen P3A Is Shown

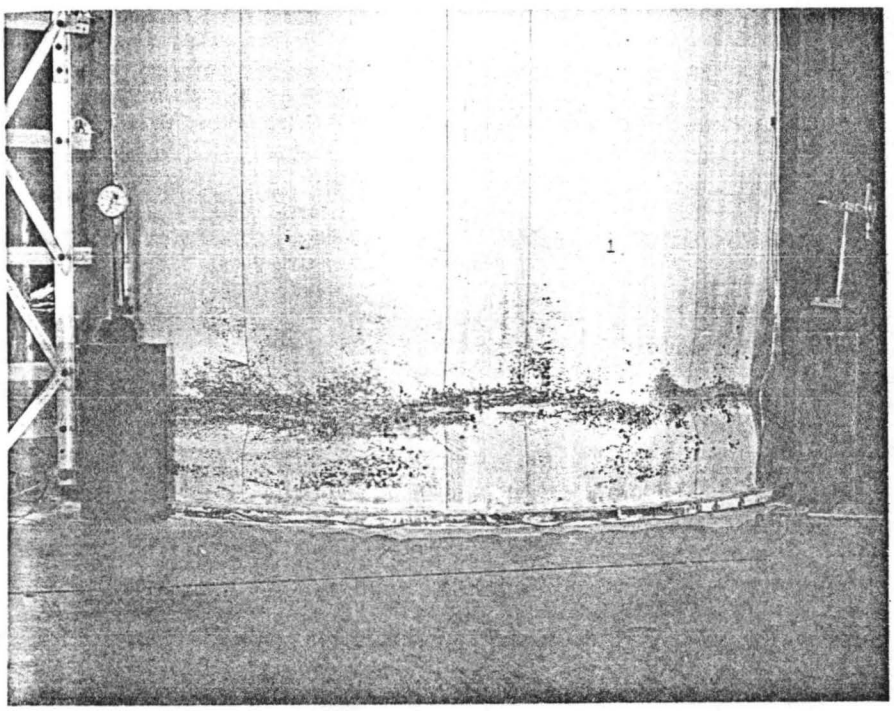

Fig. 26 Specimen P5 After Initial Buckling

Fig. 27 Side View of an Inward Lobe in Specimen P5

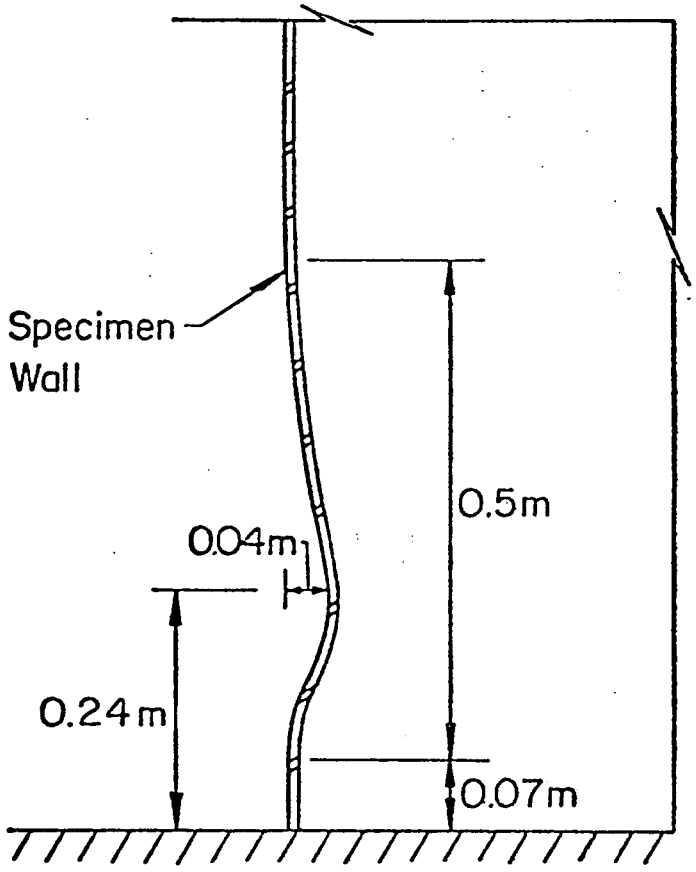

Fig. 28 Typical Geometry of an Inward Lobe in Specimen P5

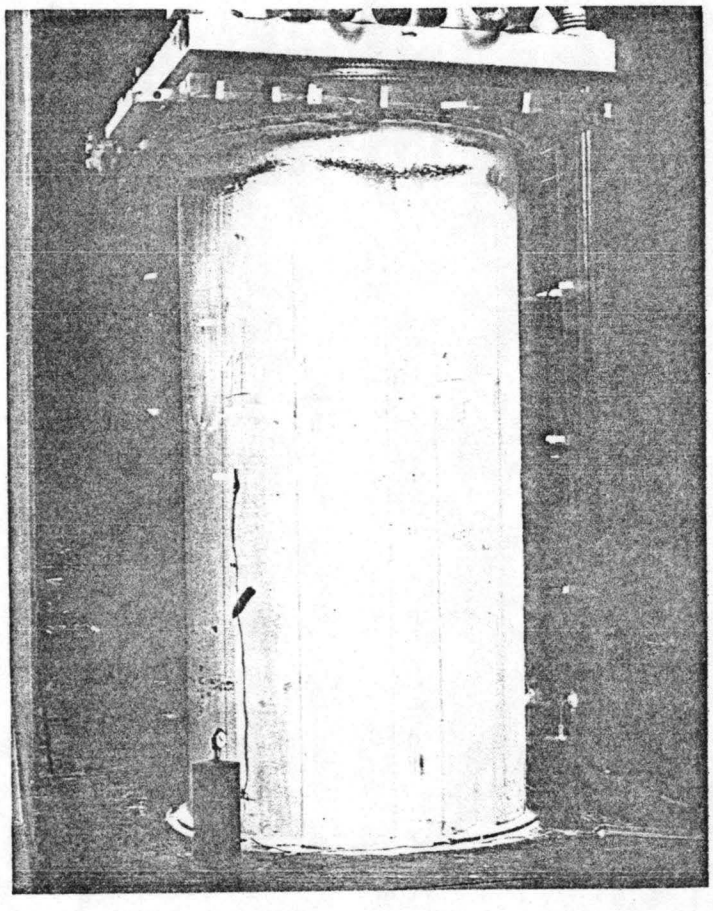

Fig. 29 Specimen P6 After Initial Buckling

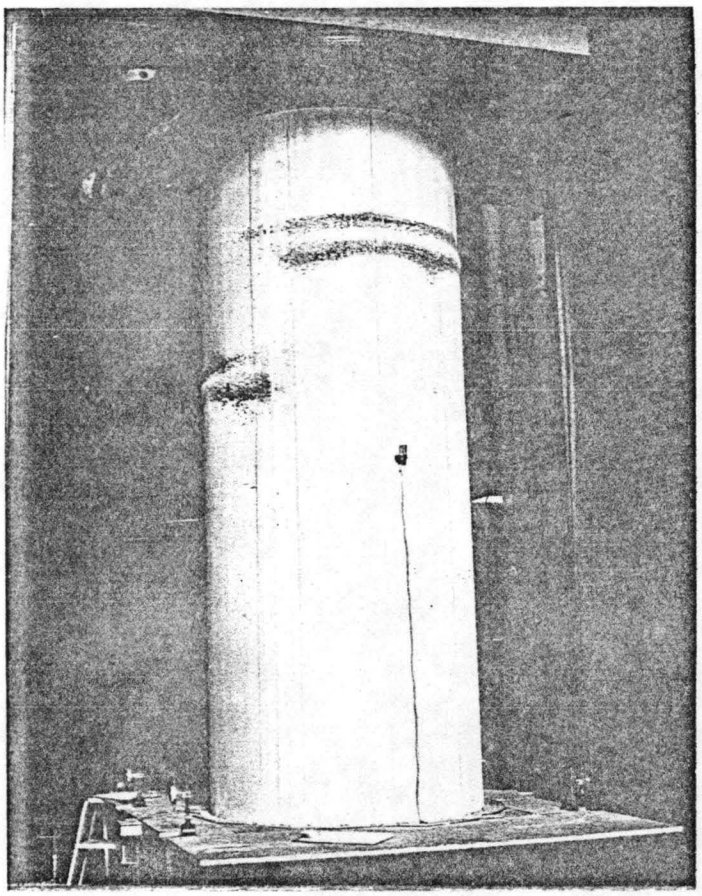

Fig. 30 Specimen P7 After Initial Buckling

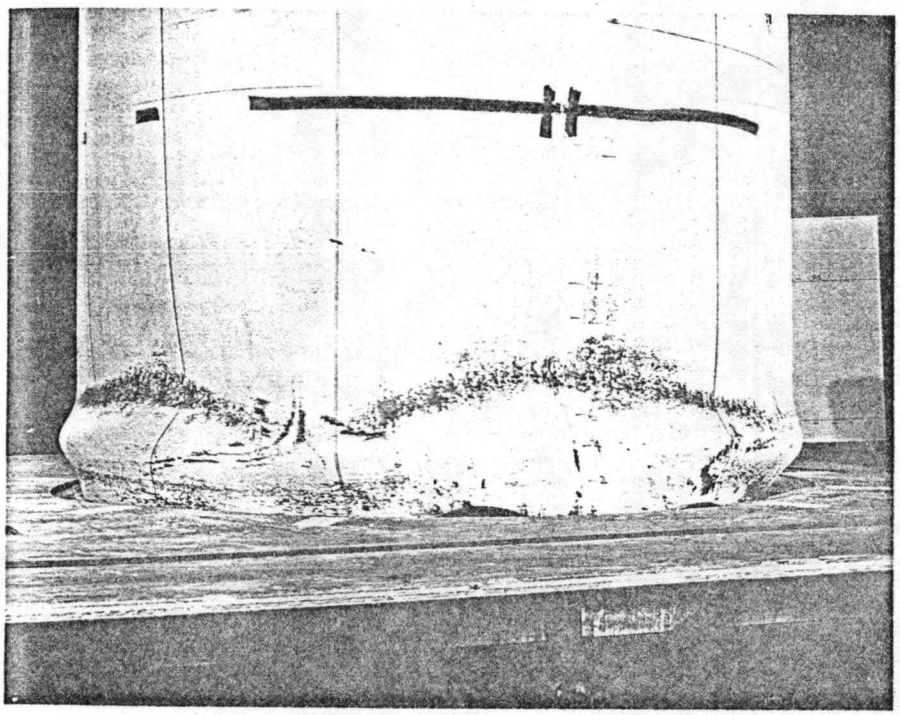

Fig. 31 Lobular Buckles in Specimen P3

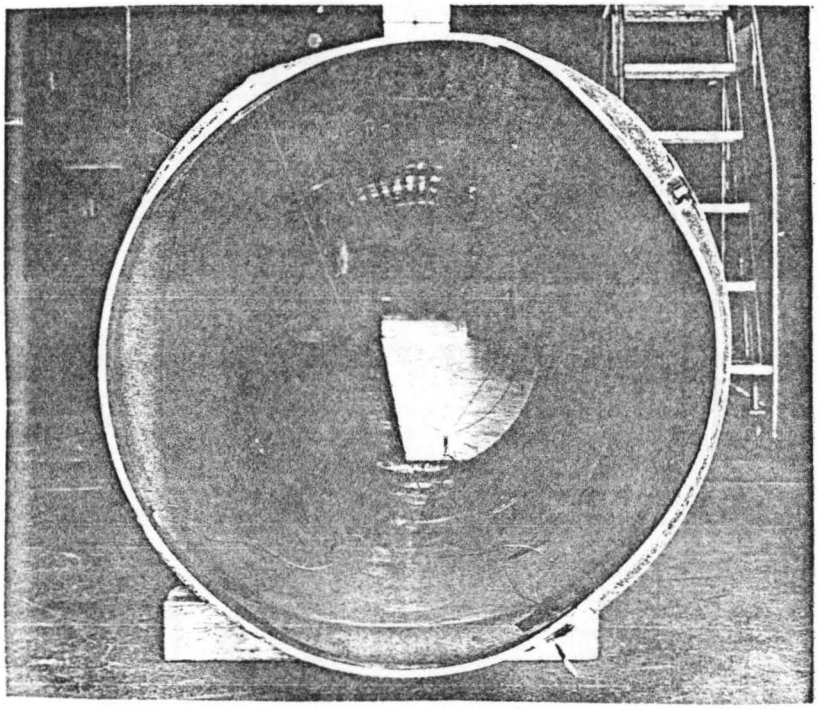

Fig. 32 End View of Specimen P1 After Testing

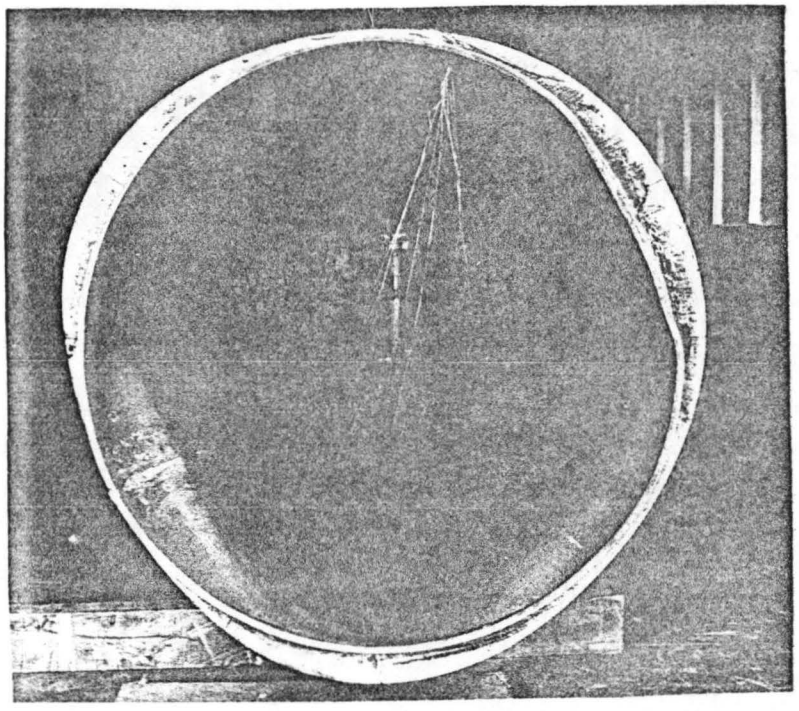

Fig. 33 End View of Specimen P2 After Testing

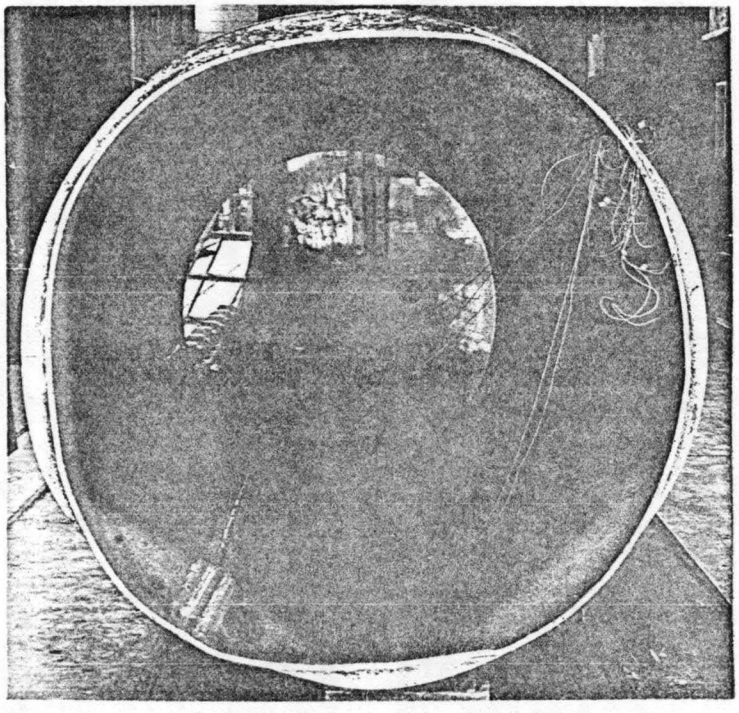

Fig. 34 End View of Specimen P3 After Testing

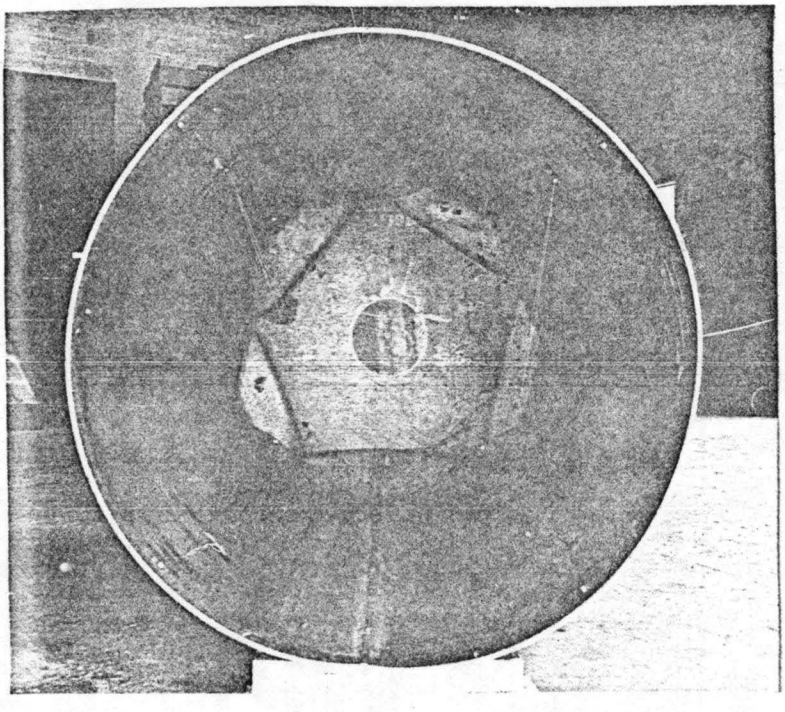

Fig. 35 End View of Specimen P3A After Testing

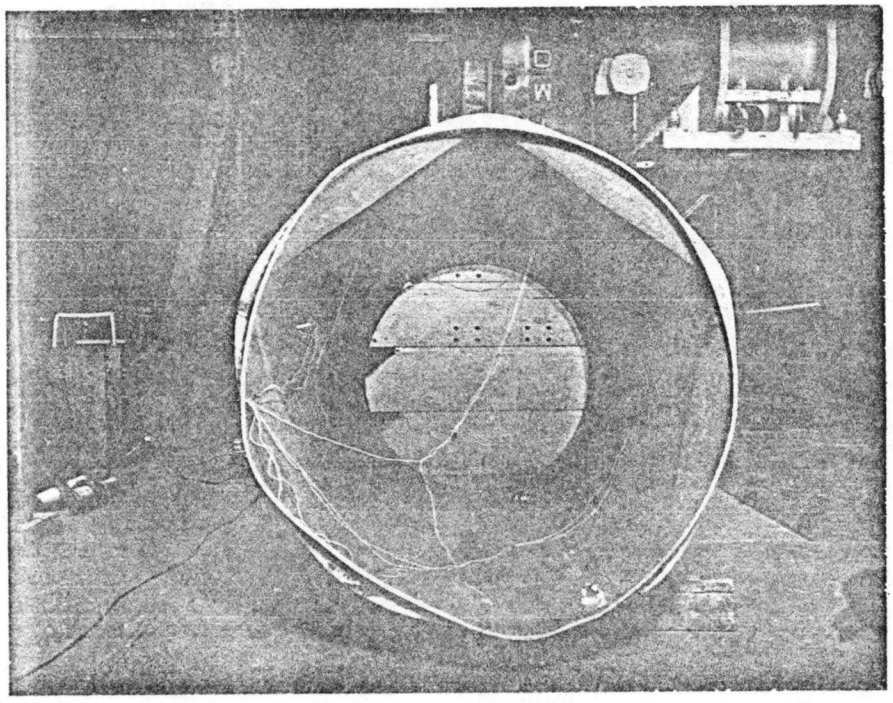

Fig. 36 End View of Specimen P4 After Testing

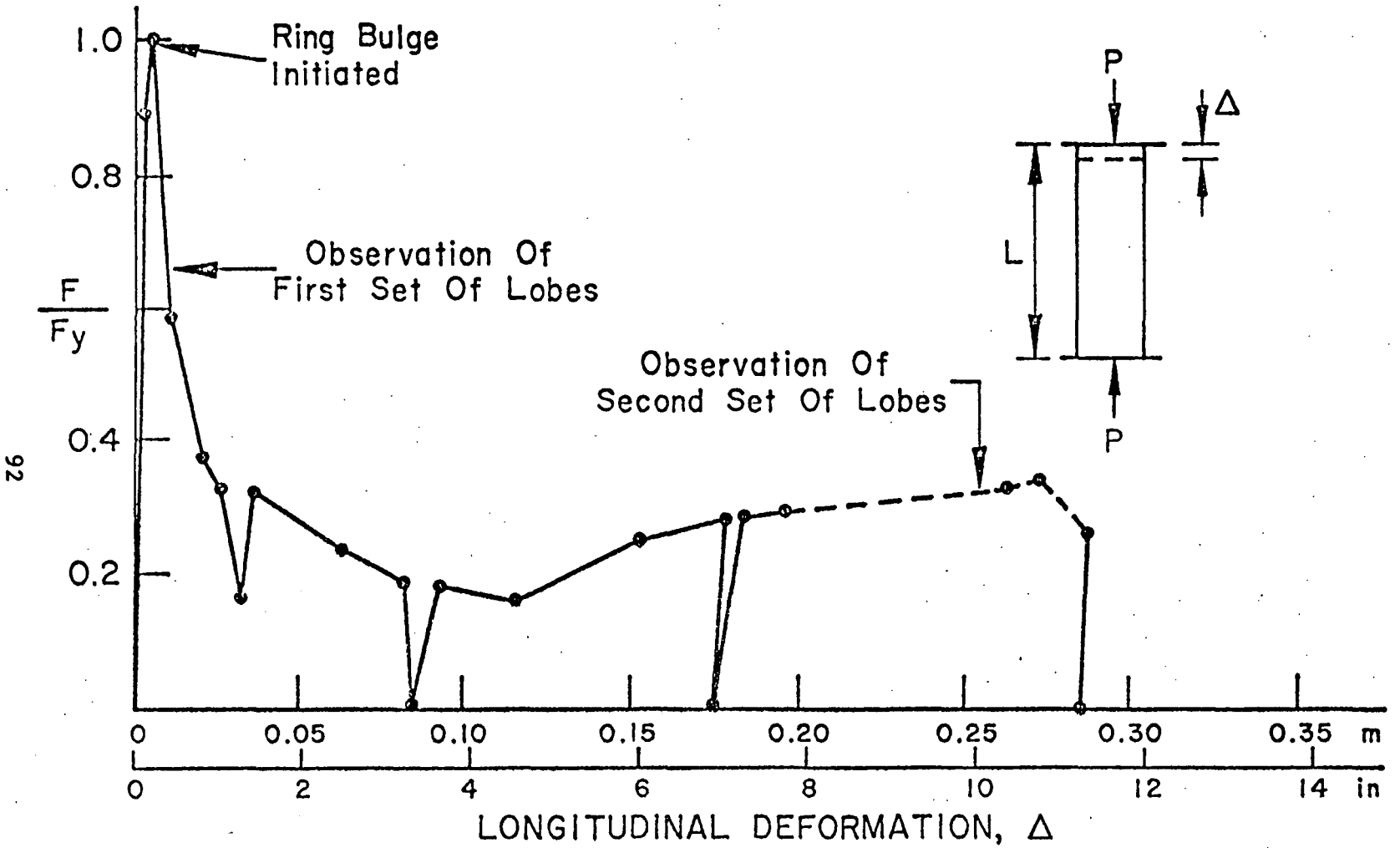

Fig. 37a Complete Average Stress-Deformation Behavior of Specimen P3A

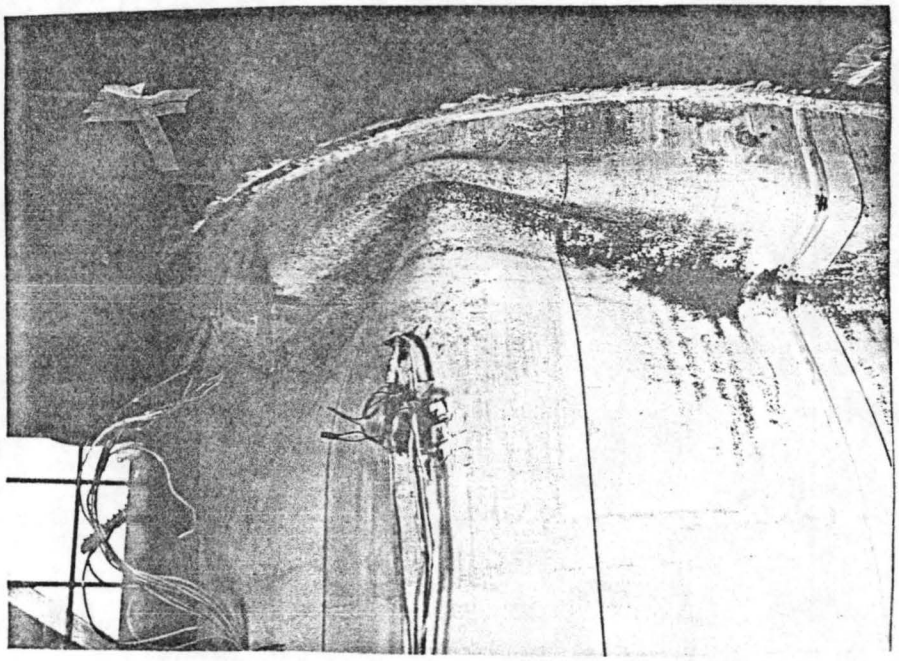

Fig. 37b First Set of Lobular Buckles in Specimen P3A

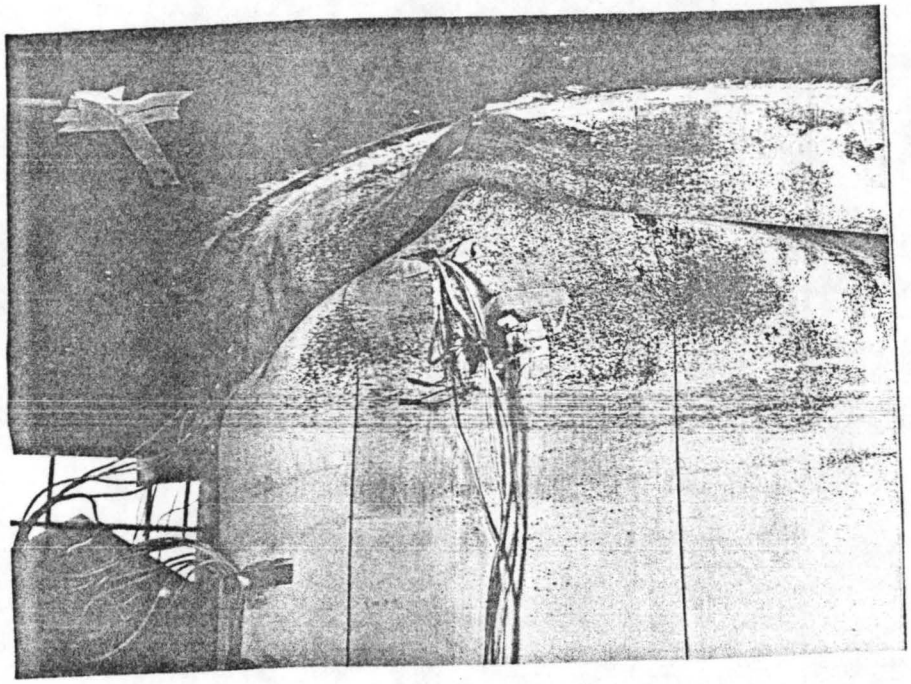

Fig. 37c First and Second Sets of Lobular Buckles in Specimen P3A

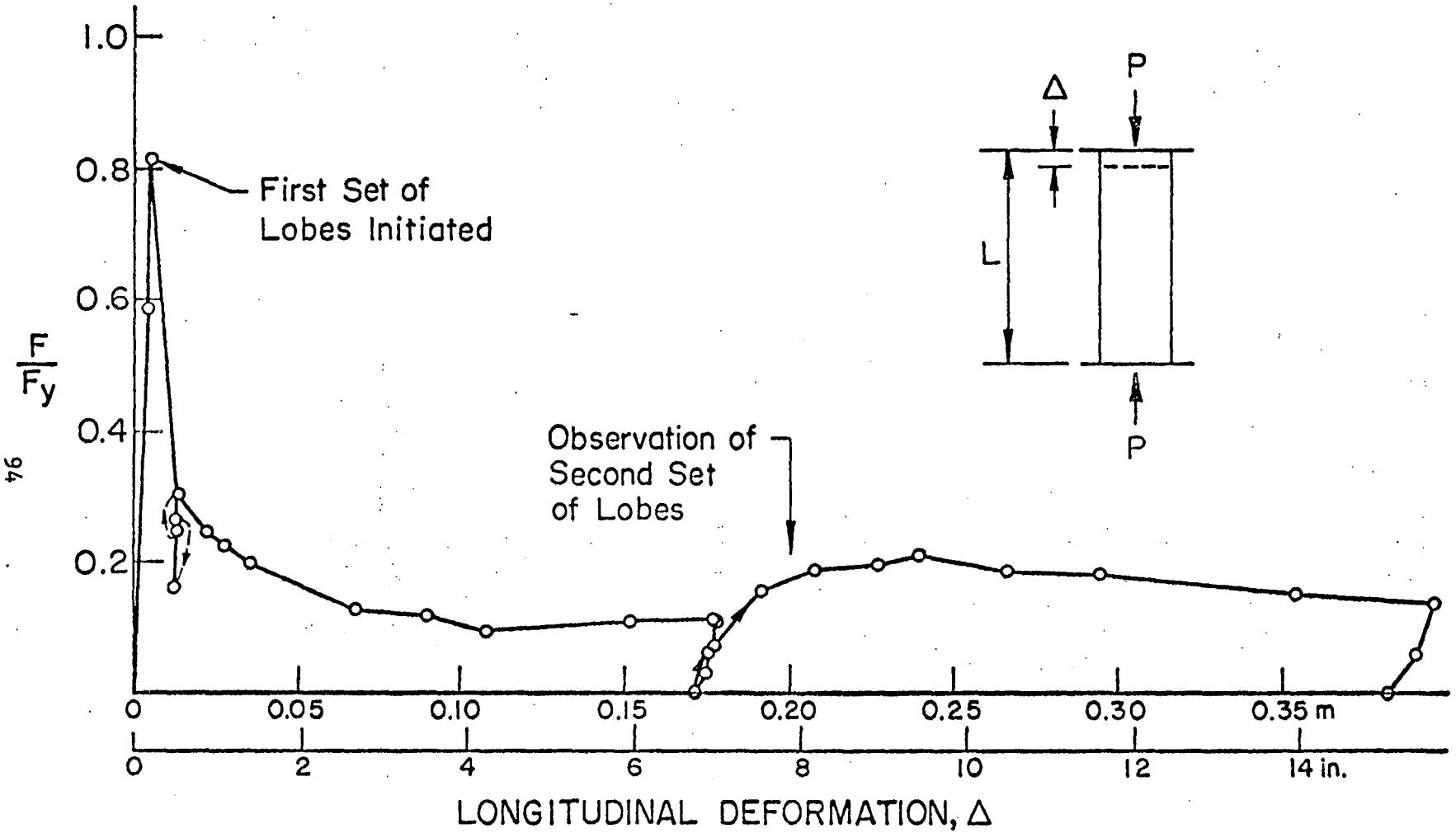

Fig. 38a Complete Average Stress-Deformation Behavior of Specimen P5

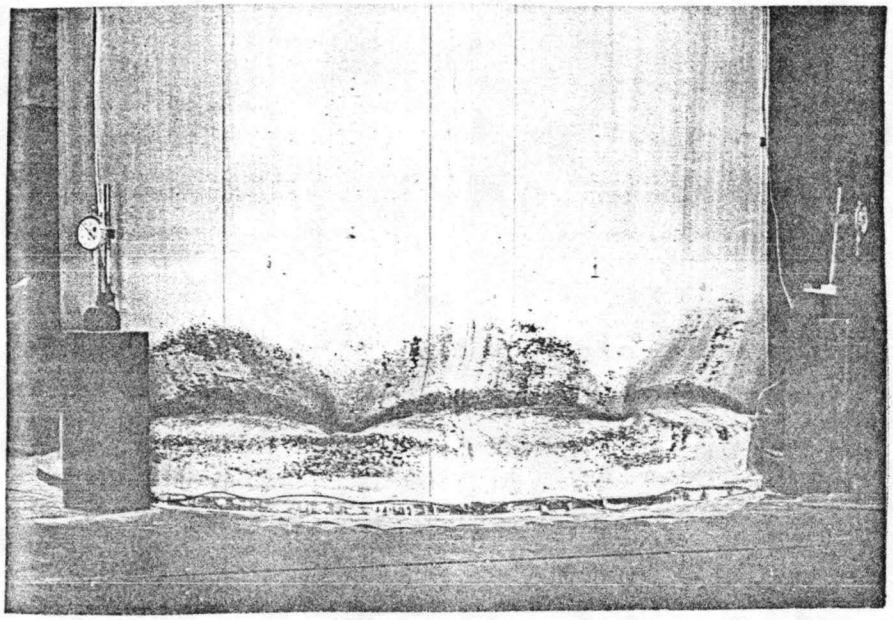

Fig. 38b First Set of Lobular Buckles in Specimen P5

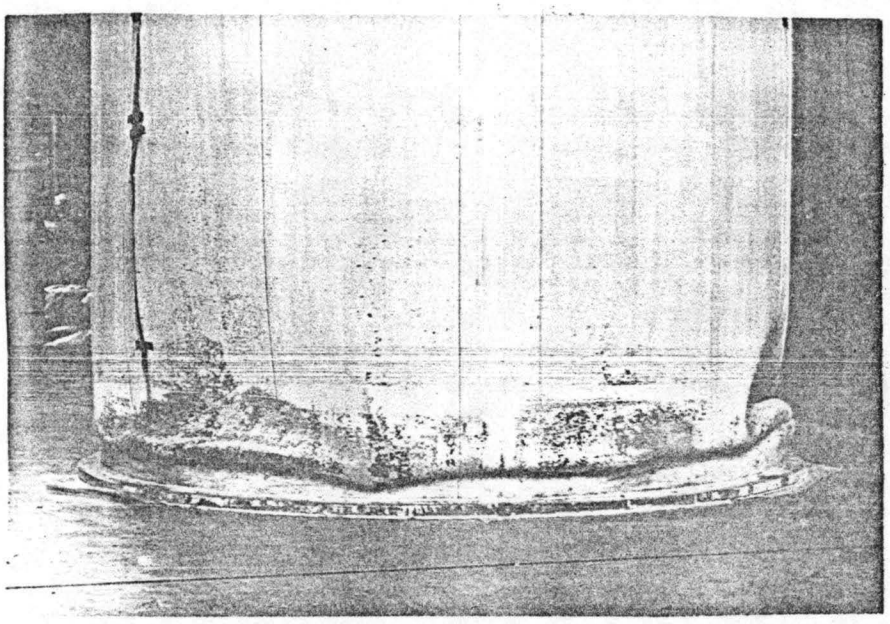

Fig. 38c First and Second Sets of Lobular Buckles in Specimen P5

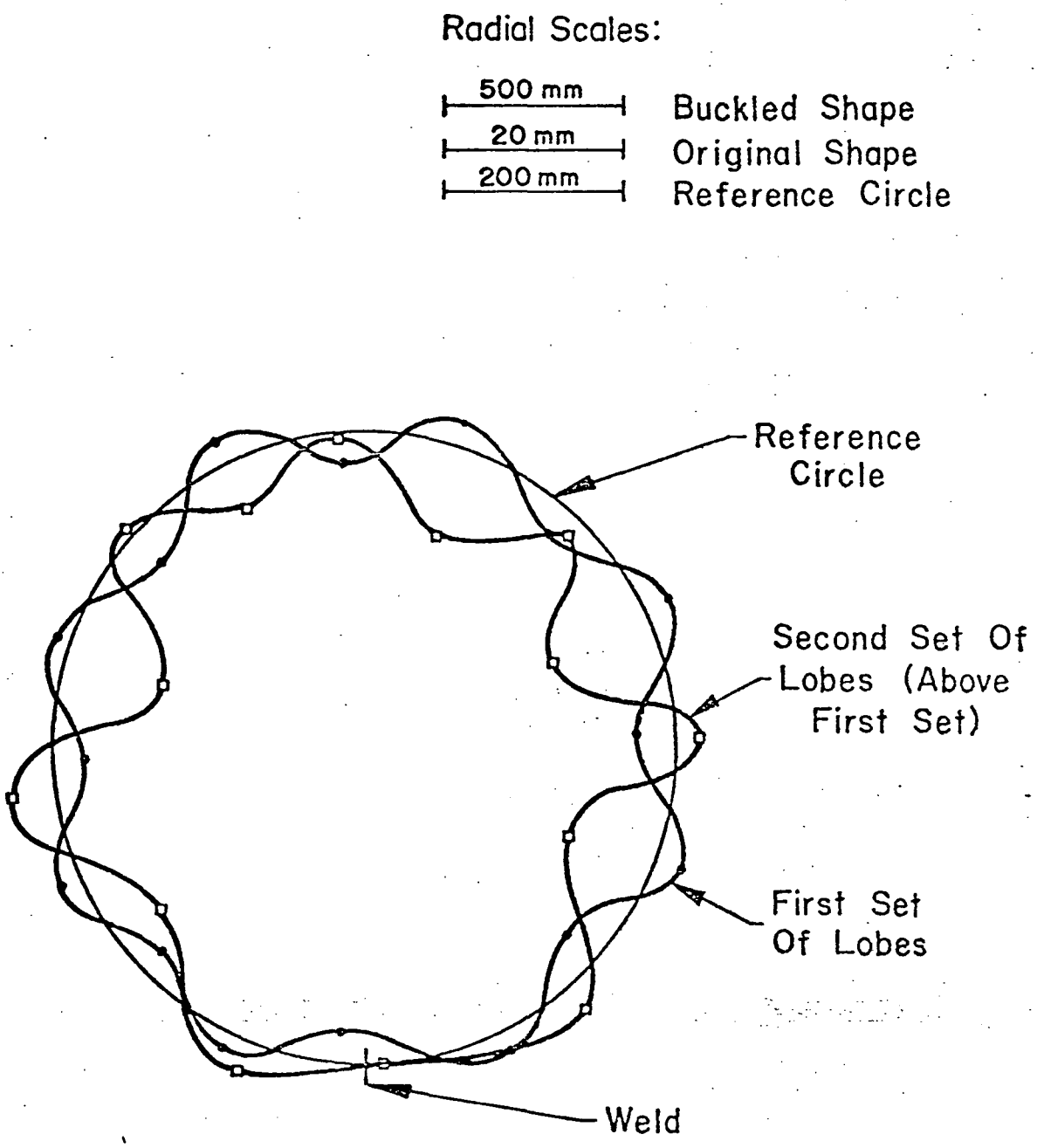

Fig. 39 Pattern of the First and Second Sets of Lobular Buckles in Specimen P5

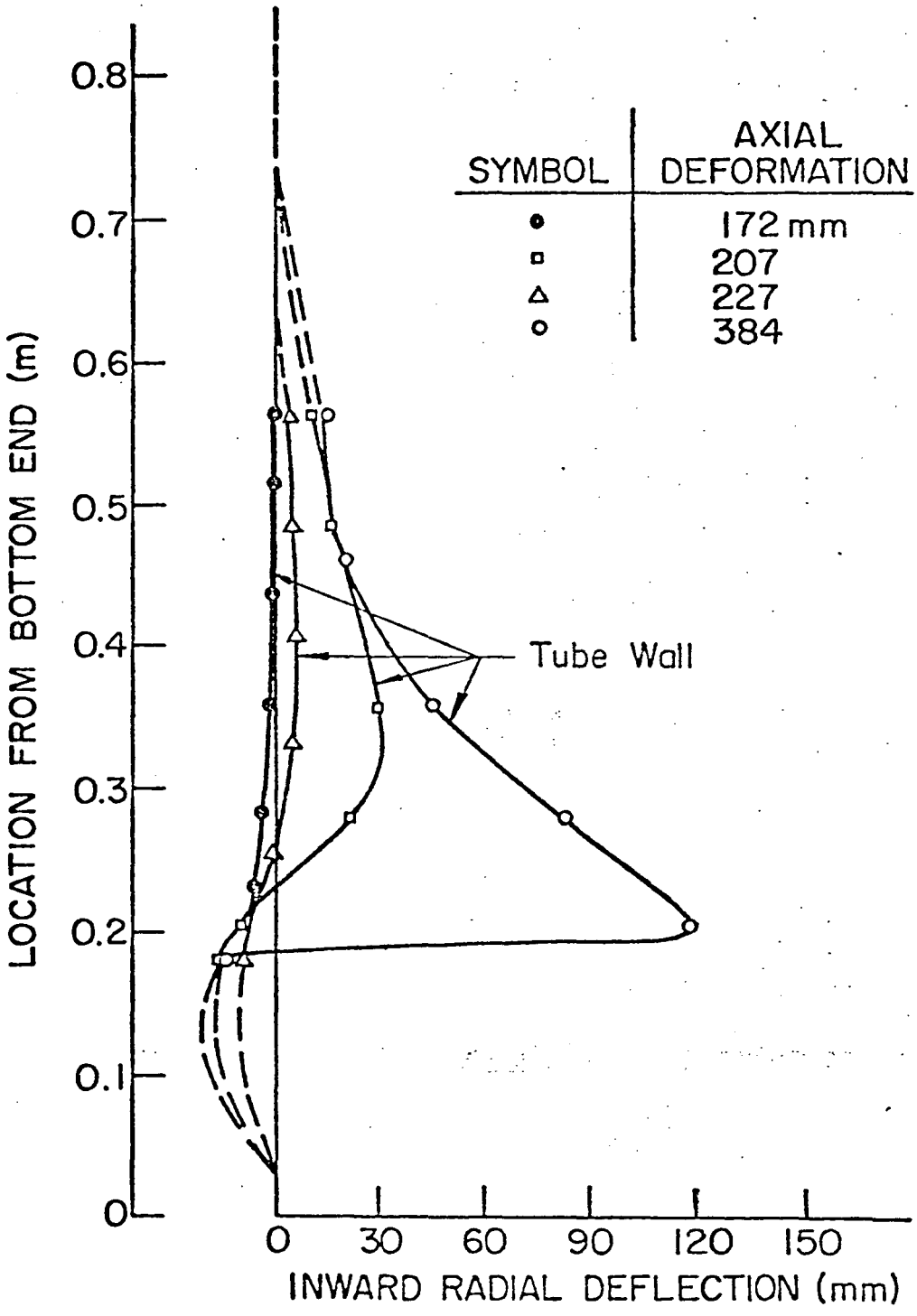

Fig. 40 Development of an Inward Lobe in the Second Set of Buckles in Specimen P5

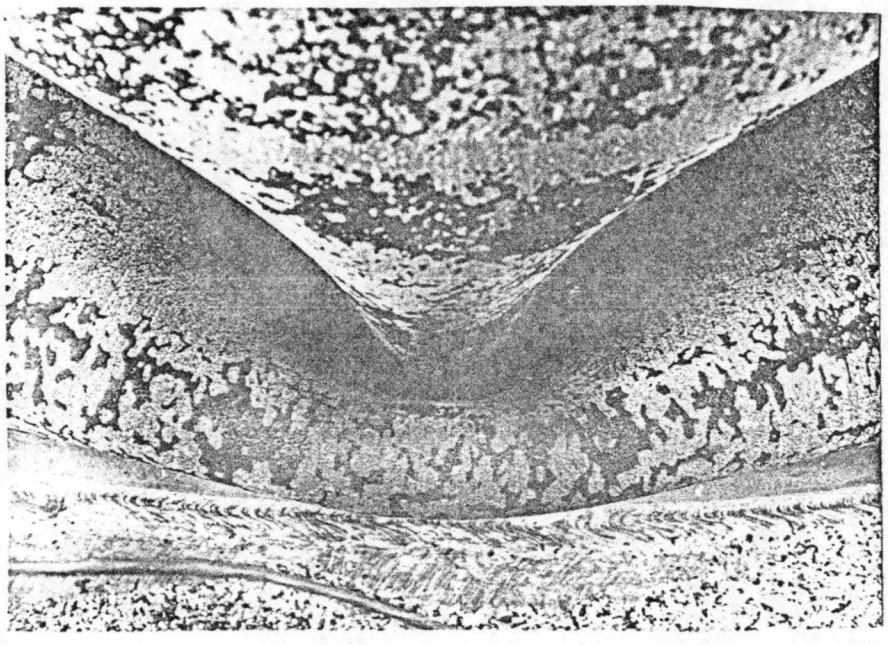

Fig. 41 Vertical, Rigid Type of Outward Lobe in Specimen P5

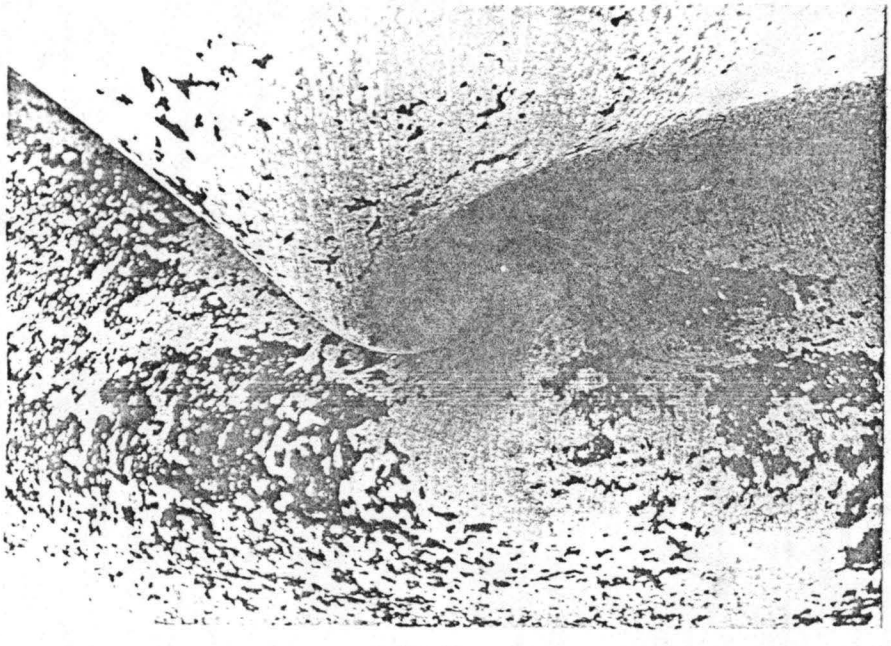

Fig. 42 Folding Type of Outward Lobe in Specimen P5

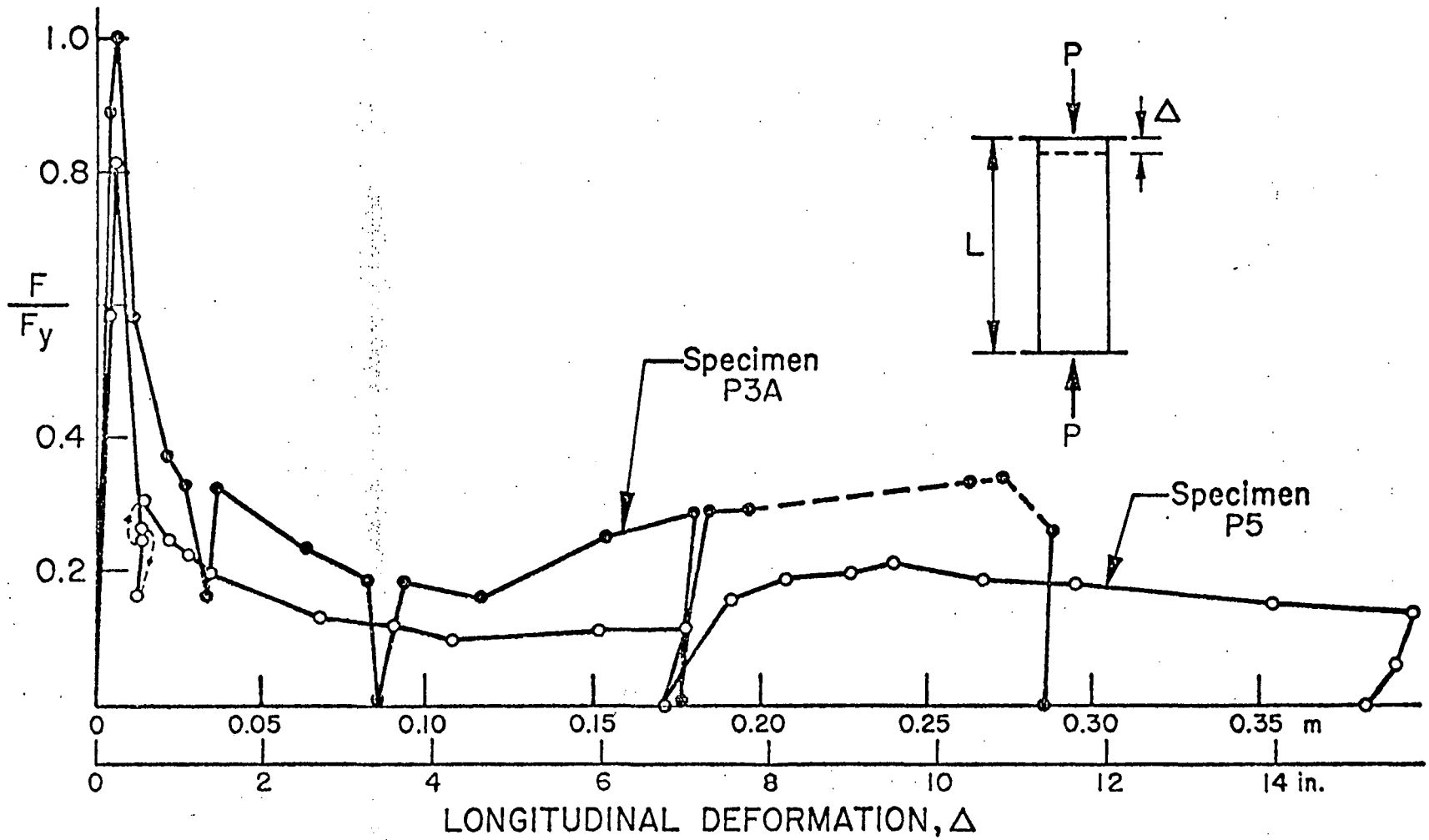

Fig. 43 Comparison of the Average Stress-Deformation Behavior for Specimens P3A and P5

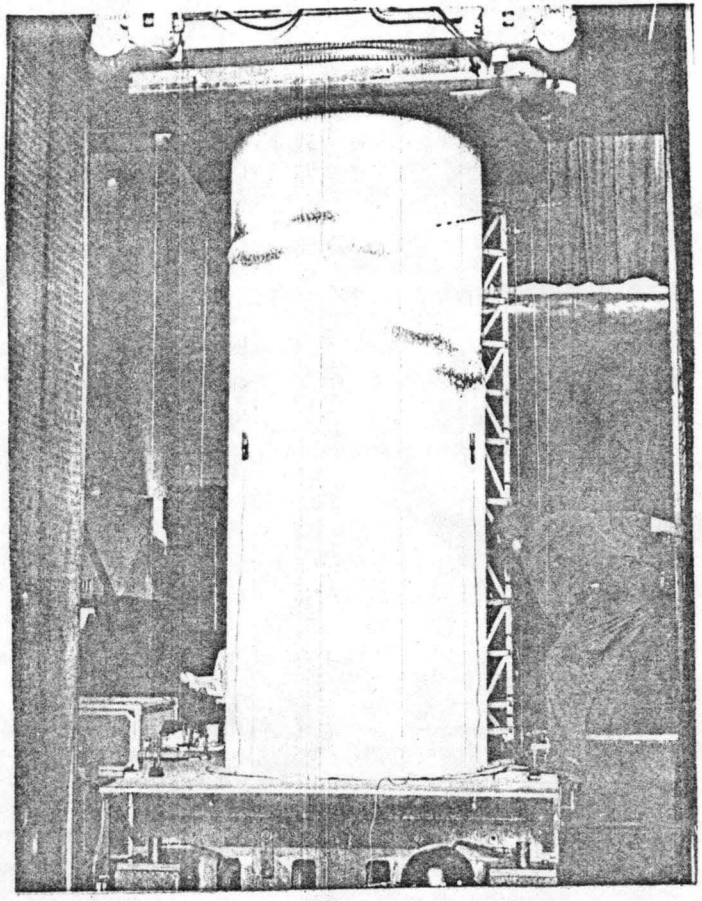

Fig. 44 The Two Levels of Buckling in Specimen P7 at One-Third of the Circumference from the Weld

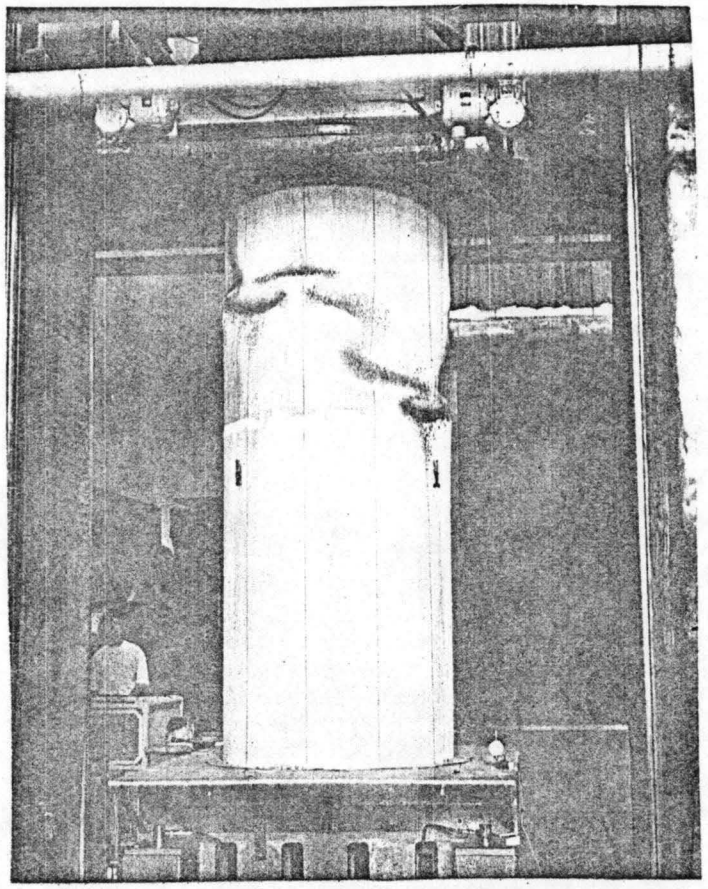

Fig. 45 "S-Shaped" Buckle Connecting the Two Levels of Buckling in Specimen P7

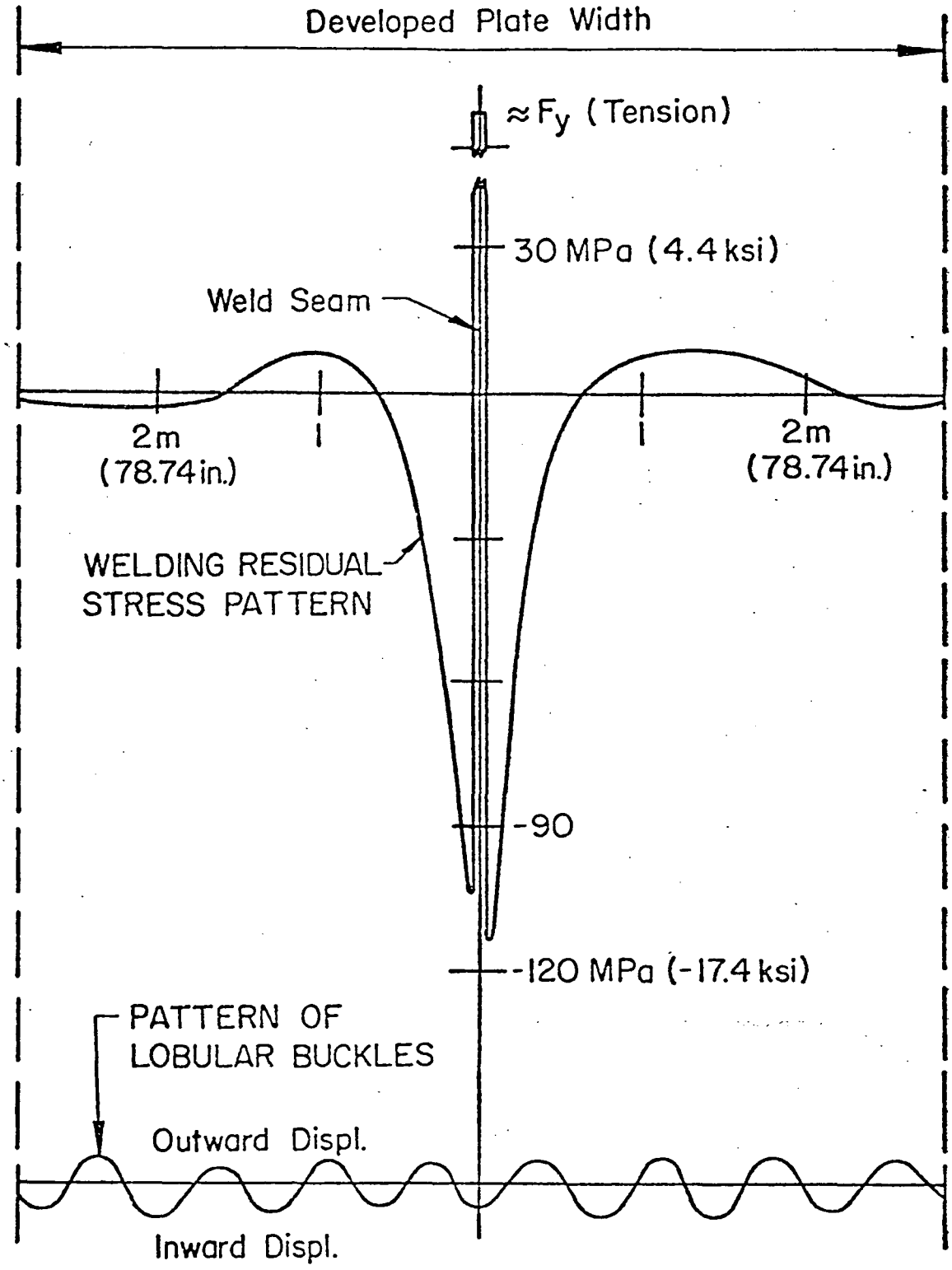

Fig. 46 Comparison of the Patterns of Welding Residual Stresses and Lobular Buckles in Specimen P5

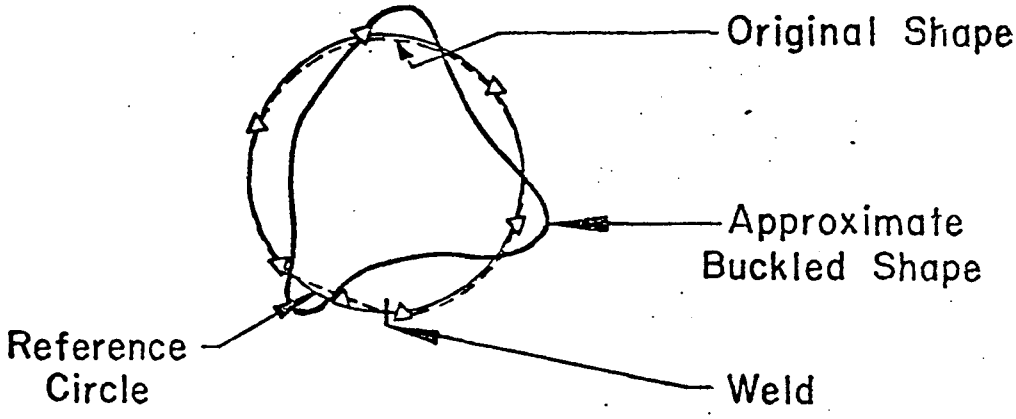

Fig. 47 The Original and Buckled Shapes for Specimen P1

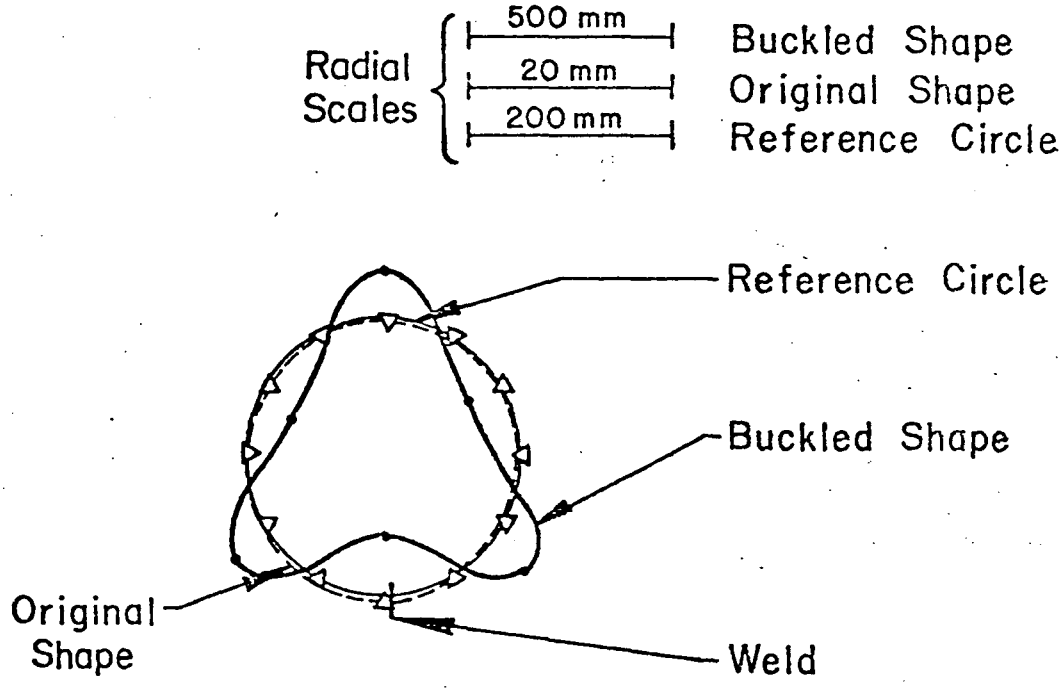

Fig. 48 The Original and Buckled Shapes for Specimen P2

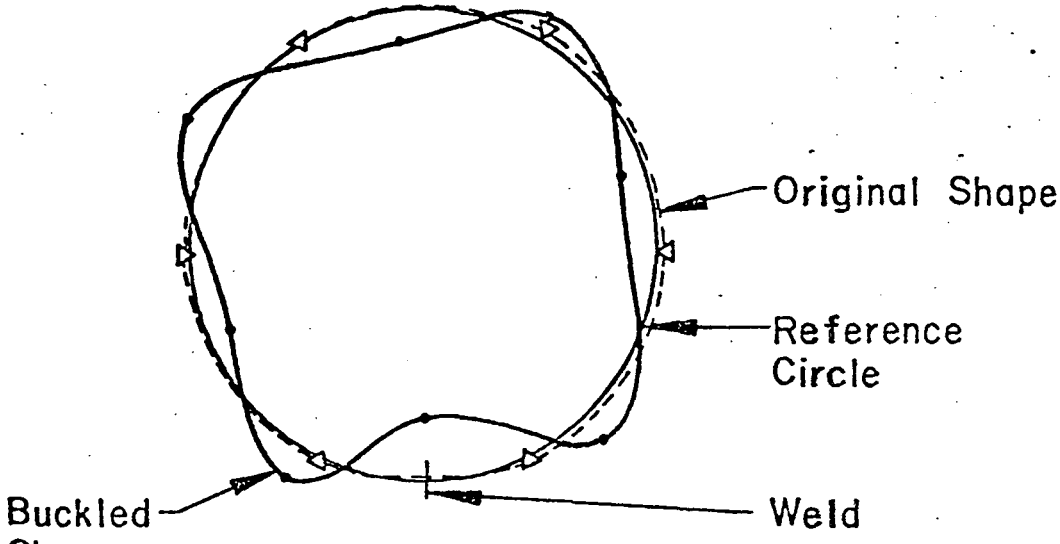

Fig. 49 The Original and Buckled Shapes for Specimen P3

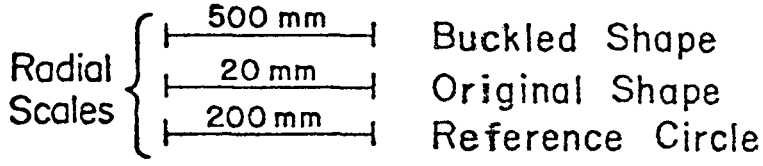

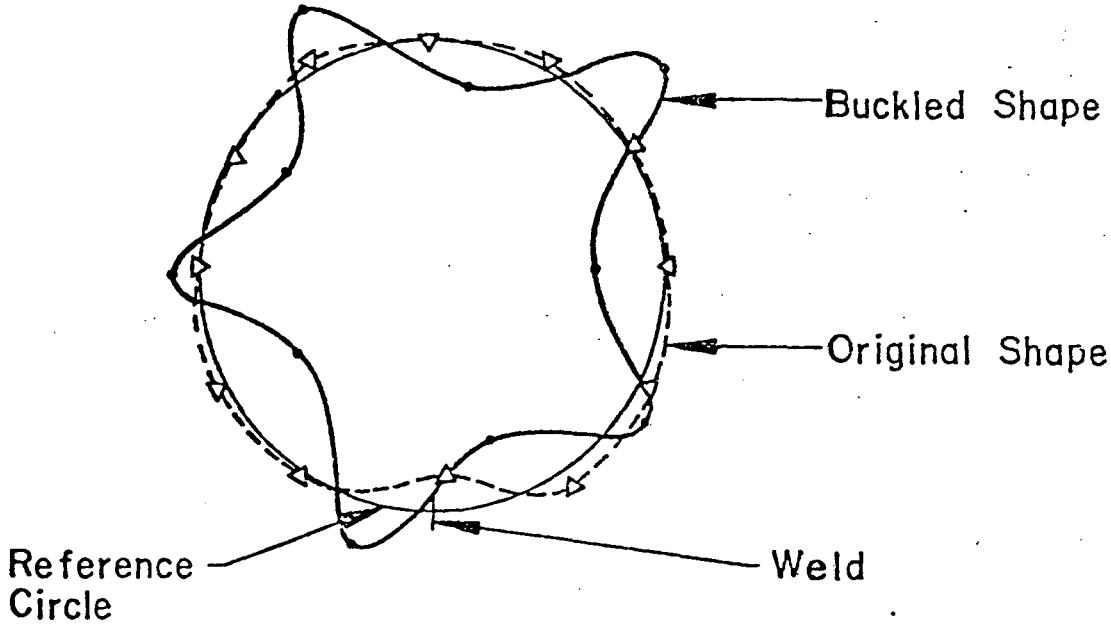

Fig. 50 The Original and Buckled Shapes for Specimen P4

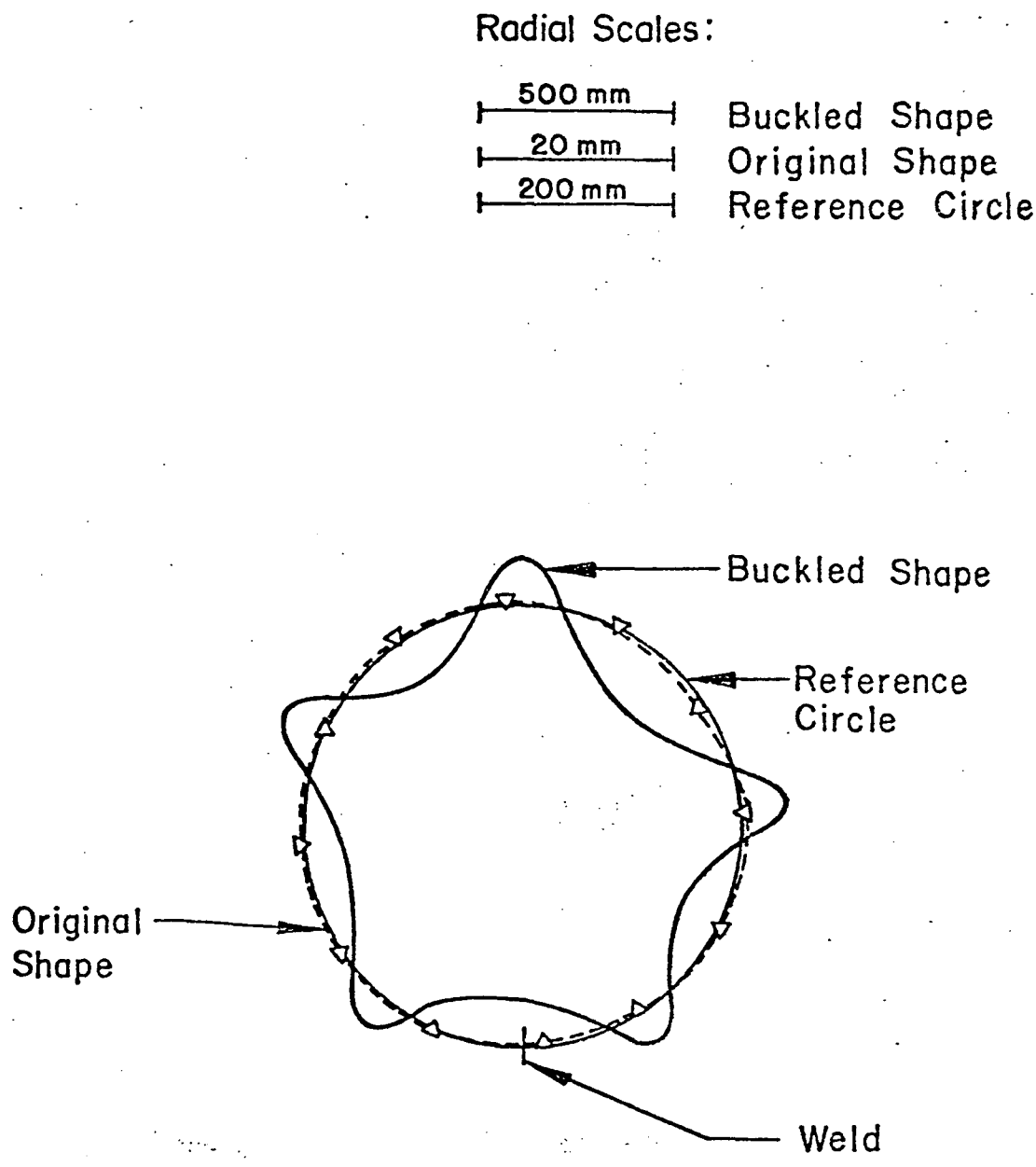

Fig. 51 The Original and Buckled Shapes for Specimen P3A

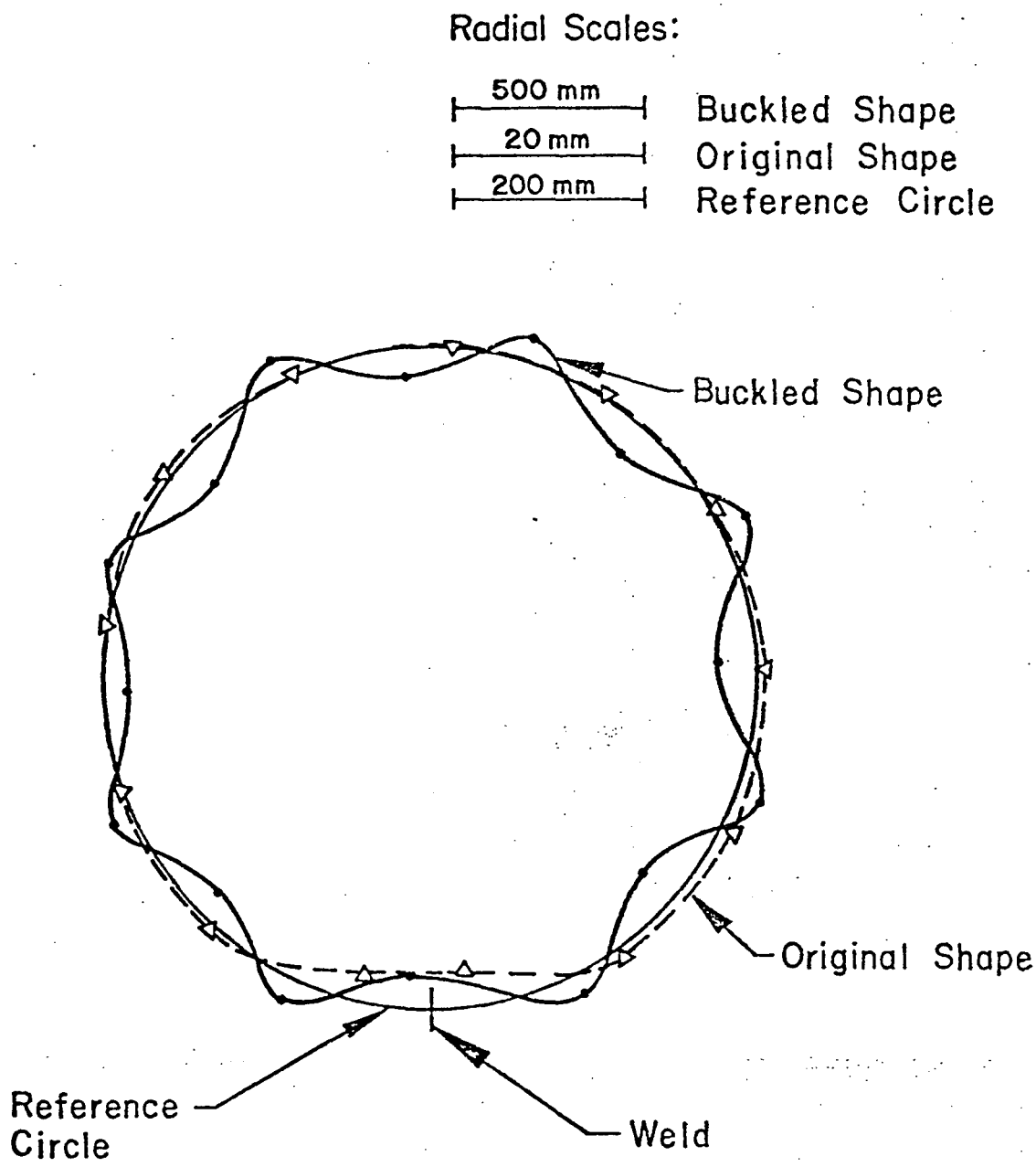

Fig. 52 The Original and Buckled Shapes for Specimen P5

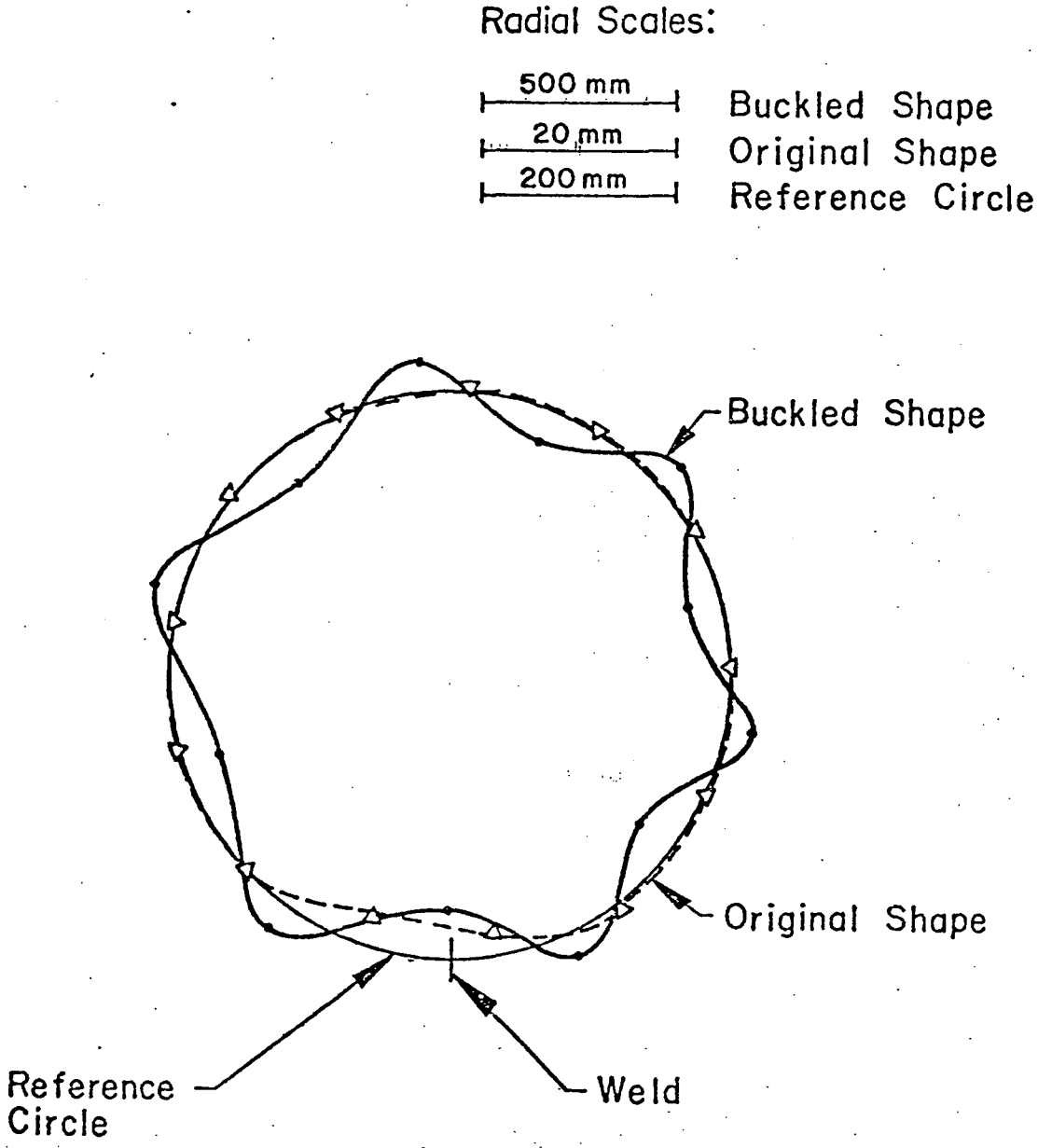

Fig. 53 The Original and Buckled Shapes for Specimen P6

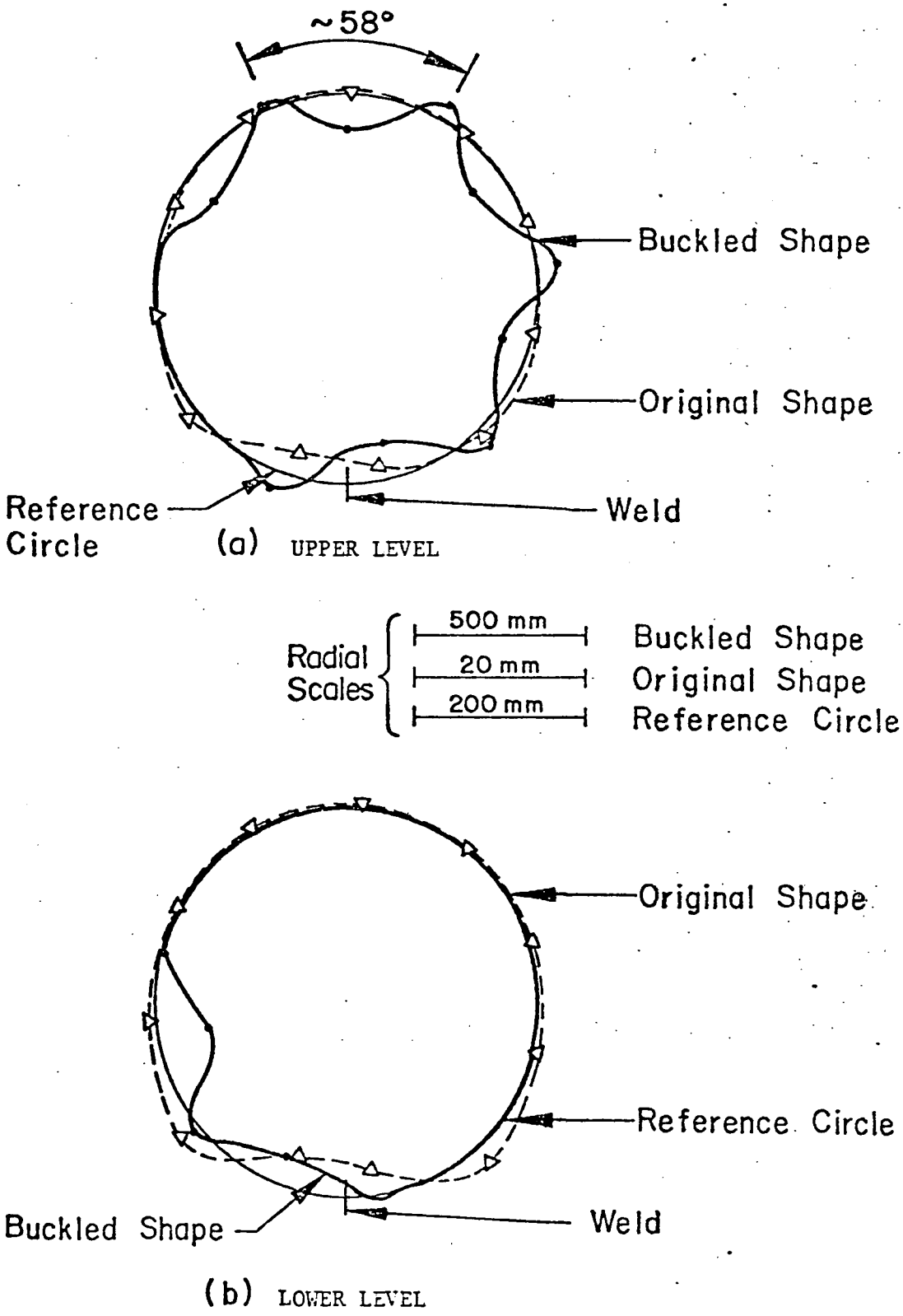

Figs. 54a & 54b The Original and Buckled Shapes for Specimen P7

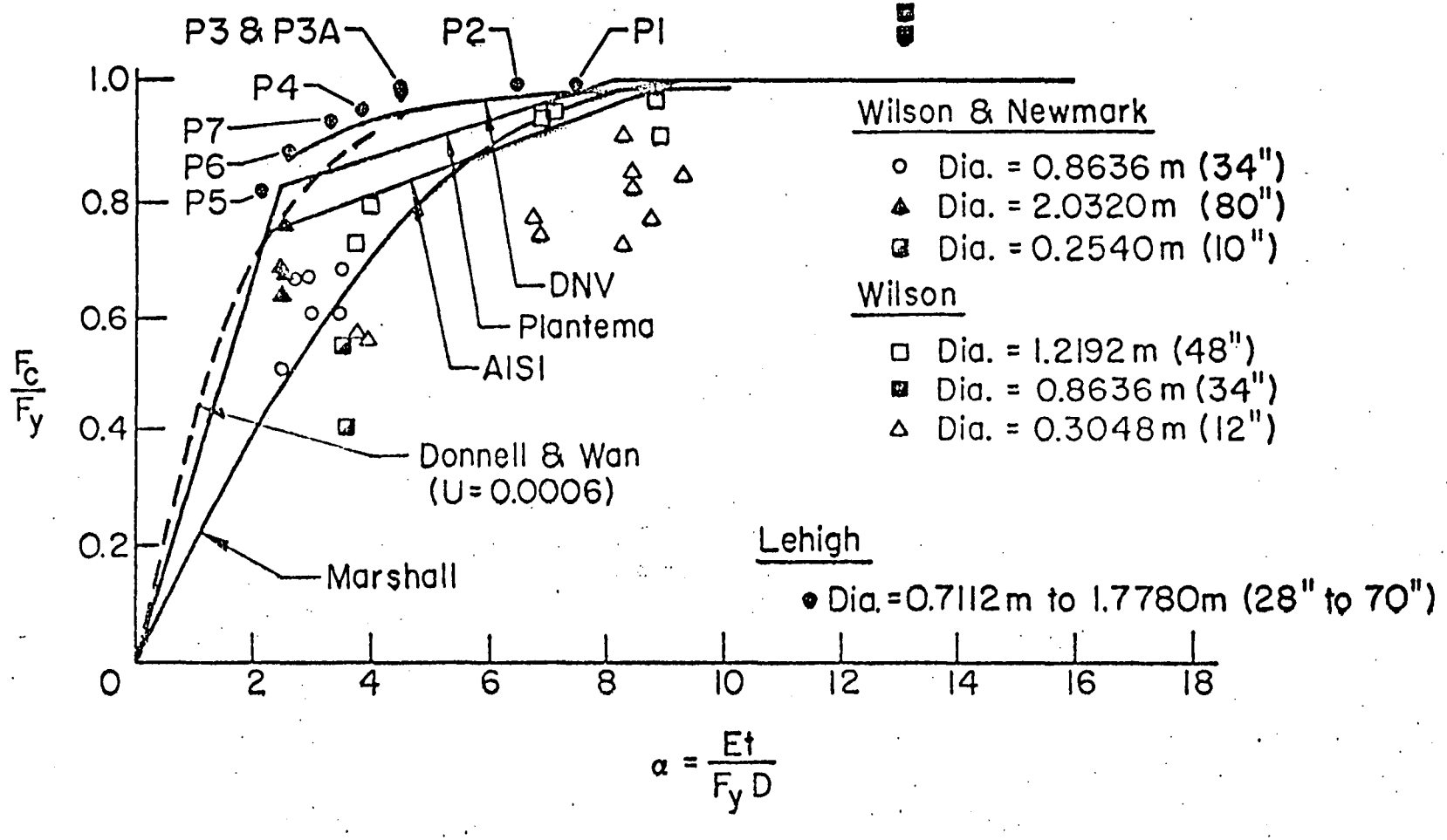

Fig. 55 Test Results of This Study In Comparison With Design Curves and Test Results of Others

12. REFERENCES

1. American Iron and Steel Institute, "Specification for the Design of Cold-Formed Structural Members," Washington, D.C., 1968, p. 25.

2. American Petroleum Institute, Division of Production, "API Specification 2B," 2nd ed., API Specification for Fabricated Structural Steel Pipe, October, 1972.

3. American Society for Testing and Materials, "ASTM Specification E8-69," Annual Book of ASTM Standards, Part 31, 1971, pp. 194-213.

4. Det Norske Veritas, "Tentative Rules for Design, Construction, and Inspection of Fixed Offshore Structures," Rule Proposal RMT-1-73, October, 1973.

5. Donnell, L. H., and Wan, C. C., "Effect of Imperfections on Buckling of Thin Cylinders and Columns Under Axial Compression," Journal of Applied Mechanics, Vol. 17, No. 1, March, 1950, pp. 73-83.

6. Guide to Stability Design Criteria for Metal Structures, Structural Stability Research Council, 3rd ed., B. G. Johnston, ed., John Wiley and Sons, Inc., New York, N.Y., 1976, pp. 261-281.

7. Koiter, W. T., "The Effect of Axisymmetric Imperfections on the Buckling of Cylindrical Shells Under Axial Compression," Proceedings, The Royal Netherlands Academy of Science, Vol. 66, Series B, Amsterdam, Netherlands, 1963, p. 266.

8. Koiter, W. T., "The Stability of Elastic Equilibrium," Air Force Flight Dynamics Laboratory Technical Report AFFDL-TR-70-25, Wright Patternson Air Force Base, Ohio, February, 1970.

9. Miller, C. D., "Buckling Stresses for Axially Compressed Cylinders," Chicago Bridge and Iron Co., Plainfield, Illinois, April, 1976, pp. 8-17.

10. Plantema, F. J., "Collapsing Stress of Circular Cylinders and Round Tubes," National Luchtraat Laboratorium, Report S.280, Amsterdam, Netherlands, 1946.

11. Rao, N. R., Lohrman, M., and Tall, L., "Effect of Strain Rate on the Yield Stress of Structural Steels," Journal of Materials, Vol. 1, No. 1, March, 1966, pp. 241-262.

12. Rao, N. R., and Tall, L., "Residual Stresses in Welded Plates," Fritz Engineering Laboratory Report No. 249.7, Lehigh University, Bethlehem, Pa., October, 1960.

13. Thin-Shell Structures - Theory, Experiment, and Design, Y. C. Fung and E. E. Sechler, ed., Prentice-Hall, Inc., Englewood Cliffs, N.J., 1974.

14. Wilson, W. M. and Newmark, N. M., "The Strength of Thin Cylindrical Shells as Columns," Bulletin No. 255, Engineering Experiment Station, University of Illinois, February, 1933.

15. Wilson, W. M., "Tests of Steel Columns, Thin Cylindrical Shells, Laced Columns, Angles," Bulletin No. 292, Engineering Experiment Station, University of Illinois, April, 1937.

13. VITA

Stephen X. Gunzelman, the son of Rita and Joseph X. Gunzelman, was born on November 5, 1949, in Baltimore, Maryland. The author grew up in Baltimore and was graduated from Archbishop Curley High School in 1967.

His undergraduate studies were conducted at Loyola College in Baltimore where he received a Bachelor of Science in Engineering-Physics in 1971. From 1971 to 1974, he worked as a project engineer for the U.S. Army Corps of Engineers in a civilian capacity at Baltimore, Maryland, and Ft. Belvoir, Virginia. During this same period, he took evening courses at George Washington University in Washington, D.C. In August, 1974, he was awarded a Research Assistantship in Civil Engineering at Fritz Engineering Laboratory, Lehigh University, and, in October, 1976, he received his Master of Science in Civil Engineering, with a structures major.